universität
wien

DIPLOMARBEIT

RNA folding kinetics including pseudoknots

Towards the design of artificial RNA switches

angestrebter akademischer Grad

Magister der Naturwissenschaften (Mag. rer. nat.)

Verfasser:	Stefan Badelt
Matrikelnummer:	0403381
Studienrichtung:	Molekulare Biologie (A490)
Betreuer:	Univ.-Prof. Dipl.-Phys. Dr. Ivo Hofacker

Wien, im August 2011

Danksagung

An dieser Stelle möchte ich mich bei all jenen herzlich bedanken, die zum Gelingen dieser Arbeit beigetragen haben:

- Meinen Betreuern Ivo Hofacker & Christoph Flamm für kompetente Unterstützung bei angenehmer und entspannter Arbeitsathmosphäre
- Meinen aktiven und ehemaligen Arbeitskollegen (agruber, berni, choener, egg, fabian, fall, hekker, ronny, sven und wolfgang) für deren Hilfsbereitschaft bei diversen größeren und kleineren Problemen
- Meinen Eltern Doris & Felix für durchgehendes Vertrauen und finanzielle Unterstützung

Prost!

Abstract

RNA molecules are essential components of living cells. Their wide range of different functions depends on the sequence of nucleotides and the corresponding structure. The majority of known RNA molecules fold into their energetically most stable conformation, as well as structurally similar *suboptimal* conformations that do not alter the specific task of the molecule. However, there are RNA molecules which can switch between two structurally distant conformations one of which is functional, the other is not. The best known examples are *riboswitches*, which usually sense various kinds of metabolites from their environment that trigger the refolding from one conformation into the other.

The rather new field of synthetic biology led to the construction of an example for a new type of riboswitches, which refold upon interaction with other RNA molecules [1]. Such RNA-triggered riboswitches are not aimed at sensing the environment, but expand the repertoire of gene-regulation. Inspired by this example, we present `RNAscout.pl`, a new program to study refolding between two RNA conformations, which can be used to estimate the performance of RNA-triggered riboswitches. The underlying algorithm heuristically computes a set of intermediate conformations that are energetically favorable and structurally related to both stable conformations of the riboswitch. Based on this refolding network, we show kinetic simulations that support the expected refolding path for our riboswitch example.

Moreover, we present `pk_findpath`, a breadth-first search algorithm to estimate *direct paths* (i. e. a small subset of all possible paths) between two different RNA conformations. Both programs `RNAscout.pl` and `pk_findpath` will be used to estimate whether natural RNA molecules are optimized to fold into their energetically most stable conformation. Thereby, we compare the new programs against existing programs of the `Vienna RNA package` [2]

Zusammenfassung

RNA Moleküle sind ein essenzieller Bestandteil biologischer Zellen. Ihre Vielfalt an Funktionen ist eng verknüpft mit der jeweiligen Sequenz und der daraus gebildeten Struktur. Der Großteil bekannter RNA Moleküle faltet in eine bestimmte energetisch stabile Struktur, bzw. ähnliche *suboptimale* Strukturen mit der gleichen biologischen Funktion. *Riboswitches* hingegen, eine bestimmte Gruppe von RNA Molekülen können zwischen zwei strukturell sehr verschiedenen Konformationen wechseln, wobei eine funktional ist und die andere nicht. Die Umfaltung solcher RNA-Schalter wird normalerweise durch verschiedenste Metaboliten ausgelöst die mit der RNA interagieren. Zellen nutzen dieses Prinzip um auf Signale aus der Umwelt effizient reagieren zu können.

Im Zuge der synthetischen Biologie wurde eine neue Art von RNA-Schaltern entwickelt, die statt einem bestimmten Metaboliten ein anderes RNA Molekül erkennt [1]. Dieses Prinzip ziehlt weniger darauf ab Signale aus der Umgebung wahrzunehmen, sondern ein weiteres Level an Genregulation zu ermöglichen. In dieser Abeit wird das Program `RNAscout.pl` präsentiert, welches die Umfaltung zwischen verschiedenen RNA Strukturen berechnet und damit die Effizienz RNA-induzierter RNA-Schalter bewerten kann. Der zugrundeliegenede Algorithmus berechnet ein Set an Zwischenzuständen die sowohl energetisch günstig, als auch strukturell ähnlich zu den beiden stabilen Riboswitch-Konformationen sind. Basierend auf diesem Umfaltungsnetzwerk werden kinetische Simulationen gezeigt, bei denen der Umfaltungsweg des RNA-Schalters vorhergesagt wird.

Des Weiteren wird das Programm `pk_findpath` vorgestellt. Der zugrundeliegende Algorithmus berechnet den besten *direkten* Umfaltungspfad zwischen zwei RNA Strukturen mittels einer Breitensuche. Beide Programme, `RNAscout.pl` und `pk_findpath`, werden verwendet um abzuschätzen ob natürliche RNA Moleküle optimiert sind um in ihre energetisch günstigste Konformation zu falten. Im Zuge dessen werden die Programme mit existierenden Programmen des `Vienna RNA package` [2] verglichen.

Contents

1 Introduction

1.1 Importance of RNA

Ribonucleic acid (RNA) made its mark in biology as a multifunctional molecule that is involved in central synthesis processes of the cell. While the importance of deoxyribonucleic acid (DNA) and proteins in cellular metabolism has been indisputable for decades, RNA has long been neglected as an intermediate during protein synthesis. Starting at latest from detection of enzymatic activities in RNA molecules [3, 4, 5] this picture slowly, but continuously changed. Over the years, the discovery of ribozymes [3], small as well as long non-coding[1] RNAs (**ncRNAs**) [6, 7, 8, 9, 10] and riboswitches [11] supported the hypothesis of RNA being also functional in itself instead of just serving as a protein-template. The 'one gene, one protein' credo, which might still be in the back of ones mind is therefore far too simple to explain developmental complexity of organisms [12].

Genome assembly & organism complexity

Taking a bird's eye view onto the humane genome [13, 14] and comparing it to other eukaryotic genomes reveals two prominent inconsistencies. The first one is known as the C-value paradox (or C-value enigma) in literature [15, 16, 17]. This paradox refers to the non-

[1] non-coding stands for non-protein-coding

existent correlation of total genome size with developmental complexity. Hence, in a search for essential genetic information that scales with organism complexity, total DNA content was revised to protein-coding sequences (about 1.5% of the human genome) and associated regulatory elements, ending up in the second inconsistency, the so-called G-value paradox [15]. This shows that the amount of protein-coding genes does not scale with organism complexity either, instead it is constant at about 20,000 sequences in many vertebrates such as human, mouse, chicken, pufferfish [18, 19, 20, 21] and apparently of no important impact when comparing the nematode worm *Caenorhabditis elegans* (19,300 genes [22]) with complex insects as *Drosophila melanogaster* (13,500 genes [23]). Moreover, most proteins can be found in numerous eukaryotes of different complexity [24]. Thus, the G-value paradox challenges the dogma that non-protein-coding sequences are either cis-regulatory and structural elements or evolutionary junk [25].

Finally, when looking at the part of non-coding DNA (98.5% in human), it seems like there is a correlation [26] especially since the ratio of non-coding DNA to total genomic DNA rises as a function of developmental complexity [27, 12]. This finding is nicely correlated with mathematical models which suggest that the quantity of regulatory molecules has to increase in a non-linear, roughly quadratic function with the number of genes [28, 29, 12]. In terms of genome evolution, this means that every new protein needs about two new regulatory RNAs to fulfill its mission, respectively that the organism complexity scales with the amount of advanced regulatory molecules instead of scaling with the quantity of available building blocks, such as proteins.

Figure 1.1 shows the composition of the human genome. The currently most examined sites of known RNA-coding sequences are introns (about 25.9%) and transposable elements (about 44.7% of the genome); parts that have long been seen as 'junk' or 'selfish' DNA. The remaining parts (about 27.9%) are characterized as 'simple sequence repeats', 'segmental duplications', 'miscellaneous heterochromatin' or 'miscellaneous unique sequences' [30].

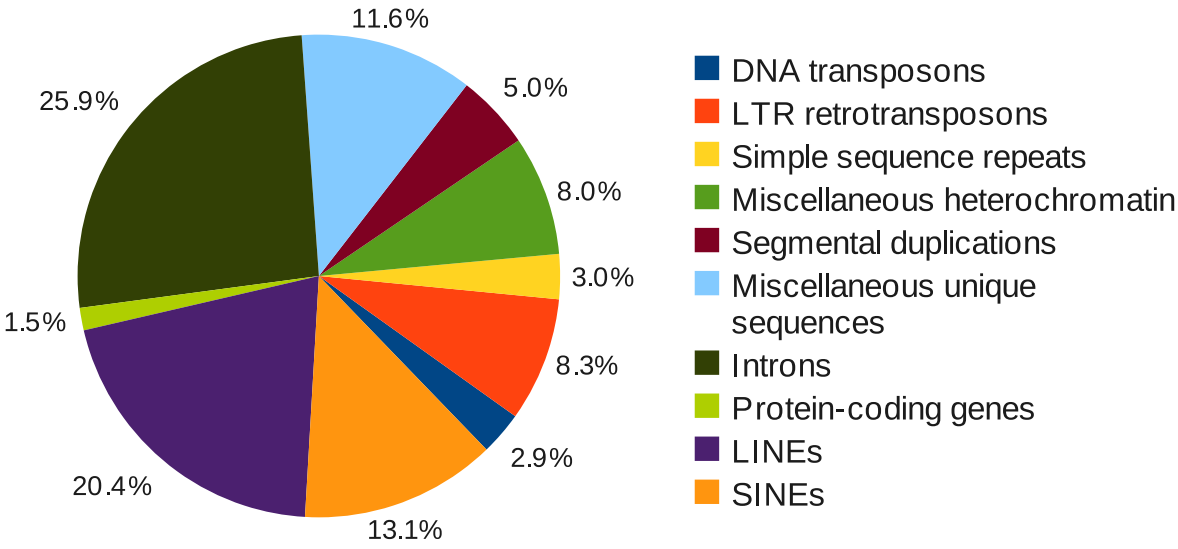

Figure 1.1: The composition of the human genome. Only 1.5% are protein-coding sequences, 25.9% are introns. 44.7% of human DNA are transposable elements (long interspersed nuclear elements (LINEs), short interspersed nuclear elements (SINES), long terminal repeat (LTR) transposons and DNA transposons). Figure reproduced from Gregory 2005 [30].

However, latest research of the ENCODE pilot project in 2007 [31] estimates that about 98% of the chromosome are transcribed. More precisely, roughly 1% of the human genome (chosen manually and by random in equal parts) was analyzed. We are far away from answering the rising questions of the particular functions of these transcripts, in fact it is even impossible to estimate whether all of these transcripts are functional or not, but the findings challenge the idea of the genome being mainly an evolutionary junkyard. Instead, it is more likely that self-splicing introns and transposable elements initiated a new level of molecular evolution by expanding the pool of regulatory molecules in eukaryotic cells [12].

Functions of RNA

The diversity of RNA sequences, sizes, structures and functions strongly suggests that we have seen only a small fraction of all functional RNAs [32]. A comprehensive review about known RNA functions would go far beyond the scope of this thesis, as RNA is involved in virtually all levels of gene and cell cycle regulation [32, 33, 34]. I will therefore provide a minimal outline of the most reviewed types of RNA, starting with classical RNAs that are involved in protein synthesis and going on with an overview of (recently) characterized ncRNAs.

The three major components of protein synthesis are ribosomal RNA (**rRNA**) that acts as an catalyst and a big coordination apparatus, messenger RNA (**mRNA**) that serves as coding-template and transfer RNA (**tRNA**) that decodes the mRNA via the delivery of certain amino acids for the emerging protein. Whereas rRNA and tRNA are merely transcribed and fold into their functional conformation spontaneously, mRNA is post-processed in eukaryotic cells, involving small nuclear RNA (**snRNA**) [35] to splice non-protein-coding parts (introns) out of the primary mRNA transcript. Some of these snRNAs are also reported to be involved in transcription initiation by RNA polymerase II [36] and probably in cell cycle regulation [37].

The family of small nucleolar RNAs (**snoRNAs**) [38] is known for the modification of other RNAs. Their length varies between 60 and 300 nucleotides, where the functional part is mainly concentrated to small regions (so-called boxes of about 18 nucleotides) that were shown to interact with rRNAs, snRNAs and mRNAs. Beyond that there are various orphan snoRNAs that cannot be associated with any target so far [34, 38]. This kind of RNA is mainly reported to be transcribed from introns; some of them are involved in tissue-specific, developmental regulation, others are involved in genomic imprinting [39, 40]. The human telomerase (hTR) enzyme needs an integral RNA subunit to provide a template for the

replication of chromosome ends. Interestingly, this RNA subunit contains the same box we know from snoRNAs, necessary for hTR accumulation and stability [38].

Micro RNAs (**miRNAs**) and short interfering RNAs (**siRNAs**) appear to be an important component of translational repression. Both are between 21 and 25 nucleotides long and influence gene expression by binding their targets via almost complementary base-pairing to suppress gene expression, or a perfect complement to trigger degradation with the RNA induced silencing complex (RISC) [41, 42], a process that is known as RNA interference (RNAi) [43]. The differentiation between miRNA and siRNA becomes indistinct as more and more research is done, but there are differences in their biogenesis. While miRNAs are derived from endogenous DNA (introns and exons of coding and non-coding transcripts), siRNAs are derived from less conserved endogenous and exogenous sources (transposons and dsRNA viruses). Nevertheless, both are finally processed by an endonuclease that cuts different kinds of precursor RNAs into small imperfect duplexes with a 2 nucleotide overhang on their 3' ends [44, 45]. So far they have been found to be associated with developmental timing, cell proliferation, left-right patterning, neuronal cell fate, apoptosis and fat metabolism in model organisms [44, 46, 47, 48], as well as neuronal gene expression [49], brain morphogenesis [50], muscle differentiation [51], stem cell division [52] and chromatin regulation [53].

Another upcoming field of interest are **long ncRNAs** with an estimated size from 200 to 10.000 nucleotides [54]. These RNAs are involved in chromatin modification [55, 56], transcriptional regulation [57, 58, 59] and post-transcriptional regulation [60, 56]. As their overall sequence conservation is very low, long ncRNAs are hard to find by comparative genomics.

In addition to these very well studied examples, the Piwi-interacting RNA (**piRNA**) is involved in the protection of the germline genome by silencing endogenous repetitive se-

quences and transposons [61]. The most recently described quelling defective/deficient RNA (**qiRNA**) may inhibit protein synthesis on DNA damage checkpoints [62, 63].

Taking into account that this brief introduction into RNA is far from complete and that new RNA representatives are reported continuously, it is not a big surprise that more and more diseases are shown to be interrelated with regulatory RNA. A few examples are RNAs that have been linked with neurobehavioral and developmental disorders and various forms of cancer [64, 65, 66, 67, 68, 69, 70].

1.2 RNA world hypothesis

A basic question that remains unclear when discussing the origins of life is the evolution of DNA, RNA and proteins. DNA is known as the genetic information storage, but does not have enzymatic activity itself. Protein synthesis requires RNA as the template and within the construction machinery. In a search for a common ancestor of life, we therefore end up with the idea that it is either RNA or an other unknown precursor molecule. Indeed, RNA can act as an auto-catalyst (ribozyme), as well as a catalyst for protein synthesis (ribosome), it can store information, replicate itself and synthesize DNA. Moreover, many co-substrates of protein enzymes contain ribonucleotides (ATP, NAD^+, FAD, Acetyl-CoA).

This lead to the idea of an RNA world [71] that induced evolution out of the primordial soup and paved the way to the first reproductive cell. However, the synthesis of the first nucleotides without protecting groups and activation steps from the primordial soup remained unreproducible for a long time and the survival of one spontaneously formed RNA molecule is still hard to comprehend. A new approach for the synthesis of pyrimidine ribonucleotides was recently published by Powner et al. [72]. The traditional strategy forms ribose and the nucleobase separately from elements in the primadorial soup, but fails to

connect these parts to form a ribonucleotide. Powner et al. [72] found an alternative way to form an activated pyrimidine ribonucleotide from plausible prebiotic feedstock molecules. It remains unclear whether it is possible to generate self regulatory RNA molecules as a next step to life from the primordial soup, but such promising research results suggest that today's life originated from spontaneously formed RNA molecules.

1.3 Synthetic biology

Traditional biological science tries to understand organic systems by the process of description, modification and re-description. While forward genetics identified changes in the genotype by their effect on the phenotype (for instance by mutagens), the newer field of reverse genetics modifies the genotype to see changes in the phenotype. Within the last years, a third level of biological science is coming up: synthetic biology. The goal of this emerging field is the departure from natural genomes that evolved for billions of years and are so highly complex in their function that they may never be completely understood. Instead, synthetic biology tries to (re-)assemble small minimal systems that fulfill predetermined functions. With this constructive approach we may be able to design new biological parts, devices and systems that do not exist in the natural world, as well as redesign existing systems to perform specific tasks.

In the last ten years, within the *first wave* of synthetic biology [73], multiple simple artificial components were developed, inspired by biological cells and electrical engineering. These genetic tools include logical switches [74, 75, 76, 77, 78], logical gates [79, 80, 81, 82, 83, 84, 85], synthetic biosensors [86, 87], cell-cell communicators [88, 89] and oscillatory networks [90, 91, 92, 93, 94, 95]. Combining these tools to somewhat more advanced units provides a basis for memory management [96, 97], response to certain input thresholds [88, 98, 99] and process-timing [100, 101]. There are also practical examples of modified cells for

image processing [102, 103, 104], cells that can break up biofilms [105], invade cancer cells [106], enhance antibiotic treatment [107] or produce an anti-malaria drug precursor molecule [108]. Moreover there are multiple strategies to build artificial molecular motors [109, 110, 111, 112, 113, 114, 115, 116], that may eventually provide a basis for a synthetic cytoskeleton.

The goal of the *second wave* of synthetic biology should be the standardization of input/output (I/O) devices that may be assembled to complex systems in a plug and play fashion [73, 117].

An ambitious challenge is to establish a small system that is somehow capable of withstanding or correcting mutations, can reproduce itself and therefore remains operational for a longer period of time. Characteristics that are generally seen to be necessary for a 'living' organism. Variations of such synthetic organisms can be utilized for eco-engineering, such as hazardous waste disposal [118], production of bio-fuels [119] and drugs [120], as well as to sense and fight cancer cells [106].

In order to construct a living system, one needs a chassis that separates the system from the environment but permits permeation between both sides (the cell wall) and an internal metabolism handling its reproduction. Such a functional metabolism that is geared to a biological cell needs multiple components that interact with each other but do not harm themselves by accidental interactions. Considering that the evaluation of each newly introduced tool in such a system needs the inspection of targeted interactions and unintentional cross-interactions on multiple levels (modified gene expression, affected RNA/protein function) the convergence to a new minimal organism is a combinatorial problem. There are two approaches for the construction of living systems. The *top-down approach* to create a minimal living cell tries to start from a small bacterial genome, such as *Buchnera aphidicola* with an estimated size of 450kb and 400 genes [121], shrinking its genome by gene deletion

as much as possible (to about 100-150 genes [122]). In contrast, the *bottom-up approach* wants to build a model organism from scratch that is completely regulated by sophisticated artificial components [123].

A basic necessity to establish a bottom-up system is the setup of artificial encapsulation and controlled cell-division. The most promising building block candidates for encapsulation are lipids, as they form dense, flexible bilayers and allow transformation in combination with trans membrane proteins[124]. Approaches to set up minimal metabolic networks within vesicles composed of different phospholipids can already be found in literature[124], but controlled cell-division failed, as it needs the internal production of lipids, amino acids and a functional cytoskeleton that defines the steric configuration within the cell, especially during cell division itself. An autonomous semi-synthetic cell, handling DNA replication, transcription, translation, cell growth and cell division should need approximately 100-150 genes [122, 125].

Coming from the RNA world hypothesis (see section 1.2, page 6), an even more minimal replication system is based entirely on fatty acid vesicles that enclose a self replicating RNA replicase [126]. The fatty acid vesicles are semipermeable for the uptake of nucleotides and RNA replication leads to swelling of the vesicle, due to osmotic pressure. This swelling results in the incorporation of new fatty acids, uncontrolled cell-division and a pH gradient that could provide energy for the uptake of small molecules [127].

1.4 Riboswitches

The importance of RNA as a low-cost regulatory molecule in the cell has been discussed in section 1.1. A particular form of both transcriptional and translational repression is carried out by riboswitches. These RNA molecules, originally reported to be located in 5'-

untranslated regions (5'-UTR) of bacterial mRNAs, are composed of an *aptamer domain* that is responsive to small metabolites and a downstream functional expression platform that can be in an ON or OFF state.

On translational level aptamer sequences of riboswitches fold into a stable conformation, that either represses the function of the expression platform or not, the switch is in OFF or ON state, respectively. A metabolite that attaches to the aptamer conformation rearranges the configuration and thereby induces a turn-over of the switch from one state to the other. Alternatively, theses aptamer regions can induce transcription termination, e.g. by the formation of a stable hairpin that causes stalling of the ribosome and therefore the release of an unfinished transcript [128].

The spectrum of known natural riboswitches is constantly expanded. Various aptamer domains can sense purine nucleobases, amino acids, vitamin cofactors, amino-sugars, metal ions and second messenger molecules [129]. Bacterial riboswitches regulating gene transcription and translation are found in the 5'-UTR; eukaryotic riboswitches are reported in introns or 3'-UTR of mRNA transcripts, involved in the regulation of splicing as well as transcription regulation [130].

Of special interest for this thesis is an engineered *RNA-triggered* riboswitch presented by Isaacs et al. [1] that is based on a cis-repressed RNA (crRNA) and a trans-activating RNA (taRNA). After transcription, the ribosome binding site (RBS) forms a stable hairpin structure with the aptamer domain, leading to a trapped (cis-repressed) OFF state. Transcription of a taRNA does induce a conformational change that resolves cis repression and induces gene translation; the switch is in an ON state (see figure 1.2). This minimal model of translational control provides a potent basis to design a library of crRNA-taRNA couples that regulate gene expression independently. In a synthetic cell, computationally optimized taRNAs could trigger gene expression of multiple crRNAs, as well as start cascades of gene

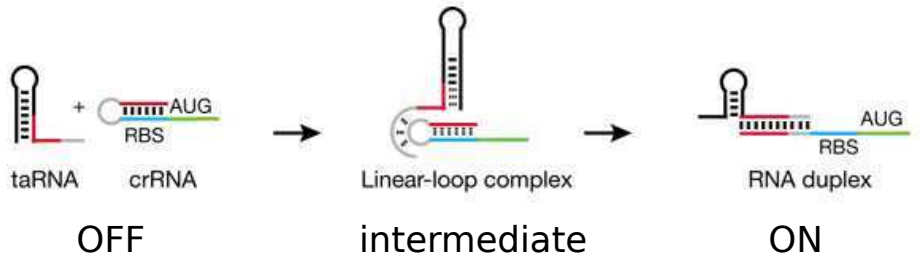

Figure 1.2: Synthetic RNA switch published by Isaacs et al. After transcription, the riboswitch is in a cis-repressed OFF state (crRNA), as the ribosome binding site (RBS) is not accessible and the therefore the transcription start side (AUG) is not functional. Upon activation with a trans-activation RNA (taRNA), the two structures interact via an Linear-loop complex conformation and finally refold to an RNA duplex structure that has an accessible RBS. Image reproduced from [1].

networks in response to molecular clocks [101].

Our goal is to model the refolding kinetics of this riboswitch, in order to establish a framework for the evaluation of new *in silico* designed riboswitches. The main challenge regards the intermediate state of the refolding path. This Linear-loop complex (schematically shown in figure 1.2) forms a structure motif that is comparatively rare and energetically hard to evaluate. Most RNA structure prediction algorithms therefore exclude such motifs, as they are predominantly interested in fast computation of frequent RNA structures. This intermediate state, however, enables a fast rearrangement of the two RNA molecules and needs to be considered for folding kinetics. In the following sections, we will therefore present the program `RNAscout.pl`, which heuristically estimates a set of intermediate structures (including the one shown in figure 1.2) that are expected to influence the refolding time. Based on this network we will simulate the change of population probabilities of individual structures and show that our results should be a good approximation of the natural behavior of the riboswitch.

Outlook

Within the following sections a detailed introduction of *in silico* RNA structure prediction (section 2) will be provided, starting with nature and representations of RNA structures. This will lead to a (historical) overview about general, *conventional* RNA folding algorithms (mainly focusing on the recursions of the `Vienna RNA package` [2]), and a short review about *pseudoknot* prediction and energetic evaluation of given pseudoknotted RNA structures. On this basis we will discuss the energy model of `RNAscout.pl`, a program to estimate folding kinetics of RNA-switches. Section 3 will explain current approaches to calculate folding kinetics, mainly dealing with conventional RNA secondary structures and the new heuristic approach of `RNAscout.pl` in RNA pseudoknot structure space. Finally section 4 discusses results of `RNAscout.pl` compared to other existing programs, and section 5 gives a short discussion and perspective towards the design of artificial RNA-triggered RNA switches.

2 RNA structure prediction

From a chemical point of view ribonucleic acid (RNA) molecules are composed of three different building blocks. Two of them, the phosphate group (PO_4^-) and the ribose (β-O-2-ribofuranose) form the backbone of RNA molecules. The 5' and 3' carbons of the ribose are bound to two oxygen atoms of the phosphate group, respectively; the 1' carbon of the ribose is connected to the third building block, the base.

There are four common types of RNA bases: Adenine (A), Guanine (G), Cytosine (C) and Uracil (U) that can interact via hydrogen-bonds to stabilize the structure (see figure 2.1). The dominating interaction motifs are the *canonical base-pairs*, which are the Watson-Crick base-pairs (AU, UA, GC, CG) [131] and the wobble pairs (GU, UG) [132]. The importance of these six base-pairs results from their isostericity, i. e. that the relative orientation of the phosphate-ribose backbone is not dramatically affected upon reversal of the particular base-pairs. Their dominance in RNA structure motifs makes these six base-pairs sufficient for reliable RNA secondary structure prediction. Although many other kinds of non-isosteric base-pair interactions are described in literature [133, 134], they have a comparatively low occurrence in nature and are neglected in most applications to speed-up (enable) structure prediction.

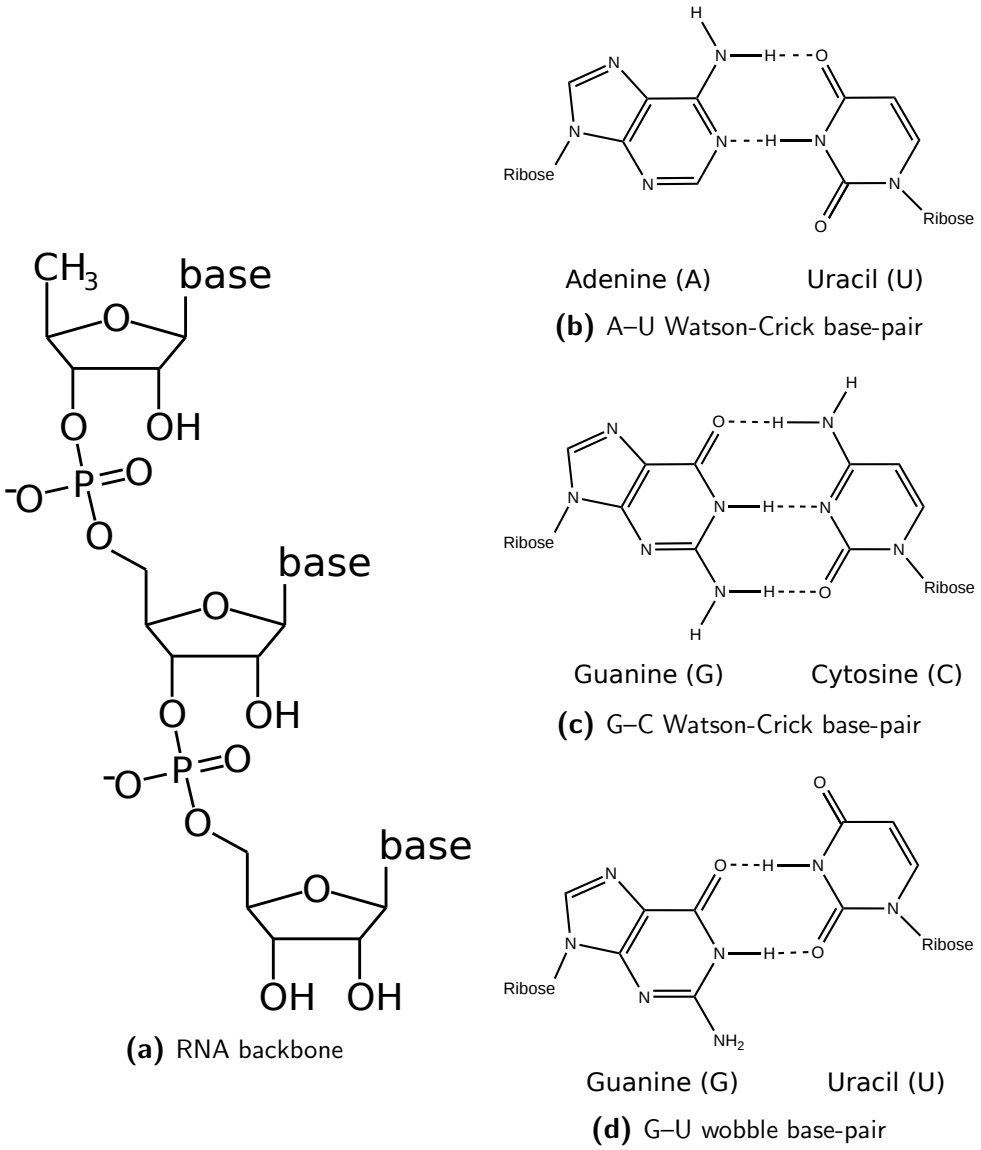

(a) RNA backbone

Adenine (A) Uracil (U)

(b) A–U Watson-Crick base-pair

Guanine (G) Cytosine (C)

(c) G–C Watson-Crick base-pair

Guanine (G) Uracil (U)

(d) G–U wobble base-pair

Figure 2.1: The building blocks of RNA molecules. **(a)** The RNA backbone is formed by phosphate groups (PO_4^-) and ribose (β-O-2-ribofuranose) molecules. Figures **(b, c, d)** show the Watson-Crick base-pairs (A–U, G–C) and the wobble pair (G–U), respectively. The individual bases form hydrogen bonds to interact; while A–U and G–U form two hydrogen bonds, the G–C base-pair forms three of them. RNAs with a high G–C content are therefore usually more stable than those with low G–C content.

2.1 Conventional RNA structure prediction

2.1.1 RNA secondary structures

Analogous to proteins, there are three different types of structured levels for RNA. A non-interacting 'open-chain' molecule can simply be described by the succession of bases. This *primary structure* (see figure 2.2a) particularly makes sense for previously mentioned mRNAs that serve as templates for translation. However, as the primary structure does not provide any information about the steric configuration, it is not descriptive in terms of non-coding RNA function.

A more advanced representation of an RNA molecule is the *secondary structure* which illustrates the base-pairing pattern but disregards the specific atomic positions in space (see figure 2.2b). The profit of this representation is that it is possible to determine whether single bases are paired or if they are accessible for molecular interactions (i. e. ribosome binding, siRNA binding, . . .). Moreover, secondary structure information serves as an indicator for molecular function (e.g. ribozyme interaction motifs, tRNA structure conservation). The RNA secondary structure representation is of importance for RNA folding algorithms, since the formation of secondary structure motifs occurs much faster than tertiary interactions. This characteristic is known as *hierarchical folding* in literature [135].

Finally, the *tertiary structure* depicts the actual configuration of the RNA molecule in space (see figure 2.2c). A number of programs that predict tertiary structures based on secondary structure prediction algorithms have recently been released (e. g. `FARFAR` [136], `iFoldRNA` [137] and `ModeRNA` [138]). Predictions become better, however, reliable tertiary structures can only be elucidated by experimental setups such as crystallography.

In terms of computational RNA biology, we define an RNA primary structure as a string

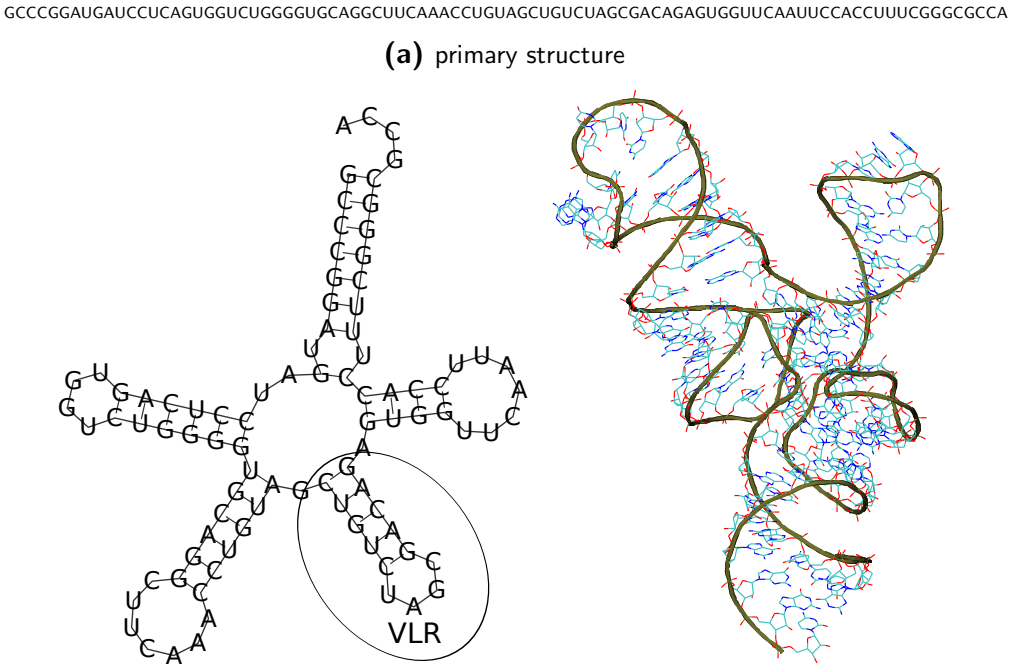

(a) primary structure

(b) secondary structure

(c) tertiary structure

Figure 2.2: Three different kinds of structure representation of the human selenocysteine tRNA [139] are shown. Usually tRNAs are composed of four stems and a variable loop region (VLR). In this case the VLR forms a fifth hairpin structure. **(a)** The primary structure as a string of nucleotides, **(b)** the secondary structure showing helices and loops in form of a squiggle plot and **(c)** the complete tertiary structure. See figure 2.3 for different kinds of secondary structure representations.

S consisting of a finite alphabet $\sum_{RNA} = \{A, C, G, U\}$, representing the four bases. The secondary structure is a set Ω of base-pairs (i, j) along the sequence of length n $[x_1, \ldots, x_n]$, which is defined by four rules.

1. If $(i, j), (i, k) \in \Omega$ then $j = k$
2. If $(i, j) \in \Omega$ then $j - i > 3$
3. If $(i, j), (k, l) \in \Omega$ and $i < k$ then $i < k < l < j$ or $i < j < k < l$
4. If $(i, j) \in \Omega$ then $(x_i, x_j) \in B\{AU, UA, GC, CG, GU, UG\}$

Rule 1 states that a base cannot form more than one base-pair. Rule 2 defines a minimum hairpin loop size of three bases. Rule 3 states that all base pairs are nested or independent of each other. Rule 4 defines the set of canonical (isosteric) base-pairs that are allowed for standard RNA structure prediction.

Each of these rules restricts the conformation space of *in silico* predictable RNA secondary structures to a biologically relevant and computationally tractable subset of possible conformations. However, increasing attention is paid to the fractional amount of non-nested structural elements, so called *pseudoknots* that violate rule number 3 and rare structural subsets that violate rules 1 and 4. Therefore, advanced RNA pseudoknot prediction algorithms focus on these problems, with the drawback that they tend to compute pseudoknots in known pseudoknot-free structure representations.

2.1.2 RNA structure representation

Graph representations

Conventional RNA secondary structures that are restricted by the rules from section 2.1.1, can be depicted as *planar* graphs, i. e. graphs that can be drawn without crossing edges.

Note that the reverse is not true, as some violations of the mentioned rules are still resulting in planar RNA secondary structures. The squiggle plot, arc plot and circular plot are three common layouts for certain kinds of planar RNA secondary structure representations.

Squiggle Plot The RNA backbone of an RNA molecule is drawn as a curved line and the formed base-pairs are straight (usually short) lines connecting the particular bases. This representation is very intuitive for small RNA structures, but becomes confusing rapidly with increasing sequence length. One advantage of the squiggle plot is the capability to represent all kinds of planar graphs. See figure 2.2b for an example of a squiggle plot.

Arc Plot / Book Embedding Arc plots consist of a straight line representing the RNA backbone from 5' to 3' end. Base-pairs are represented by arcs connecting the bases. A structure that follows the rules from section 2.1.1 can be shown on one side without arcs crossing each other (see figure 2.3a). To depict pseudoknot interactions this representation can be expanded to the *book embedding* representation. The RNA backbone is then seen as the *spine* and each set of non-crossing base-pairs as a *new page* of the book. Pseudoknot structures that can be shown with two pages of book embedding (see figure 2.6b) are also called bi-secondary structures [140].

Circle Plot The succession of bases is drawn on a circle, with the 5' and 3' end next to each other. Base-pairs are illustrated as straight lines that connect the particular bases within the circle. A conventional secondary structure does not have any lines crossing each other (see figure 2.3b), i. e. it is *outerplanar*. This representation is most restrictive, as a pseudoknot interaction results in a non-outerplanar circle plot.

Other representations

There are various other non-graph representations for RNA molecules. Three common layouts are the dot-bracket string, mountain plot and the dot plot.

Dot-bracket string This string notation is the standard input and output of the `Vienna RNA package` [2]. The alphabet of a secondary structure Ω is $\sum_{\Omega} = \{(,), .\}$, with dots representing unpaired bases and opening and closing brackets for a base-pairing upstream and downstream. A secondary structure following the rules on page 17 can always be represented by a well-formed bracket term. For structures including pseudoknots one needs to introduce new parenthesis or a second dot-bracket string. See figure 2.3c for the classical dot-bracket notation.

Mountain plot The RNA sequence is shown as a straight line. A base-pair towards the 3' end is indicated as a *uphill* line, whereas a base-pair towards the 5' end is shown by a *downhill* line. Unpaired bases result in a horizontal line (see figure 2.3d).

Dot plot A base-pair (i, j) is shown as a dot in a matrix. Indices of rows and columns correspond to the index of the sequence. The Vienna RNA dot plots show the minimum free energy base-pairs within the left lower triangle of a matrix, the base-pairing probability is shown in the upper right triangle, whereas the size of the dots proportional to the probability of the base-pair.

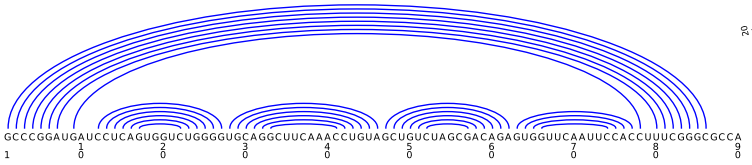

(a) Arc Plot

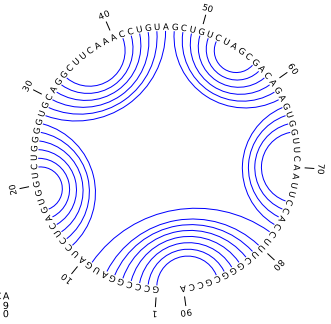

(b) Circle Plot

```
GCCCGGAUGAUCCUCAGUGGUCUGGGGUGCAGGCUUCAAACCUGUAGCUGUCUAGCGACAGAGUGGUUCAAUUCCACCUUUCGGGCGCCA
(((((((.(..(((((((....)))))))(((((.......)))))))(((((....)))))))(((.......)))))).)))))))....
```

(c) Dot-bracket string

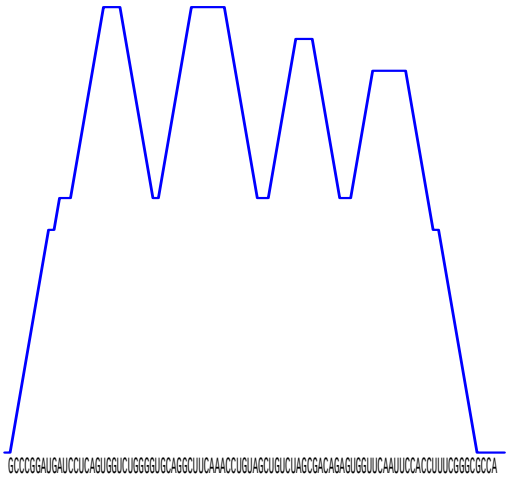

(d) Mountain plot

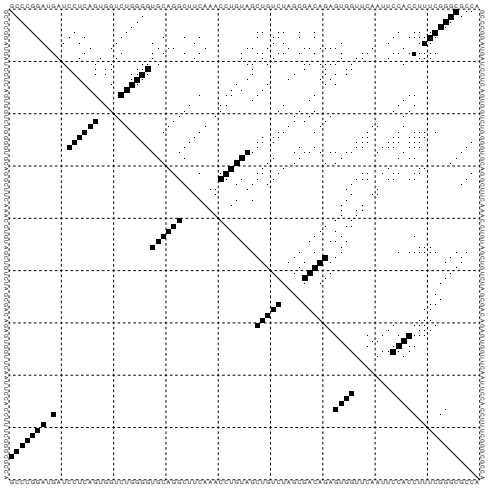

(e) Dot plot

Figure 2.3: Caption on page 21

Figure 2.3: Five different kinds of RNA secondary structure representation. **(a,b)** show RNA graph representations (images produced with JViz [141]). The Arc Plot (or Book Embedding representation) **(a)** shows the backbone on a straight line, base-pairs are arcs connecting the respective bases. The circle plot **(b)** shows the backbone drawn in a circle and base-pairs within the circle. Figures **(c,d,e)** are non-graph RNA representations. The Dot-bracket string **(c)** shows base-pairs as a well-formed bracket-term. The Mountain plot **(d)** depicts bases forming pairs towards the 5' end as uphill line, bases forming pairs towards the 3' end as downhill line. The Dot plot **(e)** shows base-pairs as dots in a matrix. Images **(d,e)** are produced with `Vienna RNA package` [2]

2.1.3 Minimum free energy structure prediction

Base-pair maximization – Nussinov algorithm

The first step towards today's folding algorithms was the Nussinov algorithm [142]. To predict the structure for a given sequence, base-pairs (x_i, x_j) score according to their stabilization potential ϵ_{x_i,x_j}. This non-thermodynamic model for structure evaluation is far too simple from today's point of view, but the dynamic programming approach to find the best-scoring structure is still a cornerstone of today's algorithms. Starting with small intervals $[i, j]$ up to the full sequence $[x_1..x_n]$, the maximum number of base-pairs within the intervals is calculated. This is done according to an decomposition into different sub-problems depending on whether base j is paired or not. This decomposition is known as a *forward recursion* to compute the best possible score for the whole sequence. The corresponding RNA secondary structure can be returned by a *backtracking routine* that reconstructs the base-pairing scheme.

Advanced energy models

Today's energy models do not focus on simple maximization of base-pairs, but utilize either experimentally determined energy parameters (in combination with models from polymer theory) or stochastic context-free grammars (SCFG) for probabilistic RNA modeling. An example for the latter is `CONTRAfold` [143]. Its RNA structure prediction method is based on *conditional log-linear models*, which generalize upon SCFGs by using discriminative training with typical thermodynamical models [143].

Experimentally determined energy parameters are for example provided by the SantaLucia [144] and Turner [145, 146] laboratories. Algorithms using these parameters uniquely decompose structures into different kinds of loops(see figure 2.4). The total free energy of an RNA secondary structure $E(\Omega)$ is then the sum of the free energies of its loops $E(L)$.

$$E(\Omega) = \sum_{L \in \Omega} E(L)$$

A loop can be described by its length, i. e. the number of unpaired bases, and the degree k, which is the number of closing base-pairs. Loops of degree $k = 1$ are called hairpin loops. They have exactly one base-pair (i, j) that closes the loop. Loops of degree $k = 2$ are either bulge loops (one unpaired strand), interior loops (two unpaired strands) or stacked pairs (no unpaired base between two base-pairs). Stacked pairs are the basic modules to build helices and stabilize structures. Finally, there are multi loops that have degree $k > 2$, and so-called exterior loops, i. e. stretches of unpaired nucleotides which are not enclosed by any base-pair. Figure 2.4 depicts all different kinds of loops.

The energy contribution of stacked pairs, small hairpins, certain interior loops and bulges are experimentally measured [148, 146] and included into secondary structure prediction programs using energy tables. Additionally, interaction penalties are provided for the formation of intermolecular base-pairs.

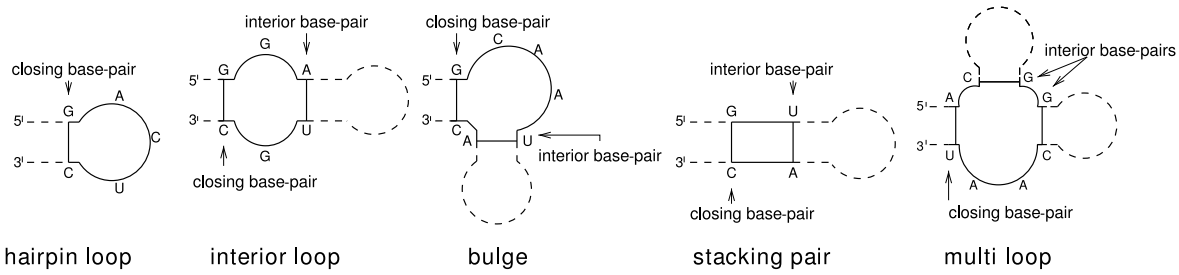

Figure 2.4: Different types of loops. Interior base-bairs and closing base-pairs separate the different loops towards the 3'/5' end of the structure and the internal part of the structure, respectively. The degree of a loop is dependent on the amount of interior and closing base-pairs. Hairpin loops have degree 1, interior loops, bulges and stacking pairs have degree 2, multi loops have a degree greater than 2. Image adapted from Flamm et al. [147]

The energy contribution of a loop is dependent on its length l (the number of unpaired bases) and the type of the closing base-pair (i, j). Large hairpin loops $H_{(i,j,l)}$ where $(l > x)$ are extrapolated logarithmically by $H_{(i,j,l)} = H_{(i,j,x)} + r * log(l/x)$, where r is a constant and x is set to 30 as default value in the `Vienna RNA package`. To keep the asymptotic time complexity of algorithms in $O(n^3)$ where n is the length of the sequence, the length of interior loops needs to be restricted. In case of the `Vienna RNA package`, the distance of the two closing base-pairs $(i, j); (p, q)$ is bound by a constant c such that $p - i + j - q \leq c$.

A multi loop energy M is composed of the cost for the formation of its closing-pair (a), the energy contribution of each branch (b) and the destabilizing energy of every unpaired base (c). This results in the following linear ansatz:

$$M = a + b * k + c * l \tag{2.1}$$

where k is the loop degree and l is the sum of unpaired bases (i. e. the loop size).

Zuker & Stiegler

Zuker & Stiegler were the first who came up with an algorithm to compute the MFE secondary structure by loop-decomposition [149]. In principle they use the same dynamic programming approach as in Ruth Nussinov's base-pair maximization, except that new terms for the type of a base-pair (i, j) are introduced. The energy contributions of a base-pair includes hairpin loop energies $H_{(i,j)}$, interior loop energies (including bulges and stacked pairs) $I_{(i,j;p,q)}$ and multi loop energies, which were originally considered as combinations of interior loops and hairpin loops.

`RNAfold` algorithm

The `RNAfold` algorithm[1] [2] is based on the principle of the recursions from Zuker & Stiegler, but came up with modifications regarding the multi loop decomposition. Figure 2.5 illustrates the recursions (we will now discuss in detail) to compute the MFE secondary structure $F_{i,j}$. The first recursion minimizes over the energy depending whether i is unpaired ($F_{i+1,j}$) or paired with a base k ($C_{i,k}$).

$$F_{i,j} = \min \begin{cases} F_{i+1,j} \\ \min_{i<k\leq j} C_{i,k} + F_{k+1,j} \end{cases} \tag{2.2}$$

The calculation of the closing pair $C_{i,j}$ is then decomposed into the hairpin case, interior loop case and the new multi loop case.

$$C_{i,j} = \min \begin{cases} H_{(i,j)} & \text{hairpin loop} \\ \min_{i<k<l<j}\{I_{(i,j;k,l)} + C_{k,l}\} & \text{interior loop} \\ \min_{i+1<u<j-1}\{M_{i+1,u} + M^1_{u+1,j-1} + a\} & \text{multi loop} \end{cases} \tag{2.3}$$

[1] `Vienna RNA package`

The multi loop decomposition differs from the former algorithm of Zuker & Stiegler, as it introduces a new term for the rightmost branch of the multi loop $M^1_{u+1,j-1}$, a term containing the rest of the multi loop $M_{i+1,u}$ and a, which is the penalty for a multi loop initiation (see equation 2.1).

To have unique terms for multi loop decomposition, $M^1_{i,j}$ can only contain the rightmost stem of a multi loop and possible unpaired bases between its rightmost base and the closing base-pair. This assures that every secondary structure is only calculated once during the forward recursion, enabling to calculate probabilities of certain conformations within the structure ensemble (see section 2.1.4). Both terms $M^1_{i,j}$ and $M_{i,j}$ can then be uniquely decomposed to:

$$M_{i,j} = \min \begin{cases} \min_{i<u<j}(u-i+1)c + C_{u+1,j} + b \\ \min_{i<u<j} M_{i,u} + C_{u+1,j} + b \\ M_{i,j-1} + c \end{cases} \tag{2.4}$$

$$M^1_{i,j} = \min \begin{cases} M^1_{i,j-1} + c \\ C_{i,j} + b \end{cases} \tag{2.5}$$

where b and c correspond to the destabilizing penalties from equation 2.1.

The computation of the forward recursions returns the MFE in $F_{1,n}$ where n is the length of the sequence; the corresponding secondary structure is then computed by the backward recursion. During this recursion, the generation of energy values in the matrices F, C, M, M^1 is traced back and the base-pairing scheme of the MFE RNA structure is returned. This algorithm requires $O(n^2)$ memory as the matrices F and C are stored for the backtracking routine and has a time complexity of $O(n^3)$ due to the size restriction of interior loops.

The algorithm of `RNAcofold` [2] is based on the same principle, but is able to fold two concatenated sequences. If there are intermolecular base-pairs, a penalty is added to the

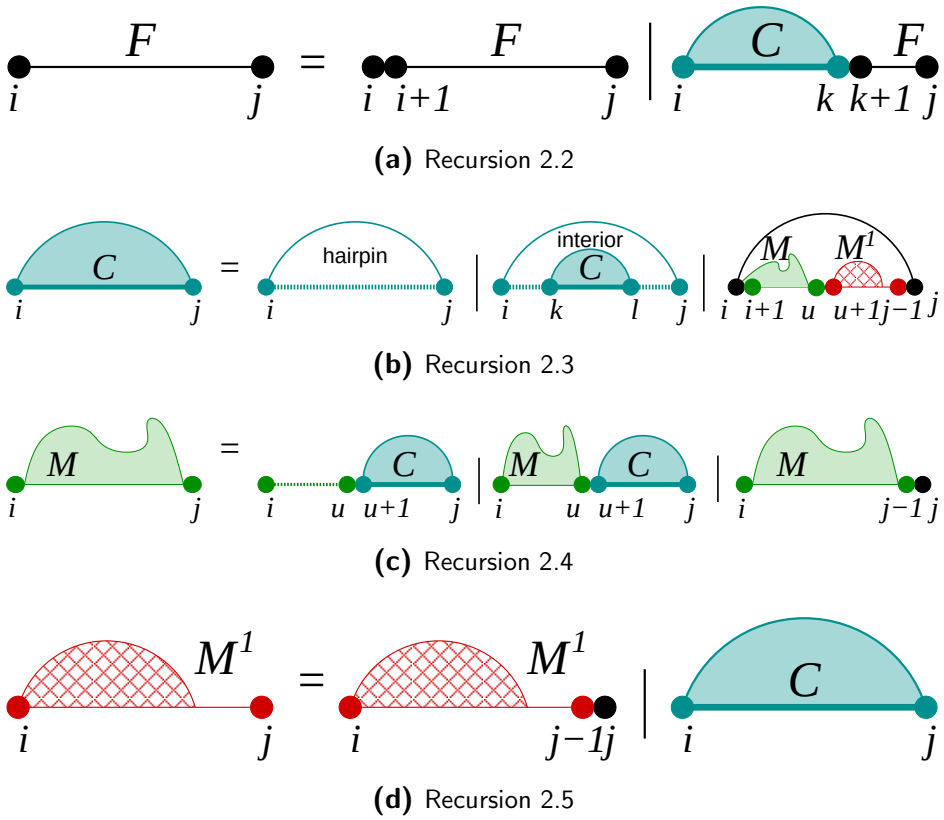

Figure 2.5: Recursions of the `Vienna RNA package`. Pictures **(a-d)** correspond to recursions 2.2-2.5 The minimum free energy of the structure interval (i, j) is stored in F. C stores energies for the case where a base-pair is formed, M and M^1 are energy tables for multi loop handling. Image adapted from Hofacker & Stadler 2008 [150]

overall MFE structure. This is important for our riboswitch example discussed in section 1.4, as we need to evaluate the energy of the RNA duplex structure (see figure 1.2).

2.1.4 Suboptimal RNA secondary structures

Of fundamental importance in RNA structure prediction is to keep in mind that there is a huge space of possible conformations. Hence, the predicted RNA structure for a given

sequence is the MFE structure according to the chosen energy model (at a certain temperature, in a certain environment). However, there is no certainty that a given RNA molecule does fold into the MFE structure, in fact it might be trapped in a local energy minimum until it is degraded. It is therefore advisable to regard all *suboptimal* conformations within a defined energy range to see whether there are structurally distant conformations that have comparable energies.

Zuker suboptimal folding

An early approach for the calculation of suboptimal structures was shown by Zuker [151]. The algorithm returns the energetically best structure for each possible base-pair which is computed from the energy terms $C_{ij} + \hat{C}_{ij}$. The term C_{ij} contains the best structure on the sub-sequence $(i..j)$ given that i and j are paired, i. e. the MFE structure *inside* the base-pair. $\hat{C}_{ij}$ contains the best possible structure from $(1..i)$ and $(j..n)$, i. e. the MFE structure *outside* the base-pair. For a sequence of length n, theoretically $\frac{n^2}{2}$ structures can be returned. In practice an RNA molecule can form far less than n^2 individual base-pairs, due to the limitations resulting from the rules discussed in section 2.1.1. An advantage of this set of suboptimal structures is that the amount of computed structures is comparatively low. A drawback, however, is that some important suboptimal structures cannot be found. Given the optimal sub-structures A and B and their suboptimal counterparts A' and B', a probably energetically very good structure $A'B'$ cannot be found.

Wuchty suboptimal folding

Wuchty et al. [152] implemented the `RNAsubopt`[2] algorithm, which is an approach to compute the *complete* suboptimal folding space. The algorithm utilizes the same forward

[2] `Vienna RNA package`

recursion discussed in the RNAfold section to track the minimum free energy of the given RNA sequence. In contrast, the backward recursion is extended to produce more than solely one (MFE) structure.

While the RNAfold algorithm searches for one best MFE structure Ω_F with a depth first search, RNAsubopt returns all structures Ω_i that have a free energy such that: $E(\Omega_i) \leq E(\Omega_F) + \delta$, where δ is the size of a user defined energy interval. RNAsubopt with $\delta = 0$ returns all MFE structures, in contrast to RNAfold which will return only one of them.

The structural ensemble returned is called a *complete* set of RNA structures, i.e. it contains the whole conformation space Q within the energy interval. Generating such a complete structure set, one has to accept that the amount of produced structures increases exponentially with the length of the sequence [153].

Stochastic sampling of suboptimal structures

An alternative to estimate an energetically wide structure space for long RNA sequences is to use the stochastic backtracking option implemented in RNAsubopt. In this case, the forward recursion additionally calculates the *equilibrium partition function* [154] and chooses the conformation space Q representing structures according to their equilibrium probability. The algorithm to compute the equilibrium partition function is similar to the discussed RNAfold forward recursions. Instead of picking the minimum, the sum over all possibilities is stored in the matrices. The former additions of loop energies are replaced by the multiplication of Boltzmann weighted energies. The Boltzmann weight $e^{\frac{-E(\Omega)}{RT}}$ is computed with the energy of the secondary structure $E(\Omega)$, the gas constant R and the absolute temperature T. The partition function Z sums over all Boltzmann weighted energy

contributions.

$$Z = \sum_{\Omega \in Q} e^{\frac{-E(\Omega)}{RT}} \tag{2.6}$$

Based on Z the probability of a certain structure Ω_i is equal to its Boltzmann weight divided by the partition function:

$$P(\Omega_i) = \frac{e^{\frac{-E(\Omega_i)}{RT}}}{Z} \tag{2.7}$$

The stochastic backtracking routine of `RNAsubopt` constitutes a secondary structure Ω with the probability $P(\Omega)$. Therefore, the suboptimal structure output derived by stochastic backtracking is not guaranteed to contain the MFE secondary structure, but it will contain a statistically representative set of structures.

2.2 RNA pseudoknot prediction

We have seen that efficient dynamic programming algorithms for RNA folding require four basic rules to define an RNA secondary structure (page 17). One of these rules ensures that every formed base-pair dissects an RNA structure into two parts that cannot interact any more. An RNA pseudoknot is known as a structural element that violates this rule such that base-pairs are crossing. Formally, a secondary structure contains a pseudoknot if there exist base-pairs $(i, j), (k, l) \in \Omega$ such that $i < k < j < l$.

2.2.1 RNA pseudoknot structures

Various kinds of crossing base-pairs result in pseudoknots of different complexity [140]. Some of them can be found in ribosomal RNA molecules [155], in the functional region of Ribonuclease P [156, 157] or are known to be involved in eukaryotic self-cleaving introns [158, 159]. In the viral kingdom, there are pseudoknotted self-cleaving RNA molecules

```
ACCCAAAUCCAGGAGGUGAUUGGUAGUGGUGGUUAAUGAAAAUUAACUUACUACUACCAUAUAUCUCUAGA&GAAUUCUACCAUUCACCUCUUGGAUUUGGGUAUUAAAGAGGAGAAAGGUACCAUG
((((((((((.(((((((..(((((((((((((((((((....)))))))).)))))))))))..)))))))...&......[[[[.[[[.[[[[[[)))))))))).....]]]]]].]]].]]]].....
```

(a) Dot-bracket including pseudoknots

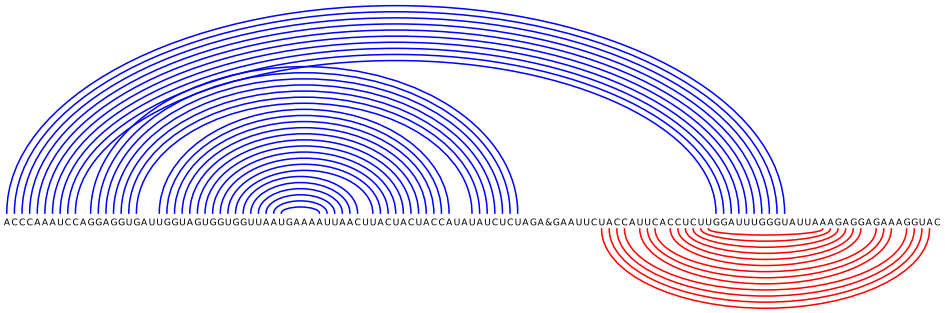

(b) 2-page book embedding

Figure 2.6: Two forms of bi-secondary structure representation. The ampersand (&) denotes the interaction of two RNA molecules. The dot-bracket notation **(a)** depicts crossing base-pairs with a second set of parenthesis, the book embedding representation **(b)** is extended with a *second page* to illustrate the pseudoknot. Both representations show the most populated transition state during a kinetic simulation of the refolding riboswitch published by Isaacs et al. [1]. The RNA molecule left of the ampersand is the trans-activation RNA, the RNA molecule on the right side is the cis-repressed riboswitch. Figure 2.6b was produced with JViz [141]

reported to be essential for replication, as well as for regulation of viral protein synthesis [158].

In this thesis we will deal with a subset of pseudoknotted structures, so called *bi-secondary* structures [140]. Every bi-secondary structure Ω is the union of two pseudoknot-free secondary structures $\Omega_c + \Omega_{pk}$. In terms of structure representation, the dot-bracket string notation illustrates a pair $(i, j) \in \Omega_c$ as '(' and ')' respectively, and a pair $(p, q) \in \Omega_{pk}$ as string '[' and ']'. Book embedding shows $(i, j) \in \Omega_c$ on the upper side, i. e. the first page of the book and $(p, q) \in \Omega_{pk}$ on the lower side, i. e. the second page of the book (see figure 2.6). A bi-secondary structure excludes all kinds of nested pseudoknot structures.

A very common bi-secondary structure is the *H-type* pseudoknot, where a hairpin loop forms base-pairs with a single-stranded region outside of the hairpin. Both helices then arrange such that they form one big helix structure together. These pseudoknots are found frequently in various kinds of RNA classes [158], e. g. the human telomerase contains an H-type pseudoknot that is essential for its catalytic function [160]. Another bi-secondary pseudoknot motif is the interaction of two hairpin loops. This *kissing-hairpin* interaction can result in a helix structure that is visually hardly distinguishable from a normal helix. A very prominent example for such an interaction is the HIV Tar-Tar* complex [161].

The pseudoknot structure motif of interest for simulations of RNA-triggered riboswitches is the linear-loop complex formation (schematically shown in figure 1.2). This initial interaction subsequently leads to a pseudoknotted transition state (see figure 2.6) which, as we will see in section 4.4, is temporary most populated during kinetic simulations. In the equilibrium distribution, the two sequences are ending up in a pseudoknot-free *RNA-duplex* formation (schematically shown in figure 1.2). Every intermediate conformation formed during this (expected) refolding path is included within the set of bi-secondary structures. The impact on refolding kinetics will be discussed in detail in section 3.2.

There exist various other defined sets of pseudoknot classes apart from bi-secondary structures. Following the book-embedding classification, the *book-thickness* (or page number) can be used as classification of more complex, nested pseudoknots [140]. Alternatively, Reeder & Gigerich define the set of predictable *simple recursive pseudoknots* [162] as those where the involved helices do not contain any bulges and have maximum possible length. A summary of pseudoknot classes traceable by different algorithms has been reviewed by Condon et al. [163] and Reidys et al. [164].

2.2.2 RNA pseudoknot folding

Pseudoknot folding algorithms include defined subsets of pseudoknots into RNA secondary structure, since exhaustive pseudoknot prediction based on loop energies has been shown to be NP-complete [165]. Some pseudoknot motifs are included in today's energy models [166, 167], but considering the amount of possible conformations, a more general energy model for pseudoknot structures would be highly desirable. A challenging aspect for the evaluation of pseudoknot interactions is the necessity to include steric and topological considerations. While the loop decomposition of standard RNA folding algorithms ensures that every predicted structure is sterically possible, there is no such guarantee for pseudoknot interactions. Instead, a predicted interaction of distant loops might be sterically impossible due to the stiffness of separating helix regions. Furthermore, an RNA helix-turn requires 11 base-pairs; in order to exceed this length, a strand forming a pseudoknot would need to wrap around the complementary strand. This is especially interesting when looking at topological constraints of RNA hybridization kinetics, as pseudoknot interactions might lead to a trapped, knotted intermediate structure [168, 169]. Taking such special cases into account, published energy models for pseudoknot folding must be substantially more complex than conventional loop-based energy models.

Heuristic approaches that do not guarantee to find the MFE secondary structure can include a wide range of pseudoknot types. `Kinefold` [170] uses stochastic folding simulations at the level of nucleation and dissociation of RNA helix regions, processes that have been shown to be the time-limiting steps of RNA folding kinetics. A related algorithm (based on the idea of iteratively forming stable stems) is implemented in `HotKnots` [171]. `DotKnot` [172] uses dot plots generated by the `Vienna RNA package` as starting point for pseudoknot construction. Alternative programs are based on genetic algorithms [173] or stochastic context free grammars [174].

Another promising approach from Cao & Chen deals with polymer physics, estimating loop entropy and handling base-pair stacking as corresponding enthalpic term [175, 176]. Limited experimentally measured loop entropy values restrict the set of predictable pseudoknots mainly to H-type pseudoknots and a few other structural elements.

Dynamic programming approaches using loop-based energy models have been implemented by Rivas & Eddy [177], Dirks & Pierce [178], Reeder & Gigerich [162], Beyer et al. [179] and Reidys et al. [164]. The corresponding set of pseudoknot structures varies between certain defined classes of H-type pseudoknots and certain examples of multiple nested pseudoknots.

2.2.3 Energy model of `RNAscout.pl`

To model the pseudoknot-like interaction of the RNA-triggered riboswitch published by Isaacs et al. [1], we will stick to a very fast and simple energy model that can handle all kinds of bi-secondary structures.

We have discussed that every bi-secondary structure Ω is the union of two pseudoknot-free secondary structures $\Omega_c + \Omega_{pk}$. However, the decomposition of a bi-secondary structure into two secondary structures is not unique, so the following rules are applied to each pseudoknot structure. Additionally to Ω, Ω_c and Ω_{pk} we introduce the temporary terms Ω_{left} and Ω_{right} to extract the pseudoknotted part of the structure, such that the leftmost base-pair and the corresponding non-crossing base-pairs are stored in Ω_{left} and the crossing base-pairs in Ω_{right}. Energy evaluation of Ω_{left} and Ω_{right} determines whether the base-pairs in Ω_{left} and Ω_{right} correspond to Ω_c and Ω_{pk} or Ω_{pk} and Ω_c respectively.

1. If $(i,j) \in \Omega$ and no $(k,l) \in \Omega$ such that $i < k < j < l$, then $(i,j) \in \Omega_c$
2. If $(i,j),(k,l) \in \Omega$ such that $i < k < j < l$, then $(i,j) \in \Omega_{left}, (k,l) \in \Omega_{right}$
3. If $E(\Omega_{right}) < E(\Omega_{left})$ then

- $\Omega_c = \Omega_c \cup \Omega_{right}$
- $\Omega_{pk} = \Omega_{left}$

else

- $\Omega_c = \Omega_c \cup \Omega_{left}$
- $\Omega_{pk} = \Omega_{right}$

This simple decomposition of pseudoknot structures identifies the number of pseudoknots, but not necessarily stores all energetically worse helices in Ω_{pk}. In case we have a helix crossing scheme A, A' and B', B, where A' and B' denote the energetically worse helices, A, B' and A', B are always evaluated together and contribute either to Ω_c or Ω_{pk}. This inexactness needs to be considered when evaluating refolding paths that contain more than one individual pseudoknot.

The structural parts Ω_c and Ω_{pk} are then energetically evaluated with the standard Vienna RNA folding algorithms and a pseudoknot initiation penalty β is added n times, where n corresponds to the amount of individual pseudoknots.

$$E(\Omega) = E(\Omega_c) + E(\Omega_{pk}) + n\beta \tag{2.8}$$

β can either be set as a loop-type independent (constant) value or adjusted depending on the type of loop interaction. Results in chapter 4 were produced using a initiation penalty β independent of the type of loop interaction. Related penalties for β are e. g. the *duplex initiation* energy of 4.1 kcal/mol [146], which is used for various RNA-RNA interaction penalties in the `Vienna RNA package`, the penalty of `DotKnot` [172] of 7 kcal/mol, the penalty of `RNApkplex` [179] of 8.1 kcal/mol or the even higher pseudoknot penalty of `pknotsRG` [162] with 9 kcal/mol. The pseudoknot interaction penalty of `RNApkplex` was shown to be most accurate in combination with the energy model of the `Vienna RNA package` [179], therefore it is used as the default β for our evaluation of pseudoknot

structures. Note, that if we are dealing with the modeling of the pseudoknot-like interaction between two different sequences, two penalties are added for the initial crossing base-pair. The pseudoknot penalty of 8.1 kcal/mol and the duplex initiation penalty of 4.1 kcal/mol for the initial interaction between two sequences.

3 Folding kinetics of RNA structures

RNA molecules are dynamic polymer chains that constantly rearrange within their environment, in order to minimize their free energy. In the following, we will focus on (re-)folding kinetics of RNA structures. In particular, the goal is to estimate the time a given RNA starting structure Ω_i needs to refold into an energetically better structure Ω_j. We will start this chapter with the definition of a *folding landscape*, which is the basis for subsequent calculations. The following sections will then discuss approaches to calculate folding kinetics within small exhaustively computable landscapes and large heuristically estimated landscapes.

A folding landscape is defined as a triple (Q, M, E).

- The conformation space Q
  $\Rightarrow$ defines the set of possible conformations
- The move-set M
  $\Rightarrow$ defines the set of possible transitions and thus dictates a neighborhood/metric within Q
- The energy (or fitness) function E
  $\Rightarrow$ A relation that assigns a real value to each conformation, defining the shape of the landscape

RNA Conformation Space (Q)

The conformation space Q of an RNA molecule can be divided into different sections of biological relevance. The minimum free energy structure Ω_F is considered as the most relevant part, followed by a set of suboptimal structures. The free energy of an open chain molecule, i. e. a completely unpaired secondary structure, is 0 kcal/mol by definition and dissects the part of relevant (suboptimal) structures from the part of irrelevant structures whose conformation energies are greater than that of the open chain molecule (at the given temperature). The amount of suboptimal structures grows exponentially with the length of an RNA molecule, such that exhaustively enumerating all suboptimal structures is feasible for small RNA sequences only. Whereas most RNA secondary structure prediction algorithms aim to compute the MFE secondary structure Ω_F, it is advisable to consider all RNA secondary structures within a certain energy range $E(\Omega_i) \leq E(\Omega_F) + \delta$ to see whether there are structurally distant conformations with comparable free energies (see section 2.1.4).

The type of conformation space (i. e. the set of structures that is included) can be of crucial impact when searching for refolding paths. In the following we will distinguish between two types of RNA conformation spaces:

- the conventional secondary structure space Q_{conv}
- the bi-secondary pseudoknot structure space Q_{pk}

Q_{conv} covers all RNA secondary structures that can be predicted by conventional RNA structure prediction; thus, it is bound by the rules on page 17. Q_{pk} covers Q_{conv} and all bi-secondary pseudoknot structures (see section 2.2). Considering that Q_{pk} is a superset of Q_{conv}, the amount of structures included within the same energy range is far higher in Q_{pk} than in Q_{conv}.

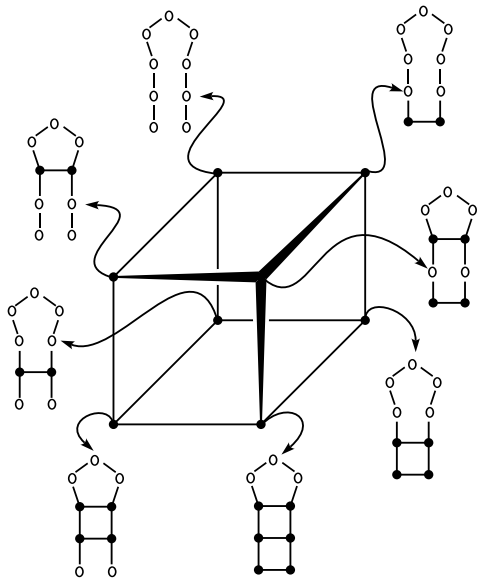

Figure 3.1: This elementary move-set for RNA structures includes only the insertion or deletion of a single valid base-pair.

The move-set (M)

The move-set M describes a notion of neighborhood and defines a metric within the conformation space Q. Hence, it must fulfill the following properties:

1. *Reversibility:* Every move has an inverse counterpart, there are no one-way moves that may lead to a trapped structure.
2. *Validity:* Every move results in a valid (neighboring) structure.
3. *Ergodicity:* Every structure Ω_i is reachable from every other structure Ω_j within Q.

The most elementary move-set one can think of for RNA structures is the insertion or deletion of a single valid base-pair (see figure 3.1).

The combination of conformation space and move-set allows to detect paths ($\Pi_{j \Leftarrow i}$) between two RNA structures Ω_i and Ω_j. A path $\Pi_{j \Leftarrow i}$ is obtained by iterative moves to

neighboring structures until a starting structure Ω_i is completely transformed into Ω_j.

The energy function E

The energy function E assigns energies to each conformation within Q. Typical energy models to score conventional RNA structures and RNA pseudoknot structures have been discussed in section 2.1 and section 2.2, respectively. The energy function determines the shape of an energy landscape, enabling to calculate whether a move (or transition) between neighboring structures is likely or not. The computation of transition probabilities will be discussed in detail in section 3.1.2.

Characterization of energy landscapes

Having discussed the general definition of folding landscapes, we are now interested in the characteristics of particular landscapes. Importantly, we would like to have parameters describing whether RNA structures can fold efficiently into their MFE secondary structure or might be trapped in local minimum conformations.

A theoretical parameter is the so-called *ruggedness* of an energy landscape. One way approach quantify the ruggedness is to compute the amount of local minima of an energy landscape [180]. Formally, for every local minimum structure Ω_i and all of its neighboring structures $\Omega_{i'}$ it holds that $E(\Omega_i) \leq E(\Omega_{i'})$. Coming from simulated annealing, another approach is to measure the *depth* of an energy landscape. The depth describes the maximum height of barrier energies separating the local minima. In the theory of simulated annealing, depth and the correlated *difficulty* of an energy landscape determine how fast the global optimum of an energy landscape can be found from arbitrary starting conformations [181]. A saddle point (or barrier structure) B_{ji} that separates two different local

minima Ω_i and Ω_j is the energetically worst structure on the energetically best path $\Pi_{j \Leftarrow i}$ within the set of all paths $P_{j \Leftarrow i}$ (see figure 3.2).

$$E(B_{ji}) = \min_{\Pi_{j \Leftarrow i} \in P_{j \Leftarrow i}} \max_{\Omega \in \Pi_{j \Leftarrow i}} E(\Omega) \tag{3.1}$$

The barrier height (H) on a path $\Pi_{j \Leftarrow i}$ can be calculated by the energy of the transition state $E(B_{ji})$ and the energy of the starting minimum $E(\Omega_i)$:

$$H_{ji} = E(B_{ji}) - E(\Omega_i) \tag{3.2}$$

Coming back to our goal to calculate (re-)folding kinetics between two RNA structures Ω_i and Ω_j, we need to compute a set of suboptimal structures, such that at least one path $\Pi_{j \Leftarrow i}$ connecting the structures can be found. The transition probability from Ω_i to Ω_j is then dependent on the energy barrier separating the two structures.

In our example of the structural rearrangement of the taRNA-crRNA couple published by Isaacs et al. (see figure 1.2), we need to find the energetically best path from the starting conformation Ω_S (two independently folded MFE conformations) to the MFE conformation Ω_F (MFE RNA duplex conformation), considering that pseudoknot transition states might shorten the best path possible within Q_{conv}. The following sections will discuss a proper way to calculate folding kinetics in a landscape based on a complete Q_{conv} and approximate approaches for calculations in a landscape based on a heuristic estimation of Q_{pk} ($\tilde{Q}_{pk}$).

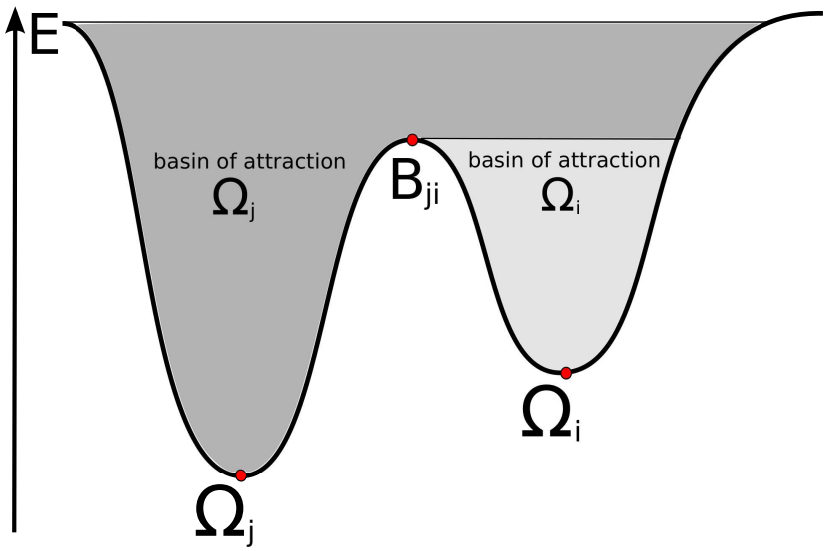

Figure 3.2: Two basins of attraction of an RNA energy landscape, their associated local minima Ω_i and Ω_j and the barrier structure (saddle point) B_{ji} separating them.

3.1 Complete conformation space

3.1.1 'barriers' – characterization of folding landscapes

Computation of a barrier tree

The program `barriers`[1] [182] computes all local minimum structures and separating barrier conformations within a certain energy range by use of a *flooding algorithm*. An energetically sorted list of Q_{conv} (produced by `RNAsubopt`) is processed starting with the MFE structure. The chosen move-set (i. e. base-pair moves) is applied to every conformation in the list generating all possible neighbors. The resulting neighborhood is utilized to classify the structures according to different cases:

[1] part of the `Vienna RNA package`

- Non of the neighboring structures has been observed before
  $\Rightarrow$ the structure is a new minimum Ω_i
- All neighbors observed belong to the same minimum Ω_i
  $\Rightarrow$ assign structure to minimum Ω_i
- Neighbors observed belong to different minima $\Omega_i, \Omega_j, \ldots$
  $\Rightarrow$ the structure is a barrier separating $\Omega_i, \Omega_j, \ldots$

A graphical illustration of this algorithm is shown in figure 3.3. If the energy range is sufficient to cover the maximum barrier, the set of local minima and barrier structures results in a so called *barrier tree*; if the energy range is not sufficient, a forest with detached barriers will be returned. The leaves of the barrier tree represent the local minima and inner nodes are saddle points separating them. The length of edges corresponds to the energy differences.

Partitioning (coarse-graining) of a folding landscape to gradient basins

As we will discuss in detail in section 3.1.2, exact computation of folding kinetics is unfeasible in exhaustively computed energy landscapes. One way to approximate folding kinetics is to partition the landscape into macro-states that summarize a certain defined set of conformations. This procedure is commonly known as *coarse-graining*.

Along with the computation of barrier trees a folding landscape can be partitioned into *gradient basins*. The important point is that all structures in Q are either separating barrier structures or are associated with exactly one local minimum. A gradient basin is the union of all structures that end up in a certain energetic minimum by a *gradient walk*. A gradient walk is defined as an iterative best energy improvement via the opening/closing of single base-pairs.

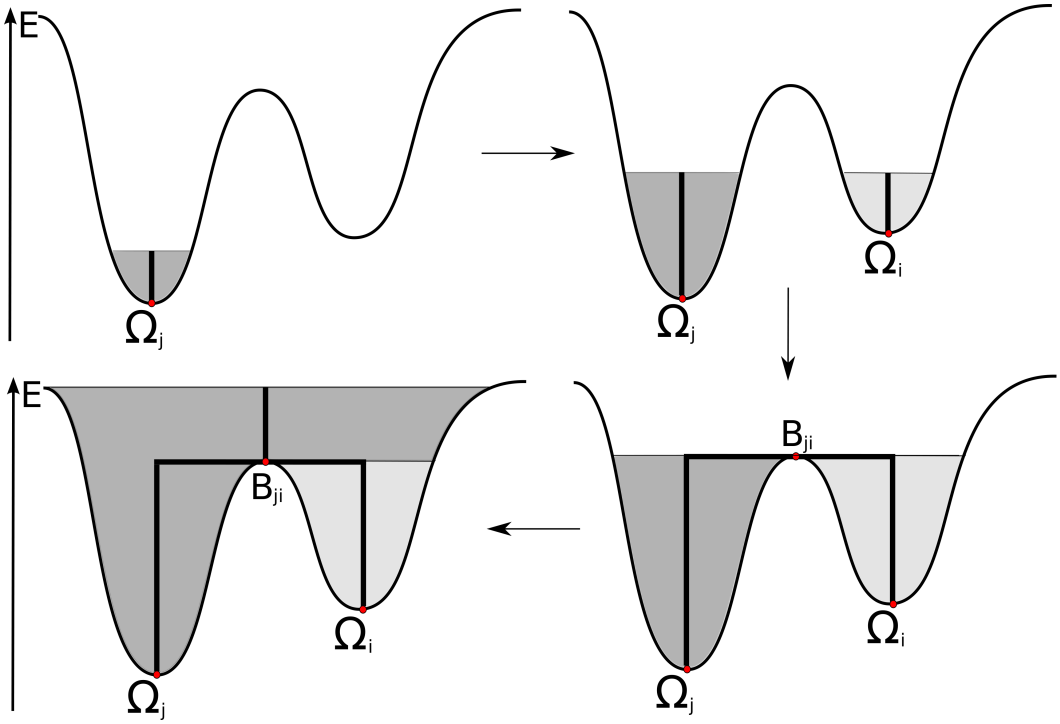

Figure 3.3: A graphical illustration of the *flooding algorithm* to generate barrier trees (implemented in the program package `barriers`). Starting from the MFE structure, an energetically sorted list of RNA conformations is processed to find local minimum structures Ω and barriers (saddle points) B.

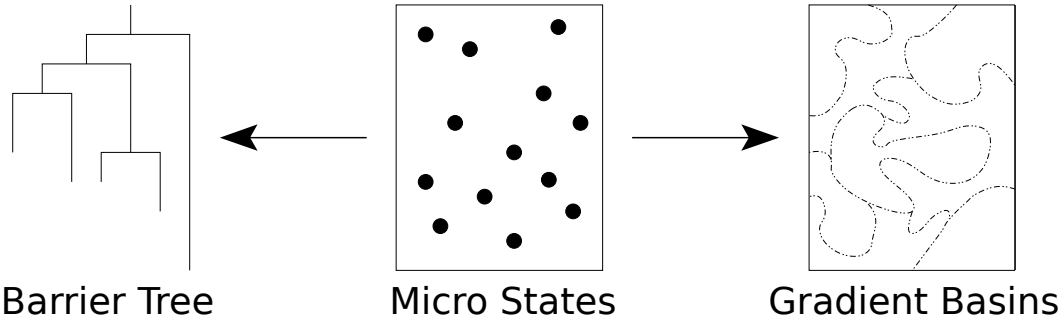

Figure 3.4: `barriers` partitions an energetically sorted list of micro-states into both a barrier-tree and gradient basins. Every micro state within the landscape has exactly one associated macro-state in both coarse-grained models. The observed barrier and minimum structures are equal in both abstractions of the folding landscape, the basins of attraction are different.

Gradient basins partition the folding landscape into macro-states that can be computed during the generation of barrier trees (see figure 3.4). Importantly, the observed barrier structures and local minima are the same for barrier trees and gradient basins. The difference, however, is that barrier trees do not consider the basins of attraction.

3.1.2 Folding kinetics using barrier trees & gradient basins

Folding kinetics as a Markov process

There are different approaches to calculate dynamics within a folding landscape. An alternative to calculations on barrier trees are Monte Carlo methods that consider every single configuration of the molecule of interest [183]. `barriers`, however, enables to model molecular dynamics as a Markov process [184]. Therefore, transition rates k_{ji} are introduced to determine the probability of a transition between neighboring structures Ω_i and Ω_j. Based on these transition rates, the following master equation can be set up to

determine the time-dependent probability of a structure Ω_i.

$$\frac{dP_t(\Omega_i)}{dt} = \sum_{j \neq i} [P_t(\Omega_j)k_{ij} - P_t(\Omega_i)k_{ji}] \tag{3.3}$$

The change in population density of a certain structure Ω_i is calculated from the sum over all incoming rates k_{ij} times the probability to be in Ω_j minus the sum of all outgoing rates k_{ji} times the probability to be in Ω_i. The overall probability to end up in a certain structure Ω_i as a function of time can be obtained by explicit solution of the master equation.

A way to numerically solve this equation is to set up a rate matrix R that contains all rates k_{ij} and the rates to remain in the current configuration, k_{ii}. Based on R, master equation 3.3 can be rewritten in matrix form, which can be integrated numerically [185]:

$$\frac{d}{dt}P_t = RP_t \tag{3.4}$$

The solution of equation 3.4 can then be calculated considering the initial and temporal distribution vectors P_t and P_0:

$$P_t = e^{tR}P_0 \tag{3.5}$$

where P_0 is the population density at the time point $t = 0$. In order to solve equation 3.5, R needs to be diagonalized. This is possible for a small rate matrix (with about 10000 states), but unfeasible for a rate matrix including all states of a conformation space. `barriers` therefore coarse-grains the folding landscape into gradient-basins (see section 3.1.1) and returns a rate matrix R connecting these macro-states. The described equations to process R are implemented in the `treekin` package[2] [182]. The corresponding thesis [186] provides a more detailed description of the mathematical background.

[2]Vienna RNA package

Modeling of transition rates

We have now found a way to numerically calculate folding kinetics on the basis of transition rates. In principle there are several ways to compute rates between neighboring structures. An important aspect that needs to be considered is *detailed balance*, i. e. ensuring that microscopic fluxes between neighboring structures are reversible. In other words, the probability of being in structure Ω_i (π_i) times the rate towards Ω_i from another state Ω_j (k_{ij}) needs to be the same as the probability of being in Ω_j (π_j) times the backward rate (k_{ji}):

$$\pi_i k_{ij} = \pi_j k_{ji} \tag{3.6}$$

On a grad scale, we need to ensure that the probability for a structure Ω_j (π_j) equals the sum of over all rates towards Ω_j (k_{ji}) times the probability to be in the respective neighboring structure Ω_i (π_i).

$$\pi_j = \sum_{i \neq j} k_{ji} \pi_i \tag{3.7}$$

`barriers` calculates rates between neighboring structures (i. e. transition rates) with the Arrhenius Law. A transition rate k_{ji} is then calculated as:

$$k_{ji} = k_0 e^{-\frac{E(\Omega_t) - E(\Omega_i)}{RT}} \tag{3.8}$$

where the transition state $E(\Omega_t)$ is the maximum of $E(\Omega_i)$ and $E(\Omega_j)$ and k_0 is a constant to adjust the time dependency of a transition. k_0 is set to 1 by default. Assuming that the transition state is always the energetically worse state of the two neighboring conformations, the Arrhenius law is the same as the Metropolis rule of simulated annealing, assuming that a transition rate k_{ji} from structure Ω_i to structure Ω_j is always 1 if $E(\Omega_i) \geq E(\Omega_j)$, and a small non-negative number calculated by the Boltzmann weighted distribution otherwise:

$$k_{ji} = \begin{cases} 1 & \text{if } E(\Omega_i) \geq E(\Omega_j) \\ e^{-\frac{E(\Omega_j) - E(\Omega_i)}{RT}} & \text{otherwise} \end{cases} \tag{3.9}$$

The rate matrix R to solve equation 3.5 contains the rates calculated by the Arrhenius Law k_{ij} and rates to remain in the current conformation k_{ii}. To ensure that the sum of probabilities for each transition from a certain state (including the transition to remain in the current conformation) is 1, the rates to remain in the current structure (the diagonal of R) is calculated by the negative sum of all outgoing rates.

$$R(k_{ij}) = \begin{cases} k_{ji} & \text{if } i \neq j \\ -\sum_{j \neq i} k_{ji} & \text{if } i = j \end{cases} \tag{3.10}$$

An exhaustive computation that considers rates between all possible conformations would result in a huge size of R even for small sequences, making the solution of the master equation unfeasible. As mentioned previously, it is necessary to coarse-grain the data set into macro-states, for example by partitioning the landscape into gradient basins. The open question is now, how to approximate rates between macro-states. If we assume that the time spent in such a macro-state is long enough to reach the internal equilibrium, we can compute rates between macro-states from the equilibrium probability of all structures within a basin. This equilibrium probability within a basin α can then be computed by the internal partition function $Z_\alpha = \sum_{\Omega_i \in \alpha} e^{-E(\Omega_i)/RT}$. The probability of a structure Ω_i in the basin α is derived by dividing its Boltzmann weight by the partition function:

$$P[\Omega_i|\alpha] = \frac{e^{\frac{-E(\Omega_i)}{RT}}}{Z_\alpha} \tag{3.11}$$

The rate connecting a basin α and β ($r_{\beta\alpha}$) is calculated from all individual rates r_{ji}, where structure $\Omega_i \in \alpha$ and $\Omega_j \in \beta$:

$$r_{\beta\alpha} = \sum_{j \in \beta} \sum_{i \in \alpha} r_{ji} P[\Omega_i|\alpha] \quad \text{for } \alpha \neq \beta \tag{3.12}$$

When using the equilibrium partition function Z to compute rates between macro-states, we approximate that it is of no impact which exact structure Ω_i is picked within the gradient

basin. An exact computation would consider $P[\Omega_i|\alpha, t, \Omega_{i_0}]$ with Ω_{i_0} being the particular state from which basin α was entered and t being the time dependency to reach state i. With the assumption that the time is long enough to reach the equilibrium probability independently from the starting state i_0, the probability can be approximated as $P[\Omega_i|\alpha]$. Note that $r_{\beta\alpha}$ can be computed during the generation of barrier trees, as we are dealing with a complete Q_{conv} where every structure belongs to a certain basin of attraction. In the following section (dealing with an heuristic $\tilde{Q}_{pk}$), we need other approximations to calculate transition rates.

3.2 Heuristically estimated conformation space

We have now discussed kinetics considering every possible conformation in the folding landscape. However, the problem of finding the best energy barrier (B_{ij}) separating two RNA secondary structures in a conformation space (Q) that excludes pseudoknots was shown to be NP-complete in 2010 [187]. In other words, exhaustive computation fails if the energy barrier is too high and therefore the relevant part of the RNA conformation space becomes computationally intractable. A number of algorithms that deal with *path finding* heuristics to estimate barrier heights have been implemented and will be discussed within this section.

If bi-secondary pseudoknot structures are included, the cardinality of Q increases to a superset Q_{pk}, making exhaustive computation unfeasible. However, sometimes there are refolding paths that have a high energetic barrier in Q_{conv} and a comparably low energy barrier in Q_{pk} (see figure 3.5). Section 3.2.2 will show an approach to estimate folding kinetics from any starting structure Ω_S into the MFE secondary structure Ω_F.

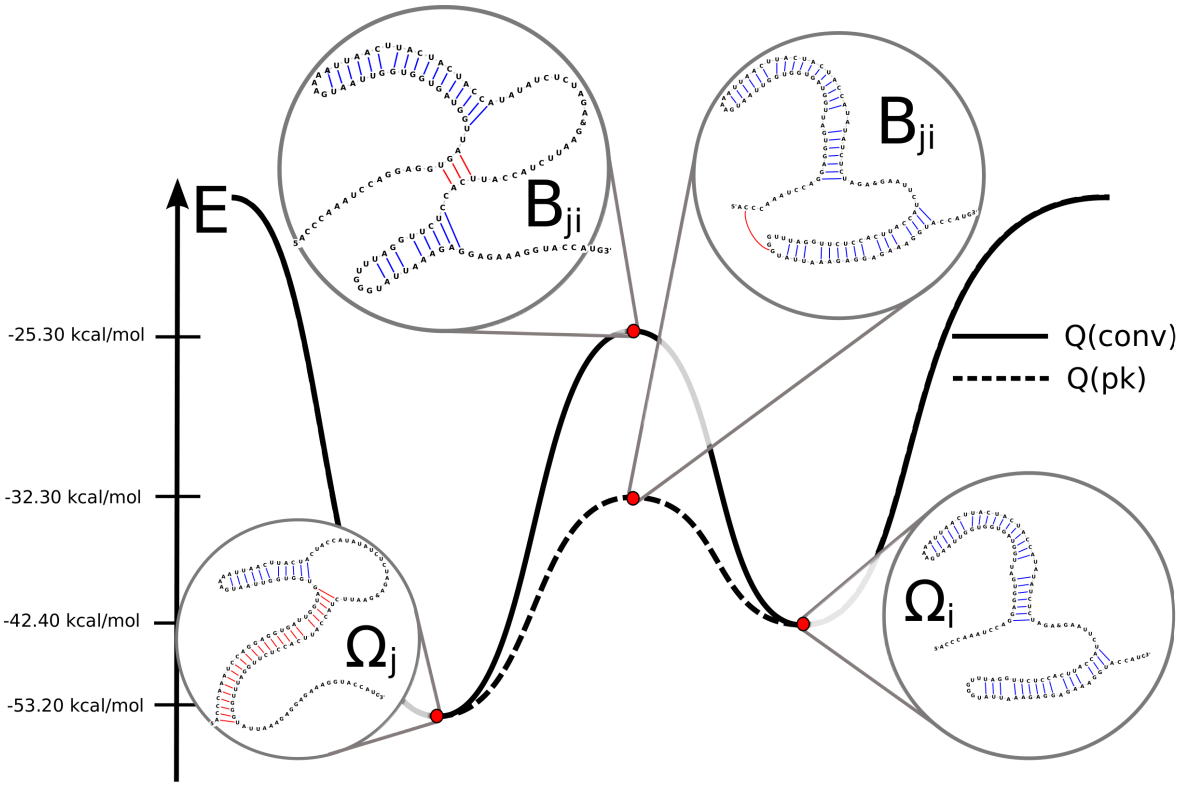

Figure 3.5: The RNA structure Ω_i is a local minimum in the energy landscape. To refold into conformation Ω_j, the time consuming step is to pass the energy barrier (B_{ji}). B_{ji} is the energetically worst structure on the best path Ω_{ji}. Within Q_{conv} the barrier height is far bigger than in the extended conformation space Q_{pk}. Barrier heights were derived from the `findpath` and `pk_findpath` heuristic respectively, the complete best paths $\Omega_{j \Leftarrow i}$ within Q_{conv} and Q_{pk} can be seen in appendix A.1 and A.2.

3.2.1 Heuristic path generation

We have discussed previously that a transition rate and the corresponding probability of a transition is proportional to the energy difference between two structures. In other words, the *height* of the energy barrier along the best path $\Pi_{j \Leftarrow i}$ determines the transition rate. The following heuristic algorithms have been implemented to determine the best path $\Pi_{j \Leftarrow i}$ in large folding landscapes. In detail, they have been implemented for a conventional conformation space Q_{conv} and the elementary base-pair move-set (see page 38). Heuristic approaches for path finding problems can be grouped into the general path heuristics and the subset of *direct path* heuristics [188]. A direct path that transforms structure Ω_1 into structure Ω_2 is generated by opening base pairs in Ω_1 that are not contained in Ω_2 and introducing base-pairs from Ω_2 that are not contained in Ω_1. The length of a direct path is therefore exactly the base-pair distance $D(\Omega_1, \Omega_2)$ and the set of structures that is evaluated for barrier estimation is excluding every structure with base-pairs $(i, j) \notin (\Omega_1 \cup \Omega_2)$. The evaluation of all direct paths is still too costly, but there are fast heuristics that estimate barrier heights on direct paths. The Morgan & Higgs heuristic [188] performs a greedy search with the following steps starting with Ω_1:

- search for base-pairs exclusively in Ω_2 that have the least number of incompatible pairs in Ω_1. Choose one randomly in case there are multiple base-pairs fulfilling this condition.
- Remove the appropriate incompatible pairs from Ω_1, add the new pair to Ω_1 and, if additional pairs can be formed, add these to Ω_1.
- Repeat this procedure with the new intermediate structure until it is transformed into the final structure Ω_2.

Another fast and simple heuristic to generate direct paths between two structures is the `findpath` routine [189]. `findpath` performs a breadth first search, generating all neighbors

of the starting structure that are one step closer to the final structure and keeps the energetically best m in memory. These candidates are then taken to produce the next best m structures. To set an upper bound for barrier energies, `findpath` pre-computes a greedy barrier energy with $m = 1$. During the subsequent breadth first search for direct paths, those exceeding the upper bound are discarded.

Barrier heights derived from direct paths, however, are often worse than their indirect counterparts. A statistical comparison of exact barrier heights and `findpath` barriers can be seen in section 4.1, page 62. The performance of the heuristic decreases with growing barrier heights. This observation is rather intuitive, as barrier heights are correlated with the base-pair distance and therefore stabilizing base-pairs are increasingly relevant.

Morgan & Higgs [188] have therefore also presented a method to heuristically estimate indirect paths. A set of low energy secondary structures is sampled and the starting and end structures Ω_1 and Ω_2 are added. The resulting set of structures is seen as the vertices of a graph. The corresponding edges are introduced by their greedy direct path heuristic discussed above. By use of a *single link cluster* algorithm the optimal path from Ω_1 to Ω_2 within the network can be determined.

Another heuristic for the generation of indirect paths has been published by Dotu et al. [190]. Their algorithm detects indirect paths with a semi-greedy *tabu search*, storing a list of the last k-visited conformations. Via iterative base-pair moves, structure Ω_1 is transformed to Ω_2. One of the energetically best neighbors (not stored in the list of visited conformations) is selected randomly and taken as the new transition state. The algorithm terminates if Ω_1 is completely transformed to Ω_2.

'pk_findpath' – direct paths in pseudoknot space

Even if both starting and end structures Ω_i and Ω_j are pseudoknot free, it is possible that the intermediate conformations on a path $\Pi_{j \Leftarrow i}$ contain pseudoknots (see figure 3.5). Especially, if there are conflicting helices that are able to form an energetically favorable pseudoknot if they are partially formed. The principle of the pk_findpath algorithm is a breadth first search with a fixed upper bound analogous to findpath [189]. In contrast to the previously described algorithm, pk_findpath operates on an enhanced folding landscape. The conformation space is extended to a set of structures that includes bi-secondary pseudoknot conformations (Q_{pk}) and base-pair moves are extended to allow every kind of crossing base-pair that results in a bi-secondary structure. The energy of conventional secondary structures is evaluated by the standard loop based energy model described in section 2.1.3; the energy of bi-secondary structures is computed by the extended energy-function from equation 2.8.

A comparison of the predicted findpath and pk_findpath barrier height for an RNA-triggered riboswitch can be seen in figure 3.5. The complete refolding paths are shown in appendix A.1 and appendix A.2. findpath predicts a pseudoknot-free refolding path with a barrier structure B_{ji} that has a free energy of -25.80 kcal/mol, whereas pk_findpath predicts a pseudoknot interaction resulting in a barrier structure with a free energy of -32.30 kcal/mol. The corresponding barrier heights regarding the energy of the starting conformation $E(\Omega_S) = -42.40$ kcal/mol are 16.6 kcal/mol and 10.1 kcal/mol, respectively.

A more general consequence of the altered landscape will be discussed in section 4.1. For small barriers, findpath and pk_findpath give the same results, as pseudoknot intermediate structures do not improve the barrier height. When comparing high barrier predictions, we do see differences in the direct path generation as pseudoknots increasingly lower the barrier energies.

3.2.2 'RNAscout.pl' – heuristic folding landscapes

As an improvement to the previously described direct path heuristics, we will now try to estimate indirect folding pathways with a small set of *related* neighboring conformations within the conformation space Q_{pk}. We will refer to this set of heuristically determined structures as $\tilde{Q}_{pk}$. The generated network of structures shall then be the basis to approximate folding dynamics of the full conformation space Q_{pk}.

In contrast to the ex ante generation of a complete Q_{conv} by the backtracking procedure of RNAsubopt, we will now discuss the generation of a partial $\tilde{Q}_{pk}$ starting from an arbitrary starting structure Ω_S and the MFE structure Ω_F. The algorithm of RNAscout.pl builds a recursive conformation graph, with vertices representing RNA secondary structures and edges corresponding to the moves that generated the connected vertices.

RNAscout.pl utilizes a larger move-set than the previously introduced base-pair moves. Structurally close conformations are lumped together into stacked, consecutive base-pairs that are opened and closed in one step. Approximations of landscapes with such large move-sets can cause problems in terms of ergodicity and reversibility (see section 3, page 38), as certain thresholds lead to non-reversible steps during the graph construction. Thus, transition rates between connected vertices are calculated in succession by use of the pk_findpath heuristic to ensure detailed balance within the generated heuristic landscape.

A conformation graph produced by RNAscout.pl allows two types of output evaluation. The first possibility is to extract the minimum barrier from the generated network. In this case, a path between any starting structures Ω_i and Ω_j can be evaluated for indirect barrier detection. A comparison of predicted pk_findpath barriers and RNAscout.pl barriers can be seen in section 4.1. However, the single best path between two structures is not sufficient to have a good approximation of the folding dynamics. Instead, we can calculate folding kinetics within the whole generated network. In this case it is advisable to stick to

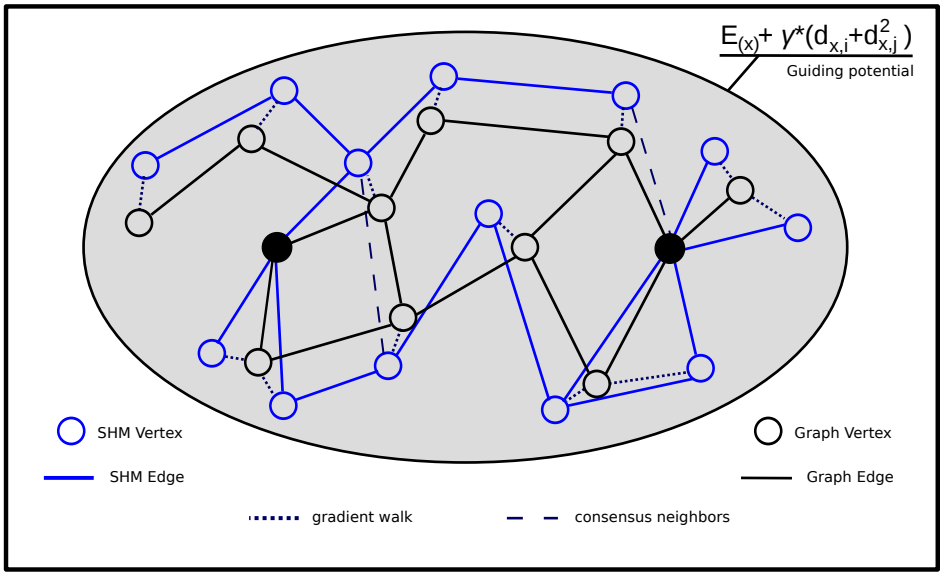

Figure 3.6: Algorithm of `RNAscout.pl`: Within guided space, a SHM network (blue) around the starting structures (black dots) is generated. The post-processing steps (gradient walk and consensus neighbor connection) generate the output graph (black) which is then utilized to estimate barrier heights or run kinetic simulations.

a path ending up in the MFE secondary structure Ω_F. Ω_F is always most populated in the thermodynamic equilibrium and usually strongly influences any refolding path $\Pi_{j \Leftarrow i}$. A simulation that does not include Ω_F will show a highly modified distribution of structures in the thermodynamic equilibrium.

The stacked helix move-set (SHM)

The stacked helix move-set (SHM), which is implemented in `RNAscout.pl`, operates on an abstraction of RNA secondary structures. In the standard representation of RNA conformations, every base is accessible for pairing and every single base-pair can be opened and closed in one step. An RNA secondary structure that can be processed with the SHM

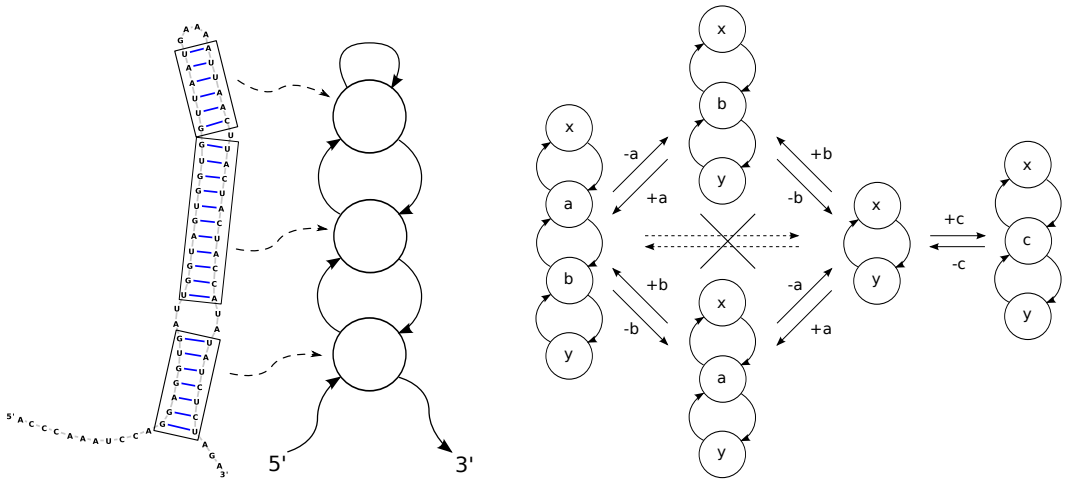

(a) stacked helix graph **(b)** stacked helix move-set

Figure 3.7: **(a)** RNA graph representation for the SHM model. **(b)** Principle of the stacked helix move-set. The opening of vertices is straight-forward as only one vertex can be removed at once. The folding of anti-parallel arcs is only allowed to introduce one new vertex to assure the symmetry of the SHM neighborhood.

is seen as a combination of consecutive stacked pairs forming a non-divisible unit (i. e. a stacked helix) and single strands that are available to form new stacked helices. Thus, whereas other definitions of a helix structure might include interior loops, bulges and hairpins, a stacked helix is delimited by any kinds of non-pairing bases. Isolated base-pairs are also seen as stacked helices that are processed by the SHM. This representation results in a 5' to 3' directed graph shown in figure 3.7a. Note that there are also arcs of size 0, e. g. if a bulge is separating two stacked helices.

Based on this graph representation, the SHM can iteratively split stacked helices to single strands or fold every combination of anti-parallel single strands (longer than n bases) to form *one* new vertex. Additionally single strands can fold alone, resulting in local hairpin formations. In principle this move-set is able to generate every type of pseudoknot structure; those that are not within the set of bi-secondary structures are discarded in the subsequent

energy evaluation.

While the opening of vertices is a straight-forward procedure where only a single vertex can be split at once, the folding of arcs needs to explicitly avoid the possibility to introduce more than one vertex at once to ensure the symmetry of the SHM neighborhood. Thus, if the optimal folding of arcs results in $n > 1$ vertices, n neighboring conformations are generated, each containing one different new vertex. An optimal solution containing all n vertices can only be found after n steps of neighbor generation.

The folding of single arcs for local hairpin formations is done using the `RNAsubopt` algorithm (see section 2.1.4), with an energy range δ that is calculated as the difference between the energy of the whole RNA structure Ω_i and the total energy range within guided space (see below). Folding of two anti-parallel arcs uses the `RNAduplex` algorithm. This algorithm is similar to `RNAcofold` (see section 2.1.3) but does not allow intramolecular loops. In case of a duplex interaction, we do not allow suboptimal interactions.

Building a recursive conformation graph

A heuristic $\tilde{Q}_{pk}$ is generated by a recursive call of the SHM, until no new structures are found. The initial set of conformations contains the starting structures Ω_i and Ω_j that shall be connected with at least one path $\Pi_{j \Leftarrow i}$. The selection of RNA secondary structures that are further processed in a new round of the SHM is parameter-dependent on both their energetic relevance and structural affinity to the starting structures (discussed in detail below).

After termination of the recursive SHM call, two post-processing steps are applied to enhance the performance of the generated network. Note, that so far there is no certainty that a path $\Pi_{j \Leftarrow i}$ was generated, instead it is likely that two different sets of conformations evolved from both Ω_i and Ω_j, with a structurally close, but not connected set of RNA

secondary structures.

RNA molecules tend to minimize their free energy and fold into local minimum structures. A refolding path is therefore more reasonable if it connects different local minimum conformations instead of move-set dependent intermediate states. The first post-processing step assigns every RNA secondary structure to the next best local minimum conformation. This method was previously introduced as a *gradient walk* that iteratively opens or closes single base-pairs to improve the energy until a local minimum is found. During this step, different vertices can be merged to one local minimum that combines the edges of its predecessors.

In a second post-processing step structurally related conformations that are not neighbors within the conformation graph, are identified and connected with additional edges. There are various ways to define structurally related, neighboring conformations. One of them depends on the base-pair distance. In other words: Ω_i and Ω_j are related if $D(\Omega_i, \Omega_j) < n$ where n is a user defined parameter. `RNAscout.pl` uses a parameter-independent definition of related conformations. Ω_i and Ω_j are related if all base-pairs in Ω_i are also formed by Ω_j. In other words, the base-pairs formed by Ω_i are a subset of those formed by Ω_j. New edges for neighboring conformations are thus connecting structures where one conformation is comprised in the other one. Two structures that have a base-pair distance of 2, such that one base-pair $(p, q) \in \Omega_i$ and $(p, q) \notin \Omega_j$ whereas the other base-pair $(k, l) \in \Omega_j$ and $(k, l) \notin \Omega_i$ are not seen as neighbors by this model. On the other hand, if the open chain is generated during the SHM, it is connected to every other structure within the network during this post processing step.

Guiding potential as a soft boundary

Exhaustive computation of a conformation space considers all RNA secondary structures Ω_i with $E(\Omega_i) \leq E(\Omega_F) + \delta$ (see section 2.1.4). In order to restrict the cardinality of $\tilde{Q}_{pk}$,

while keeping a structural related network around the best path $\Pi_{j \Leftarrow i}$, a second parameter is introduced that favors conformations related to the initial structures. `RNAscout.pl` restricts the relevant conformation space with a soft boundary, the *guiding potential* (Γ), that is added to the energy of each RNA secondary structure Ω_x, resulting in a relevance score P:

$$P(\Omega_x) = E(\Omega_x) + \Gamma(\Omega_x) \tag{3.13}$$

Γ is composed of the base-pair distance $d_{x,i} = D(\Omega_x, \Omega_i)$ and $d_{x,j} = D(\Omega_x, \Omega_j)$ and a user defined guiding stringency γ.

$$\Gamma(\Omega_x) = \gamma(d_{x,i} + d_{x,j})^2 \tag{3.14}$$

The selection of RNA secondary structures that will be part of the recursive conformation graph is based on an ex ante computation of the direct path barrier found by `pk_findpath` (B_{ij}^{pkf}). For any structure Ω_x that is part of a direct path between Ω_i and Ω_j holds that $d_{x,i} + d_{x,j} = d_{i,j}$, such that we can write the soft boundary for the conformation graph as:

$$P(\Omega_x) = E(\Omega_x) + \gamma(d_{x,i} + d_{x,j})^2 \leq E(B_{i,j}^{pkf}) + \gamma(d_{i,j})^2 + \delta \tag{3.15}$$

The combination of energy range and guiding potential creates an RNA structure space around the best $\Pi_{j \Leftarrow i}$, with the two user defined parameters:

1. δ to adjust the size of the conformation graph
2. γ to adjust the shape of the conformation graph

δ needs to be sufficiently high to include the barrier structure within the set of vertices. γ allows to shrink the conformation graph if a high δ is necessary. However, a high γ excludes structures that differ strongly from the direct path between starting and end structure. Considering that the stacked helix move-set needs an energy range sufficient to open whole helices, it might not be possible to find the direct path between starting and

end structure. In contrast, a low γ results in a huge amount of generated structures before a potential barrier is found.

Figure 3.6 shows a summary of the `RNAscout.pl` algorithm:

1. the guiding potential is calculated from the starting structures
2. the recursive SHM network is generated within guided space
3. SHM vertices are assigned to local minima via gradient walks
4. comprised local minima are connected with new edges

3.2.3 Folding kinetics in a heuristic conformation space

Now that we have a heuristic image of the bi-secondary structure space in form of connected (edges) local minima (vertices), the goal is to calculate folding kinetics from Ω_S to Ω_F.

Folding kinetics as a Markov process

As we have discussed in section 3.1.2, there are several approaches to estimate molecular dynamics between RNA secondary structures. Analogous to section 3.1.2 we will handle the molecular dynamics between RNA secondary structures as a Markov process. The underlying master-equation to determine the time-dependent probability of a structure Ω_i was shown in equation 3.3, which can be solved numerically by use of a rate matrix R (see equation 3.5).

Calculation of transition rates

In the heuristic conformation space, we estimate barriers between connected local minima with the `pk_findpath` algorithm. This approximation should be sufficient, as connected local minima were generated from single stacked helix neighbors or are comprised in each other. The transition rate k_{ji} between two local minima Ω_i and Ω_j is computed by the Arrhenius law considering the energetic difference between the `pk_findpath` barrier B_{ij}^{pkf} and the starting minimum $E(\Omega_i)$:

$$r_{ji} = r_0 e^{-\frac{E(B_{ji}^{pkf}) - E(\Omega_i)}{RT}} \tag{3.16}$$

In contrast to `barriers`, that coarse-grains all conformations within an energy range into gradient basins, `RNAscout.pl` considers solely local minimum conformations. A computed rate matrix R does therefore contain the rates r_{ji} instead of $r_{\beta\alpha}$.

Comparison of simulations, influence of the soft boundary

A comparison between kinetic simulations of macro-states produced by `barriers` and the conformation graph generated from `RNAscout.pl` will be shown in section 4.3. Additionally to the performance comparison against `barriers` we will discuss the influence of the user defined network parameters δ and γ on kinetic simulations.

As we are primarily interested in the population density of starting structure Ω_S and the MFE structure Ω_F, we focus on the distance of the trajectories from Ω_S and Ω_F computed by different simulations. The absolute distance D of trajectories in different simulations can be computed in the following way:

$$D = \sum_t (\Omega_S^I(t) - \Omega_S^{II}(t)^2 + (\Omega_F^I(t) - \Omega_F^{II}(t))^2 \tag{3.17}$$

where $\Omega_S^I(t)$ denotes the population density of starting structure Ω_S in simulation I at a time point t.

4 Computational results

The following computational results are divided into four subsections. The first two are dealing with the general distribution of barrier heights and the performance of `Vienna RNA package` heuristics on barrier height estimation. The underlying data set of RNA sequences is taken from the RNAstrand database [191]. In total, 1198 sequences with a length between 30 and 200 nucleotides have been evaluated.

The last two subsections show the performance of kinetic simulations within heuristically estimated folding landscapes. Section 4.3 compares various simulations on small folding landscapes with `barriers`, whereas section 4.4 finally summarizes the results for the large folding landscape analysis of a synthetic riboswitch.

4.1 Barrier heights of RNA sequences

We previously discussed that the maximum barrier height in a folding landscape is a crucial parameter for its *difficulty*. In the theory of simulated annealing, this parameter is the decisive factor whether the global optimum of a folding landscape can be reached for sure [181]. In a similar manner, very high barrier heights of RNA folding landscapes may prevent the RNA molecule from folding into the MFE secondary structure. Instead, the molecule might be trapped in a probably nonfunctional local minimum conformation. We therefore

expect that functional RNA sequences tend to optimize their folding paths by avoiding high energy barriers, such that the suboptimal conformations can refold into the MFE secondary structure quickly and the MFE secondary structure is highly populated in the cell.

In contrast to ordinary RNA molecules, bistable RNA-switches are expected to have a high maximum barrier, separating two functional local/global minimum conformations. Usually, switching between these conformations is triggered by an independent catalyst that lowers the barrier energy.

As mentioned previously, the barrier height (H_{ji}) on a path $\Pi_{j \Leftarrow i}$ can be calculated as the difference of the energy of the transition state $E(B_{ji})$ and the energy of the minimum $E(\Omega_i)$ where we start (see equation 3.2).

1198 natural sequences (differing in at least one base) were processed to compute energy barriers of the corresponding folding landscapes. To this end, up to 5×10^6 suboptimal structures with an energy $E(\Omega) \leq 3$ kcal/mol were computed by `RNAsubopt`. As the physical stability of RNA molecules depends on stacking energies, starting with an open chain RNA molecule, the first base-pair closed does always result in a positive free energy. The positive energy cut-off is chosen to avoid that the open chain RNA secondary structure (0 kcal/mol) forms a detached local minimum when computing the energy landscape. A sorted list of the suboptimal RNA secondary structures was processed with the program package `barriers` to partition the landscape into gradient basins and corresponding barrier trees (see section 3.1.1). As default, `barriers` partitions the landscape into macro-states that have a minimum basin height of 1 kcal/mol, i. e. observed barriers that are lower than this threshold are merged into one gradient basin (and the corresponding leaf of the barrier tree). To decrease the amount of small barriers, the tree size was limited to 100 local minima. Furthermore, trees for every sequence were recomputed with a minimum barrier height of 3 and 5 kcal/mol and duplicate entries within the three barrier trees per sequence

were discarded.

Due to the limited amount of suboptimal structures, `barriers` occasionally returned a forest instead of a single barrier tree. In this case, some local minima that were obtained, were not connected to neighboring basins (i. e. detached) as the barrier height exceeded the computed part of the folding landscape. In total, `barriers` returned 210228 local minima, 200719 of them in combination with a barrier height to the next local minimum, 9509 without an associated barrier height. The total maximum barrier height derived from these barrier trees was 15.6 kcal/mol, the maximum detached barrier height was 14.20 kcal/mol.

In order to search for the maximum barrier height within the folding landscapes, all forests returned by `barriers` were post processed with the `findpath` heuristic, searching for direct paths in the conventional conformation space. The cut-off for the `findpath` breadth first search was set to 50. After this step, all forests were returned as reconnected barrier trees where the maximum barrier could be determined. Beware that – especially for very high barriers – direct path heuristics might not be sufficient to find the minimum barrier height.

For statistical comparison, we generated a second data set of *random* structures. As physical stability of RNA secondary structures is known to depend on stacking energies, the RNAstrand sequences were randomly shuffled preserving the dinucleotide composition. Based on these shuffled sequences with same length and dinucleotide composition we will assess the question whether natural RNA molecules are optimized to have low maximum barriers.

Figure 4.1a shows the distribution of the maximum barrier height per sequence. Note that there is no length or MFE dependency included within this comparison. For this reason, figure 4.1b shows a histogram depicting the difference of barrier heights between every single RNAstrand sequence and its randomly shuffled counterpart. Higher barriers for shuffled sequences result in a positive value, lower barriers in a negative value.

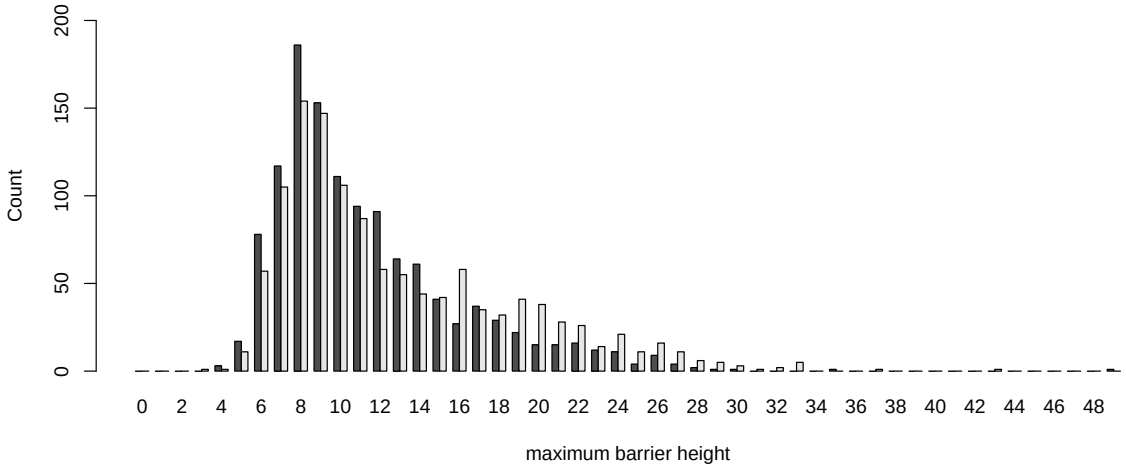

(a) 30-200 nucleotides

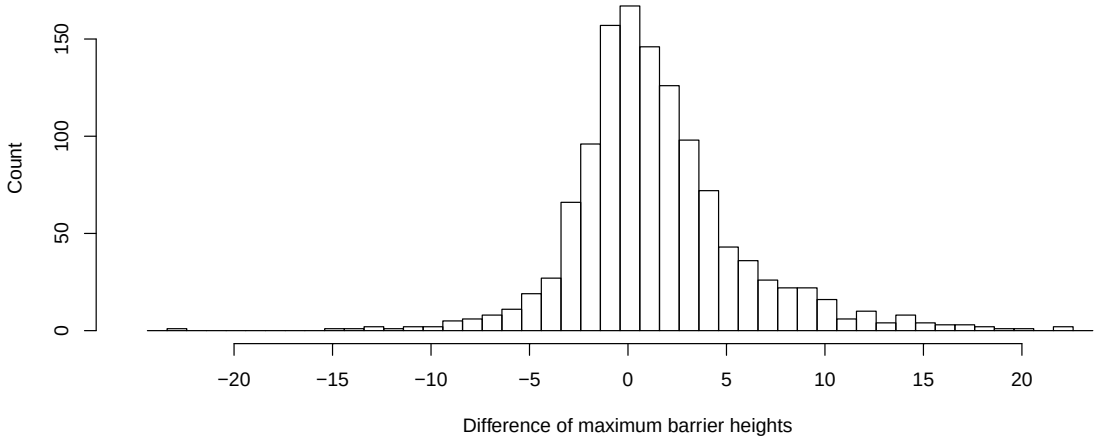

(b) 30-200 nucleotides

Figure 4.1: Distribution of maximum barrier heights. Natural sequences with a length ranging from 30-200 nucleotides are compared against dinucleotide shuffled counterparts. **(a)** Dark bars represent natural sequences, light bars show the distribution of barrier heights from shuffled sequences. **(b)** A histogram depicting the difference of barrier heights between individual natural sequences and shuffled counterparts ($H_{shuffled} - H_{natural}$).

The new maximum barrier heights derived from the RNAstrand data set range from 4 to 49 kcal/mol. The distribution of the RNAstrand sequences has its peak at 8 kcal/mol, which is comparatively low. In total, 186 of 1198 sequences have the maximum barrier at about 8 kcal/mol. There are 78 and 117 smaller barriers around 6 and 7 kcal/mol, respectively. Barriers below that threshold are extremely rare (20 in total). The remaining amount of barrier heights decreases between 9 kcal/mol (153 sequences) and 24 kcal/mol (11 sequences). Higher barriers (23 in total) range up to 49 kcal/mol, but they are all estimated by `findpath` routine.

The length of sequences included within this statistical comparison varies between 30 and 200 nucleotides. However, as we are dealing with natural sequences from the RNAstrand database, there are predominantly small sequences:

- 168 sequences with 30-50 nucleotides
- 788 sequences with 51-100 nucleotides
- 248 sequences with 101-150 nucleotides
- 25 sequences with 151-200 nucleotides

This partially explains the left shift of the distribution, but even if these smaller subsets are examined separately, one can see an optimization towards lower barrier heights irrespective of the sequence length (see figure 4.2).

When inspecting the shuffled sequences in figure 4.1a and the bar-plots in figure 4.2, we observe a similar shape of the distribution compared to the original RNAstrand sequences, underlining the importance of preserving the dinucleotide content. However, in contrast to natural sequences, the distribution of random counterparts is shifted to higher maximum barriers as a whole, which supports the hypothesis that barrier heights of natural sequences are optimized.

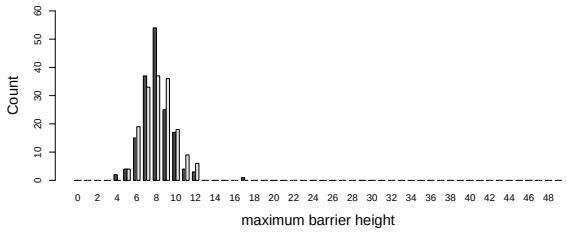

(a) 30-50 nucleotides

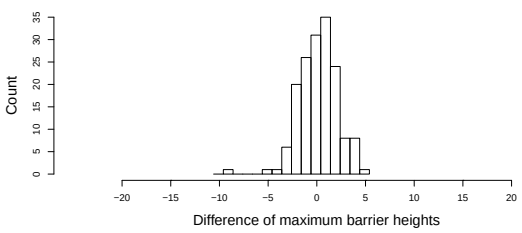

(b) 30-50 nucleotides

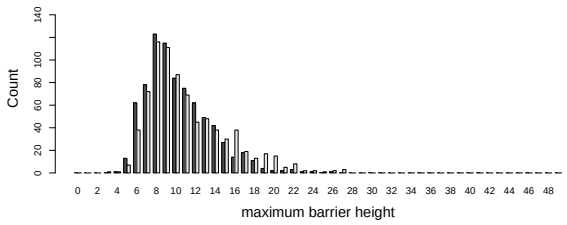

(c) 51-100 nucleotides

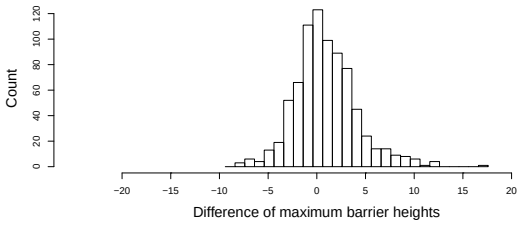

(d) 51-100 nucleotides

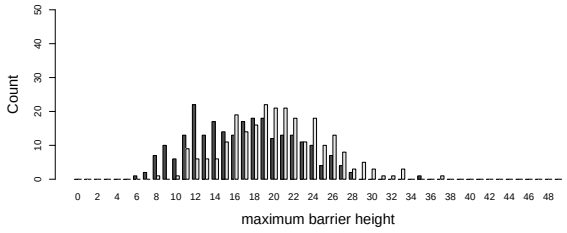

(e) 101-150 nucleotides

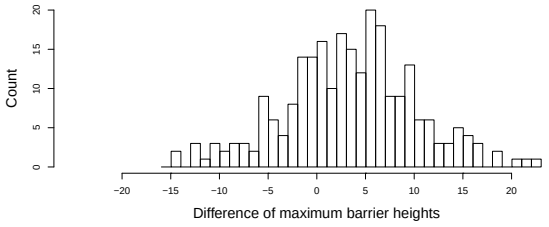

(f) 101-150 nucleotides

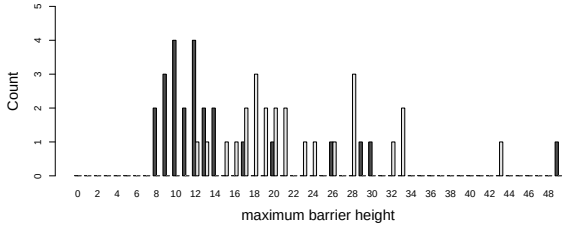

(g) 151-200 nucleotides

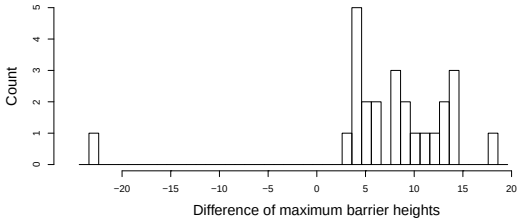

(h) 151-200 nucleotides

Figure 4.2: Caption on page 68

Figure 4.2: Distribution of maximum barrier heights. The data set of figure 4.1 is split into four length dependent groups. On the left side **(a, c, e, g)** one can see the frequency of barrier heights from natural sequences (dark bars) and dinucleotide shuffled sequences (light bars). On the right side **(b, d, f, h)** one can see histograms depicting the difference between natural sequences and their dinucleotide shuffled counterparts ($H_{shuffled} - H_{natural}$). Note, that the scale of the y-axis differs between the individual figures.

Histograms in figures 4.1b and 4.2 compare barrier heights of individual sequences to their randomly shuffled counterparts. Higher barriers for shuffled sequences result in a positive value. The results clearly show that barrier optimization increases with the length of the sequence, which is quite intuitive, as longer sequences have more potential to optimize their refolding pathways.

4.2 Comparison of path-finding heuristics

We will now evaluate the performance of heuristics to recompute known barrier energies. In the previous section, obtained barrier trees were post processed with the `findpath` routine and the maximum barrier per sequence was computed. In this section, *all* barrier heights within the original barrier trees (or forests) were recomputed with the three heuristics contained in the `Vienna RNA package`:

- `findpath` to estimate the best direct path in a folding landscape based on the conventional conformation space Q_{conv}
- `pk_findpath` to estimate the best direct path in a folding landscape based on the bi-secondary structure conformation space Q_{pk}
- `RNAscout.pl` to estimate the best indirect path in a folding landscape based on the

bi-secondary structure conformation space Q_{pk}

The breadth first search of the direct path heuristics (`findpath` and `pk_findpath`) was limited to keep the best 100 structures in memory. The parameters to restrict the size and shape of the `RNAscout.pl` network (see equation 3.15), were adjusted automatically. The guiding stringency γ is calculated from the estimated `pk_findpath` barrier height between the input structures Ω_i and Ω_j (H_{ji}^{pkf}):

$$\gamma = \frac{H_{ji}^{pkf}}{10} \tag{4.1}$$

Equation 4.1 is based on the hypothesis that high barriers estimated from direct paths, will also result in high barriers when considering indirect paths. A stringent guiding potential will therefore allow to raise the energy range δ without an extreme expansion of network vertices (i. e. intermediate structures). δ is set to 2 kcal/mol, but is increased by 1 kcal/mol if either the generated network does not contain a path $\Pi_{j \Leftarrow i}$ (i. e. it is not connected) or if it consists of less than 500 vertices. On the other hand, if more than 1500 intermediate structures are generated and the graph is still not connected, or if the memory requirements of the program exceed 20 GB, the calculations are stopped and no output is returned. Recomputation of these barrier heights would require to vary the γ parameter, which is not done in this comparison. For simplicity, these barrier heights are excluded from the data set.

`barriers` always computes the minimal barrier heights within the input conformation space. Still, dealing with the same conformation space, `findpath` can predict better barrier heights. This observation results from an approximation we have discussed in section 2.1.3. To reduce the time complexity of RNA folding algorithms from $O(n^4)$ to $O(n^3)$, the length of interior loops is limited to 30 base-pairs. Thus, `RNAsubopt` excludes structures exceeding this cut-off from the conformation space. This restriction should not influence the computational results when searching for minimum free energy structures or energetically stable

suboptimal structures, as large interior loops cause high energetic penalties. However, when searching for saddle points separating different local minimum conformations, energetically unfavorable conformations become important to measure barrier heights. Furthermore, length restriction of interior loops results in the computation of *false* local minimum conformations. If unpaired regions longer than 30 base-pairs are not allowed, the algorithm computes a local minimum conformation *given that* it does not contain an interior loop longer than 30.

Table 4.1 shows the ratio between lower, equal and higher barrier height computations when comparing the heuristics to `barriers`. The data set therefore contains all attached, but no detached barriers heights.

The results can be split into three major sets. Between 0.5 and 6.4 kcal/mol, the majority (i. e. more than 50%) of heuristically determined barrier heights are equal to the results returned by `barriers`. From 6.5 to 9.4 kcal/mol, the majority of heuristically determined barrier heights is higher than those computed by `barriers` and finally, barriers higher than 9.5 kcal/mol are rarely predicted by the individual heuristics. The last set of barriers greater than 9.5 kcal/mol, however, is comparatively small, making statistical comparison error-prone.

Generally, predictions of `findpath` and `pk_findpath` show the same results when comparing the total amount of lower, equal and higher estimates. When inspecting the ratio of equal to higher estimated barrier heights, the accuracy decreases with increasing barrier heights. This indicates that refolding paths with high barriers are predominantly indirect paths. Interestingly, the amount of lower barrier height estimates is around 10%, which is higher than we expected, because interior loops of size greater 30 are energetically unfavorable. In search for saddle point conformations, it is therefore advisable to increase the maximum interior loop size.

barriers	findpath			pk_findpath			RNAscout.pl			MINIMUM		
(kcal/mol)	l	e	h	l	e	h	l	e	h	l	e	h
0.5 – 1.4	705	27068	1006	705	27068	1006	740	25518	2521	756	27694	329
1.5 – 2.4	1904	35280	2235	1904	35280	2235	1964	34476	2979	1969	36649	801
2.5 – 3.4	3796	41030	5980	3796	41030	5980	3952	42754	4100	4042	44645	2119
3.5 – 4.4	2302	22517	5310	2302	22517	5310	2452	24045	3632	2498	25388	2243
4.5 – 5.4	889	7456	3625	889	7456	3625	949	7618	3403	984	8633	2353
5.5 – 6.4	356	2964	2665	356	2964	2665	397	2917	2671	411	3612	1962
6.5 – 7.4	153	1008	1196	153	1008	1196	173	1027	1157	177	1299	881
7.5 – 8.4	48	333	539	48	333	539	66	350	504	67	457	396
8.5 – 9.4	22	143	234	22	143	234	30	124	245	32	174	193
9.5 – 10.4	7	39	115	7	39	115	8	43	110	8	59	94
10.5 – 11.4	5	7	60	5	7	60	8	12	52	8	15	49
11.5 – 12.4	1	6	22	1	6	22	1	5	23	1	9	19
12.5 – 13.4	2	0	13	2	0	13	2	0	13	2	0	13
13.5 – 14.4	0	0	1	0	0	1	0	0	1	0	0	1
14.5 – 15.4	0	0	2	0	0	2	0	1	1	0	1	1
15.5 – 16.4	0	0	1	0	0	1	0	1	0	0	1	0

Table 4.1: Barrier heights, computed by the program package `barriers`, are compared to three different heuristics. Columns `findpath`, `pk_findpath` and `RNAscout.pl` show the amount of (lower | equal | higher) estimated barrier heights. The last column (MINIMUM) contains the best predictions (i. e. the minimum) from all three heuristics compared to `barriers`

RNAscout.pl predicts more equal barrier heights and less higher barrier heights than the direct path heuristics in general. The amount of lower estimated barrier heights is increased to direct path heuristics, indicating that some of these estimations result from indirect pseudoknotted intermediates that could not be found by direct path heuristics and barriers.

The last column shows the minimum of all heuristic barrier height estimations. The difference to the best heuristic (RNAscout.pl) shows that there are barrier heights where the direct path heuristics performed better than RNAscout.pl. These results are predominantly caused by small local rearrangements. As an example, given a local minimum consisting of a helix with the complementary strands A and B, and another minimum forms a slightly shifted helix of same length A' with B', then the structures are neither neighbors within the stacked helix move-set nor comprised in each other. RNAscout.pl will therefore not see these conformations as neighbors; instead, it connects the structures with a transition state that (in worst case) has no base-pair of both helices inserted. For such small rearrangements, a direct path heuristic is usually sufficient. The set of pk_findpath better/worse predictions is therefore not completely included within the set of RNAscout.pl predictions.

The fact that there is no difference between the heuristics findpath and pk_findpath, might have two reasons: Firstly the interaction penalty for an initial pseudoknot base-pair is 8.1 kcal/mol, which cannot be compensated by the insertion of small helix regions. Secondly, local rearrangements, such as the relocation of a bulge loop or the shift of a whole helix region do not allow to form pseudoknot structures. Instead, pseudoknot transition states occur predominantly between secondary structures that differ in whole helix regions, such that pseudoknotted transition states allow the partial formation of both helices. Apparently, within the RNAstrand data set, the amount of such distant rearrangements is little or non-existent. However, differences between findpath and pk_findpath can be seen with lower pseudoknot penalties (data not shown). A pseudoknot penalty of 4.1

kcal/mol (i. e. the duplex initiation energy) shows a lot of lower barrier energies starting when inspecting medium and high barriers from 6.4 to 16.4 kcal/mol.

The difference between barrier height predictions from the individual programs is shown in figure 4.3. Figure 4.3a contains the same data as discussed in table 4.1, i. e. all attached barriers computed by `barriers` (disregarding the barrier heights where recomputation with `RNAscout.pl` failed). Figure 4.3b compares predictions for detached barrier heights, i. e. heights that could not be determined by `barriers`, due to the limited amount of suboptimal structures. For simplicity, we computed the minimum barrier height to the MFE secondary structure for every detached barrier (again disregarding the barrier heights where recomputation with `RNAscout.pl` failed).

Comparing the different programs in figure 4.3a, we see that the main variation between `barriers` and all heuristics is concentrated to a small range. This range as a whole is shifted to higher barrier estimations with increasing precomputed barrier heights. `RNAscout.pl` results show that there are more outliers of very high estimated barrier heights. Interestingly, we see differences when comparing the barrier heights computed by direct path heuristics, as there are a few cases where indirect paths lower the barrier height. `RNAscout.pl` compared to the direct path heuristics shows many better predictions.

Figure 4.3b also shows that `pk_findpath` performs better at a small amount of refolding paths. With increasing barrier heights, `RNAscout.pl` shows increasing deviations in both lower and higher barrier predictions.

These observations underline that `RNAscout.pl` is susceptible to false barrier estimation from local rearrangements that can be computed by `findpath`, but occasionally returns very bad results with the automatically adjusted guiding stringency. Instead, direct path heuristics show less bad estimations, but a higher amount of small differences. The minimum of the heuristics should therefore give a good estimation of the real barrier heights.

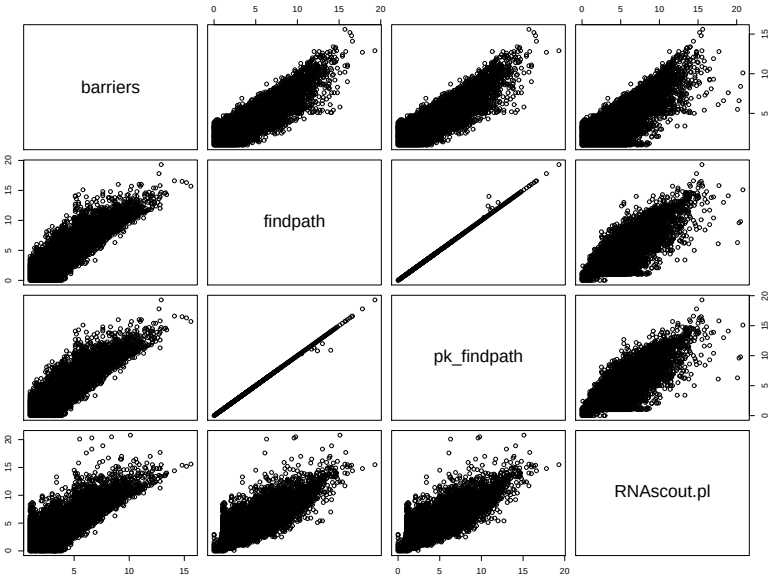

(a) Correlation plot of barrier predictions

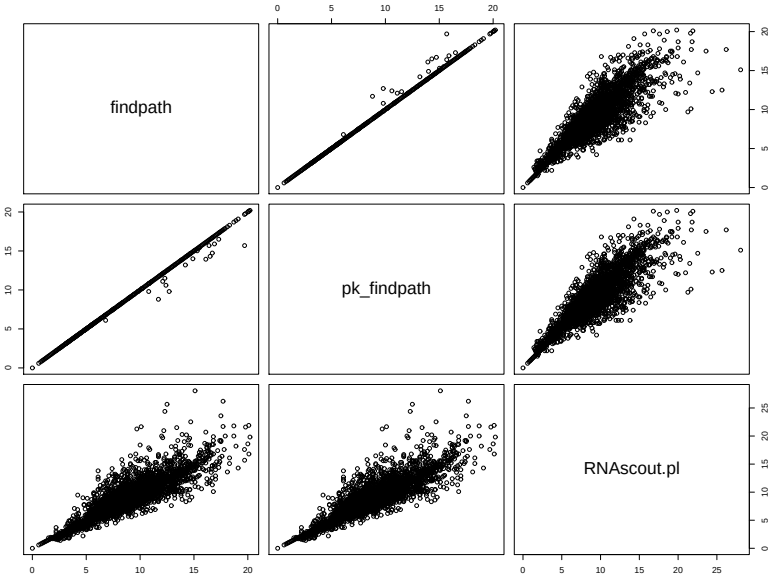

(b) Correlation plot of barrier predictions

Figure 4.3: Barrier heights computed by the different programs are compared to each other. **(a)** compares all programs, **(b)** compares predictions for barrier heights that could not be determined by `barriers`.

The histograms in figure 4.4a depict the differences between barrier heights computed by `barriers` and `RNAscout.pl` predictions. Apparently, the majority of predictions is equal. The main differences between predicted barriers range from -2 to 2 kcal/mol, while the amount of higher predicted barriers is greater than the amount of lower predicted barriers. The histogram in figure 4.4b contains the difference between `barriers` and the minimum over all heuristics. As expected, the amount of worse predicted barriers is smaller, the amount of equal and better predicted structures is higher.

As a concluding remark of this section we see that `RNAscout.pl` does enhance the prediction of barrier heights, but it is advisable to consider the `pk_findpath` heuristic as an upper bound for network generation. In contrast to the current approach, `RNAscout.pl` would not stop network expansion if it has more than 500 RNA secondary structures, but expand until at least the `pk_findpath` barrier height is found. This, however, is too time consuming for the evaluation of all barrier heights from the RNAstrand data set, as it would require the variation of both network parameters γ and δ to keep the network size computationally tractable. However, we will see in the following section that recomputation of single barrier heights with variable parameters can strongly influence the performance of `RNAscout.pl`.

4.3 Comparison of kinetic simulations

The following section compares the accuracy of heuristic `RNAscout.pl` networks with coarse-grained `barriers` landscapes. Different coarse-grained landscapes from a manually selected sequence were generated with `barriers` and folding kinetics based on these landscapes were calculated with `treekin`. The simulations have then been compared to heuristic landscapes that consider solely the local minima obtained from barrier trees. Saddle points are recomputed with all three heuristics, transition rates are calculated by

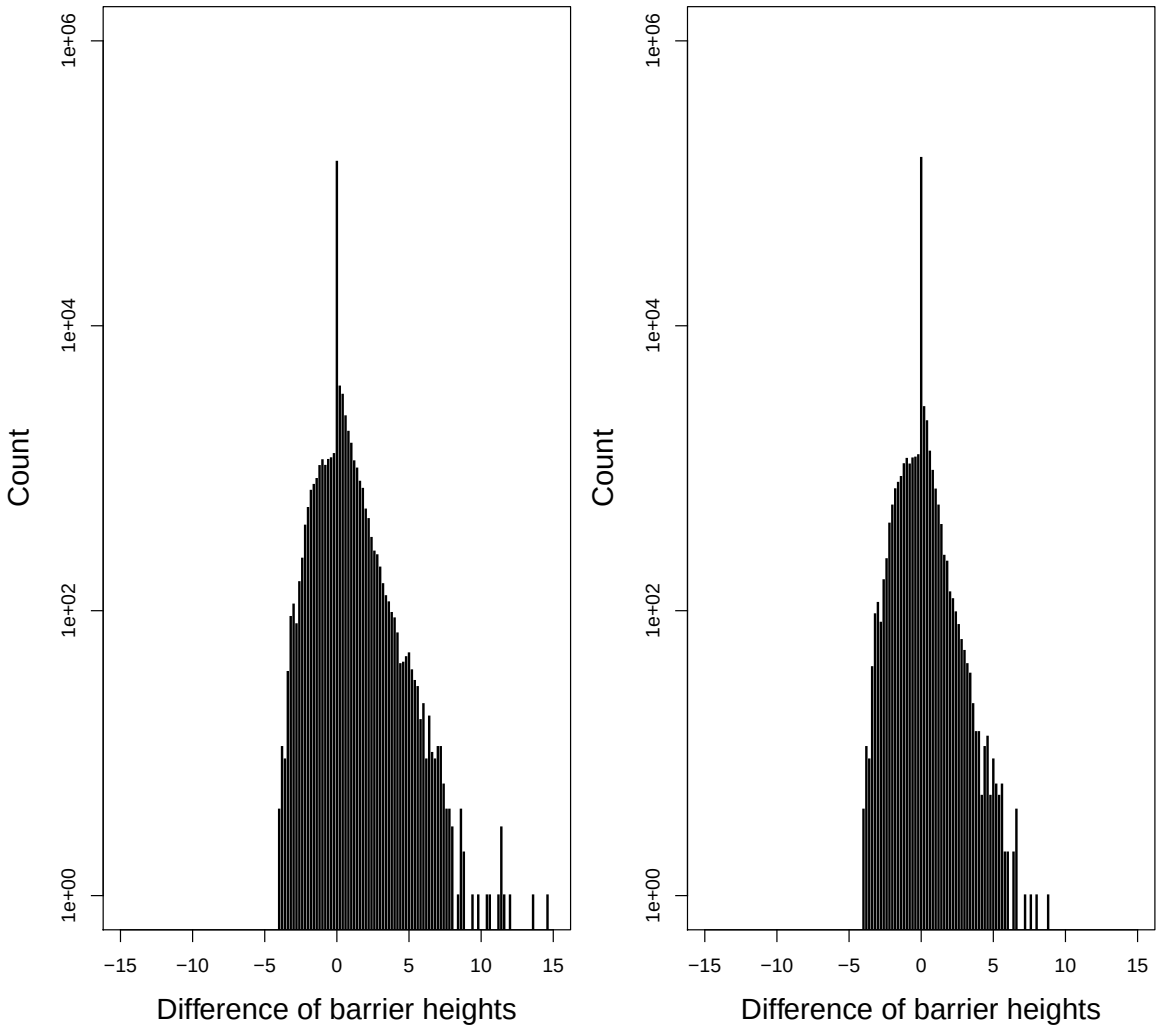

(a) $H_{\texttt{RNAscout.pl}} - H_{\texttt{barriers}}$ **(b)** $H_{heuristics} - H_{barriers}$

Figure 4.4: Difference of barrier height predictions. **(a)** `RNAscout.pl` against precomputed barriers from the `barriers` package. The majority of predictions is equal, main differences range from -3.9 to 7.7 kcal/mol. **(b)** the minimum prediction of direct and indirect path heuristics against the `barriers` package. The amount of equal predictions increases significantly, while the amount of higher estimations is lower.

Arrhenius kinetics as it is done in the `RNAscout.pl` algorithm (see section 3.2.3).

Subsequently, an `RNAscout.pl` network was generated from a manually selected starting conformation and the MFE conformation. The network parameters δ and γ (see equation 3.15) were varied to measure their influence on the size of the generated network, the minimum barrier height found and the refolding kinetics on subsequent `treekin` simulations. The results obtained from `RNAscout.pl` networks are then compared to an exhaustively computed folding landscape from `barriers`.

Influence of the basins of attraction

To measure the accuracy of `RNAscout.pl` we searched the previously generated barrier trees for small sequences with many energetically trapped local minima (i. e. minima with high minimum barriers). To increase the complexity of the problem, the conformation we start our simulations with should not be directly connected with the MFE conformation, but should firstly lead to an energetically trapped intermediate structure and then refold into the MFE secondary structure. The RNA folding landscape of the signal recognition particle SRP_00209 [192] contains a path fulfilling this properties. Tables 4.2, 4.3a and 4.3b represent three barrier trees with a minimum barrier height (H_{MIN}) of 1, 3 and 5 kcal/mol, respectively. The minimum free energy computed for SRP_00209 is -35.70 kcal/mol. The energy range δ for `RNAsubopt` was set to 13.30 kcal/mol, which results in 5139059 structures up to a free energy of -22.40 kcal/mol. We decided to compute all barrier trees such that they cover the local minimum structures up to a free energy of -31.80 kcal/mol, which is the energy of the selected conformation we will start our simulations with.

As we have discussed in section 3.1.1, `barriers` returns a set of RNA secondary structures, where each conformation represents the minimum of a certain basin of attraction. Rates between the local minima are calculated considering the internal equilibrium partition

GGCCCCUACGUGGUGUCAUCUCGCUGAACUUCCCCCAGGACCGGAAGGUAGCAAGGGUAGGUGGGCUCUGGCAGGUGCGUGAGGGGUCUUCACGUUU

ID	Structure (Ω)	$E(\Omega)$	N	H	N	H
1	((((((((((((.(((((.((((((.....(((.....(((....))).....)))..))))))...))))))..))))))).))))).....	-35.70	0	11.43	0	13.30
2	((((((((((((.(((((.((((((.....(((.....(((....))).....)))..))))))...))))))..))))))).))))).....	-35.40	1	2.30	1	2.30
3	((((((((((((.(((((....(((..((((((.....(((....))).....)))..))))))...))))))..))))))).))))).....	-35.40	1	7.30	1	7.30
4	((((((((((((.(((((....(((..((((((.....(((....))).....)))..))))))...))))))..))))))).))))).....	-35.10	3	2.30	3	2.30
5	((((((((((((.(((((....(((..(((((.(((....))).....)))..))))))...))))))..))))))).))))).....	-35.10	1	7.00	1	7.00
6	((((((((((((.(((((....(((.(.((((((.....(((....))).....)))..))))))...))))))..))))))).))))).....	-34.90	3	1.70	3	1.70
7	((((((((((((.(((((....(((.(.((.(((.....(((....))).....)))..))))))...))))))..))))))).))))).....	-34.90	3	3.60	3	3.60
8	((((((((((((.(((((....(((..((((.(((....(((....))).....)))..))))))...))))))..))))))).))))).....	-34.80	5	2.30	5	2.30
9	((((((((((((.(((((.(((((....((.(((.....(((....))).....)))..))))))...))))))..))))))).))))).....	-34.70	1	1.60	1	1.60
10	((((((((((((.(((((....(((.(.((((((.....(((....))).....)))..))))))...))))))..))))))).))))).....	-34.60	4	1.70	4	1.70
11	((((((((((((.(((((....(((.(.((.(((....(((....))).....)))..))))))...))))))..))))))).))))).....	-34.60	5	1.70	5	1.70
12	((((((((((((.(((((....(((.(.((.(((.....(((....))).....)))..))))))...))))))..))))))).))))).....	-34.60	7	2.30	7	2.30
13	((((((((((((.(((((.(((((....((.(((.....(((....))).....)))..))))))...))))))..))))))).))))).....	-34.40	1	1.60	1	1.60
14	((((((((((((.(((((....(((.(.((.(((....(((....))).....)))..))))))...))))))..))))))).))))).....	-34.30	8	1.70	8	1.70
15	((((((((((((.(((((.((((((.....(((....(((....))).....)))..))))))...))))))..))))))).))))).....	-33.90	1	5.70	1	**6.00**
16	((((((((((((.(((((.((((((.....(((....(((....))).....)))..))))))...))))))..))))))).))))).....	-33.60	15	2.30	15	2.30
...						
47	((((((((((((.(((((.((((((...(((((.....)))))..........))))))...))))))..))))))).))))).....	-31.90	1	7.60	1	7.60
48	((((((((((((.(((((.(((((....((...(((...(((....))).....)))..))))))...))))))..))))))).))))).....	-31.90	19	2.30	19	2.30
49	((((((((((((.(((((.(((.....((((.(((....(((....))).....)))..))))))...))))))..))))))).))))).....	-31.90	36	2.30	36	2.30
50	((((((((((((.(((((...(.(...(((((.....(((....))).....)))..))))).)...))))))..))))))).))))).....	-31.90	3	2.10	3	2.10
51	((((((((((((.(((((...(.(...((((.(((....(((....))).....)))..))))).)...))))))..))))))).))))).....	-31.90	5	2.10	5	2.10
52	((((((((((((.(((((.(((((.....(((((.....(((....))).....)))..))))))...))))))..))))))).))))).....	-31.80	1	1.40	1	1.40
53	((((((((((((.(((((.(((((.....((.(((....(((....))).....)))..))))))...))))))..))))))).))))).....	-31.80	15	1.30	15	1.30
54	((((((((((((.(((((....((((..(((((.....)))))..)))).(((((.....)))))..))))))...))))))).))))).....	-31.80	47	7.00	47	7.00

Table 4.2: An energetically sorted set of local minima from the signal recognition particle SRP_00209. The RNA sequence is shown above the table. The first five columns show standard output of the program package `barriers` with a minimum barrier height H_{MIN} of 1 kcal/mol. For each Structure(Ω), the free energy ($E(\Omega)$) and the minimum barrier height (H) to the next neighboring structure (N) is shown. N refers to the ID of the (neighboring) structure. The last two columns, the second (N,H) pair, is recomputed with the heuristics discussed in section 3.2 and represents the minimum of their predictions. Bold values underline inaccuracy of the heuristics.

GGCCCCUACGUGGUGUCAUCUCGCUGAACUUCCCCCAGGACCGGAAGGUAGCAAGGGUAGGUGGGCUCUGGCAGGUGCGUGAGGGGUCUUCACGUUU

ID	Structure (Ω)	$E(\Omega)$	N	H	N	H
1	(((((((((((.(((((.((((((.....(((.....(((....))).....)))..))))))...))))))..))))).))))).....	-35.70	0	13.30	0	13.30
2	(((((((((((.(((((....(((..(((((((.....(((....))).....))).)))).)))..))))))..))))).))))).....	-35.40	1	7.30	1	7.30
3	(((((((((((.(((((....(((..((((.(((.....(((....))).....))).)))).)))..))))))..))))).))))).....	-35.10	1	7.00	1	7.00
4	(((((((((((.(((((....(((.(.((.(((.....(((....))).....)))..)))..))))))..))))).))))).....	-34.90	2	3.60	2	3.60
5	(((((((((((.(((((.((((((.....(((....(((....))).....)))..))))))...))))))..))))).))))).....	-33.90	1	5.70	1	**6.00**
6	(((((((((((.(((((.((((((.....(((.....(((....))).....)))..))))))...))))))..))))).))))).....	-33.30	1	4.20	1	**5.20**
7	(((((((((((.(((((.((((((.....(((...(((....))).....)))..))))))...))))))..))))).))))).....	-33.30	1	6.00	1	**7.00**
8	(((((((((((.(((((....(((..((((..(((...(((....))).....)))..))))))...))))))..))))).))))).....	-32.80	1	5.50	**3**	5.50
9	(((((((((((.(((((.(((.....(((((((.....(((....))).....)))..)))))))...))))))..))))).))))).....	-32.50	2	4.20	2	4.20
10	(((((((((((.(((((.((((((.....(((.....(((....))).....)))..))))))).))))...))))))..))))).))))).....	-32.20	1	3.40	1	3.40
11	(((((((((((.(((((.(((.....((((.(((....(((....))).....)))..)))).)))...))))))..))))).))))).....	-32.20	1	4.20	2	4.20
12	(((((((((((.(((((.((((((...(((((.........)))))..........)))))))...))))))..))))).))))).....	-31.90	1	7.60	1	7.60
13	(((((((((((.(((((....(((((..(((((.........)))))..)))))..((((......))))))))))...))))))..))))).))))).....	-31.80	12	7.00	12	7.00

(a) $H_{MIN} = 3$

GGCCCCUACGUGGUGUCAUCUCGCUGAACUUCCCCCAGGACCGGAAGGUAGCAAGGGUAGGUGGGCUCUGGCAGGUGCGUGAGGGGUCUUCACGUUU

ID	Structure (Ω)	$E(\Omega)$	N	H	N	H
1	(((((((((((.(((((.((((((.....(((.....(((....))).....)))..))))))...))))))..))))).))))).....	-35.70	0	13.30	0	13.30
2	(((((((((((.(((((....(((..(((((((.....(((....))).....))).)))).)))..))))))..))))).))))).....	-35.40	1	7.30	1	7.30
3	(((((((((((.(((((....(((..((((.(((.....(((....))).....))).)))).)))..))))))..))))).))))).....	-35.10	1	7.00	1	7.00
4	(((((((((((.(((((.((((((.....(((.....(((....))).....)))..))))))...))))))..))))).))))).....	-33.90	1	5.70	1	**6.00**
5	(((((((((((.(((((.((((((.....(((...(((....))).....)))..))))))...))))))..))))).))))).....	-33.30	1	6.00	1	**7.00**
6	(((((((((((.(((((....(((..((((..(((...(((....))).....)))..))))))...))))))..))))).))))).....	-32.80	1	5.50	**3**	5.50
7	(((((((((((.(((((.((((((...(((((.........)))))..........)))))))...))))))..))))).))))).....	-31.90	1	7.60	1	7.60
8	(((((((((((.(((((....(((((..(((((.........)))))..)))))..((((......))))))))))...))))))..))))).))))).....	-31.80	7	7.00	7	7.00

(b) $H_{MIN} = 5$

Table 4.3: An energetically sorted set of local minima from the signal recognition particle SRP_00209. The RNA sequence is shown above both tables. The first five columns show standard output of the program package `barriers` with a minimum barrier height H_{MIN} of 3 kcal/mol **(a)** and 5 kcal/mol **(b)**. For each Structure(Ω), the free energy ($E(\Omega)$) and the minimum barrier height (H) to the next neighboring structure (N) is shown. N refers to the ID of the neighboring structure. The last two columns, the second (N,H) pair, is recomputed with the heuristics discussed in section 3.2 and represents the minimum of their predictions. Bold values underline inaccuracy of the heuristics.

functions of the corresponding basins. `treekin` simulations based on the three different coarse-grained landscapes can be seen in the first column of figure 4.5. The ID of the trajectory corresponds to the ID of the structure in tables 4.2 4.3a and 4.3b.

Generally the results can be split into three parts. The first addresses the starting conformation, which has ID 54, 13 and 8 in the three different barrier trees. Independently of the coarse-graining, the population of this structure behaves similarly, but decreases faster when increasing the minimum barrier height. Supposedly, aggregation of small basins to one big gradient basin alters the influence of small rates (high barriers) to neighboring basins relative to high rates (small barriers) within the equilibrium distribution of the merged basins.

The second part of the simulation regards the population of intermediate states. The simulation on the most detailed landscape ($H_{MIN} = 1$) behaves as expected. While the population of the starting basin decreases, the transition basin (table 4.2: 47) increases. In contrast, $H_{MIN} = 3$ and $H_{MIN} = 5$ simulations compute the MFE secondary structure basin as highest populated intermediate. The population of the transition basin (table 4.3a: 12 and table 4.3b: 7) is comparatively low.

The last difference can be seen in the equilibrium distribution of the gradient basins. The MFE conformation basin is highest populated in every simulation, the rest of the basins are not sorted according to their best local energy, as the amount of structures within the basins plays a crucial role. Because small basins are merged into one basin when raising the minimum barrier height, the remaining representing structures are distributed differently. For this reason, the equilibrium distribution is strongly dependent on the minimum barrier height.

The simulations considering gradient-basins are now compared to simulations of a heuristic image of the folding landscape. The gradient basins were sacrificed and the local minima

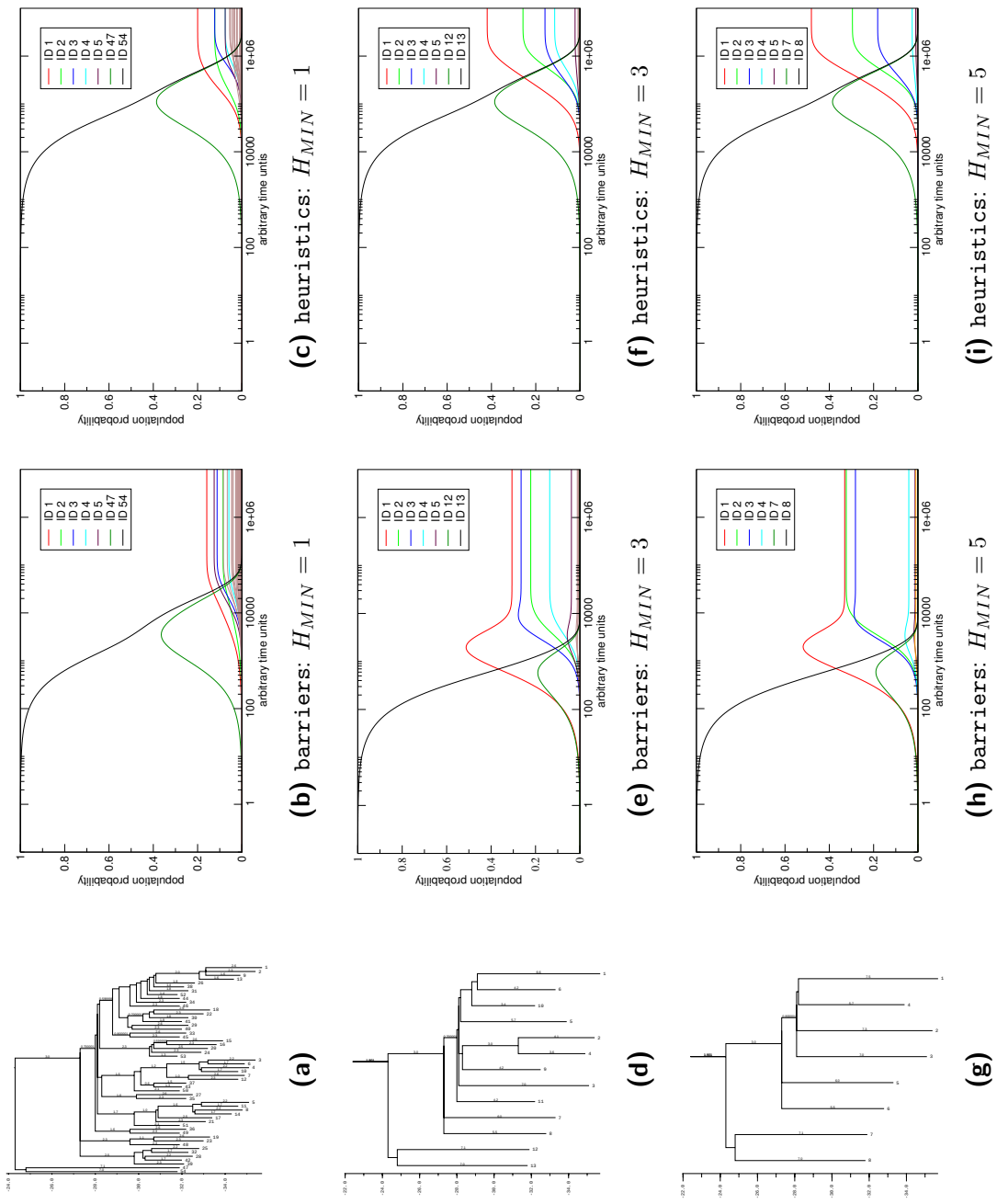

Figure 4.5: Caption on page 82

Figure 4.5: Comparison of `treekin` simulations based on different representations of an RNA folding landscape. All simulations start with 100% population of the same RNA conformation and end in the equilibrium distribution. The IDs from the trajectories correspond to the RNA secondary structures from the respective barrier trees **(a, d, g)**. **(b,c)** table 4.2, **(e, f)** table 4.3a, **(h, i)** table 4.3b. **(b, e, h)** Simulations based on coarse-grained landscapes computed by `barriers` with a minimum barrier height of 1, 3 and 5, respectively. **(c, f, i)** Simulations based on heuristic re-computation of barrier trees with a minimum barrier height of 1, 3 and 5, respectively.

within the barrier trees were reconnected with the best prediction of the three heuristics of the `Vienna RNA package` (`findpath`, `pk_findpath` and `RNAscout.pl`). Tables 4.2 4.3a and 4.3b compare the results of heuristic barrier trees to the exhaustively computed ones by `barriers`. The majority of barrier heights is equal, small differences can e. g. be seen if heuristic barriers are worse than the exact ones (table 4.2: ID 15) or if the minimum barrier found connects different basins (table 4.3a: ID 8).

Simulations based on these recomputed barrier trees were done using Arrhenius kinetics discussed in section 3.1.2. Figure 4.5 shows the results of the simulations in the second column. Interestingly, the trajectories of the starting conformation and the intermediate conformation behave similar in all three simulations. Compared to `barriers`, they are all close to the simulation based on the lowest coarse-graining, apart from the fact that the lack of gradient basins alters the dwell times of certain structures and therefore the time scale is distorted. Coming from this example, the heuristics are closer to the coarse-grained simulation with $H_{MIN} = 1$ than coarse-grained landscapes with huge gradient basins. In equilibrium, the structures are distributed exclusively according to their free energy.

Network size												
δ \ γ	2.0	1.0	0.9	0.8	0.7	0.6	0.5	0.4	0.3	0.2	0.1	0.0
0.1	18	37	38	39	42	54	75	78	91	136	264	479
0.5	21	40	41	41	54	74	81	113	125	171	347	592
1.0	27	46	51	59	75	85	111	126	157	272	479	1021
1.5	28	52	69	81	103	109	133	171	226	362	633	1466
2.0	31	79	90	108	126	138	168	218	372	519	847	
2.5	38	110	117	130	149	195	252	338	495	627	1140	
3.0	54	131	143	167	196	246	319	443	583	891	1615	
3.5	69	156	172	191	256	315	431	584	789	1129		
4.0	80	176	203	259	297	436	561	751	984	1731		
4.5	91	221	242	310	428	560	738	927	1451			
5.0	104	256	328	472	548	727	951	1297				

Table 4.4: Amount of structures within the `RNAscout.pl` network dependent on the user defined parameters δ and γ. Background colors indicate the predicted barrier height. Dark gray: $H = 9.40$ kcal/mol; white: $H = 7.50$ kcal/mol.

`RNAscout.pl` compared to an exhaustive computed folding landscape

We will now evaluate the `RNAscout.pl` output if only the starting structure Ω_i and the MFE structure Ω_j from figure 4.5 are given. First of all, table 4.4 shows the influence of γ and δ for this specific network. In this case, the graph is already connected (i.e. there is a path $\Pi_{j \Leftarrow i}$) with $\delta = 0.1$ kcal/mol and $\gamma = 2.0$, which are very restrictive parameters. The estimated minimum barrier height, however, is 9.40 kcal/mol with these parameters. Expanding the network (e. g. with the parameters $\delta = 2.5$ kcal/mol and $\gamma = 0.4$) lowers the estimated barrier height to 7.50 kcal/mol.

We can expect that the simulations based on networks with estimated barrier heights of 9.40 kcal/mol will compute a longer refolding time, than those with a minimum barrier height of 7.50 kcal/mol. We will refer to changes in the refolding time as *qualitative* changes, that are very important to measure the efficiency of a refolding path.

On the other hand, the higher the amount of vertices, the more we converge to the results of a simulation in the full conformation space. This convergence should predominantly influence the population size of individual structures in respect to similar suboptimal structures, but should not influence the refolding time between different local minima. These changes will be seen as *quantitative* changes that are of little importance to measure the efficiency of a refolding path, as the refolding time is not affected. A quantitative description of population density in a heuristically estimated conformation space is risky, as energetically good but structurally distant conformations might not be found and the basins of attraction are not included for the individual local minima. We will therefore focus on a good qualitative description with respect to the time scale.

Figure 4.6a shows changes in the population of starting and MFE trajectory for a constant guiding stringency $\gamma = 0.4$ and the variation of the energy range δ from 0.1 kcal/mol to 5.0 kcal/mol. The simulation based on the smallest network ($\delta = 0.1$ kcal/mol), shows both starting and MFE trajectories mainly between 90% and 100%, due to the low amount of competitive structures. Small expansions of the network (up to $\delta = 2.0$ kcal/mol) do not influence the barrier height and thus, weakly influence the trajectories. We can see quantitative changes in the population density and small qualitative changes in the refolding time.

Further network expansion to $\delta = 2.5$ kcal/mol lowers the minimum barrier height and heavily influences the refolding time. The quantitative changes, in contrast, do only influence the time period when the new transition state is detected. In equilibrium, the

population of the MFE secondary structure remains constant. Even higher values of δ, up to the biggest network generated with $\gamma = 0.4$ and $\delta = 5.0$ kcal/mol solely result in quantitative changes. At $\delta = 3.5$ kcal/mol, the population of the MFE secondary structure in the equilibrium decreases and finally with $\delta = 5.0$ a new structure is included that differs from the starting structure in solely two base-pairs. This energetically worse, but nearly equal structure populates immediately, but does not influence the refolding time.

Figure 4.6b shows a `treekin` simulation based on the most detailed rate matrix we can compute with `barriers`. The rates within the matrix are not rates connecting macro-states (basins of attraction) but micro-states (single structures). Usually a sequence of 97 nucleotides length is too long to calculate full dynamics. However, in this case, the structures within our energy range do all have a constant part of 50 nucleotides. The remaining dynamic part of 47 nucleotides is small enough to compute micro-rates. We find that this full simulation predicts a similar behavior of the starting trajectory compared to the `RNAscout.pl` network with $\delta = 5.0$. The first upcoming sequence was previously merged into the gradient basin of the starting sequence (see figure 4.5). The population of the MFE secondary structure seems very small, which is expected if all suboptimal structures are considered without being merged into gradient basins. Note that the timescale in figure 4.6a and 4.6b is slightly different, but the behavior of the trajectories is comparable.

While figure 4.6a shows the changes with increasing energy range and a guiding potential of $\gamma = 0.4$, table 4.5 shows the computed distances of the trajectories (see equation 3.17) for γ ranging from 2.0 to 0.4. Similarly to $\gamma = 0.4$, the main changes in the positions of the trajectories are found when a lower barrier is obtained. If the barrier height remains constant, there are only small qualitative changes in the population density. The last change including the slightly modified, energetically worse starting sequence is only found with the smallest guiding stringency. We therefore conclude that simulations based on networks that found the lowest barrier heights are sufficient for a qualitative description of the refolding

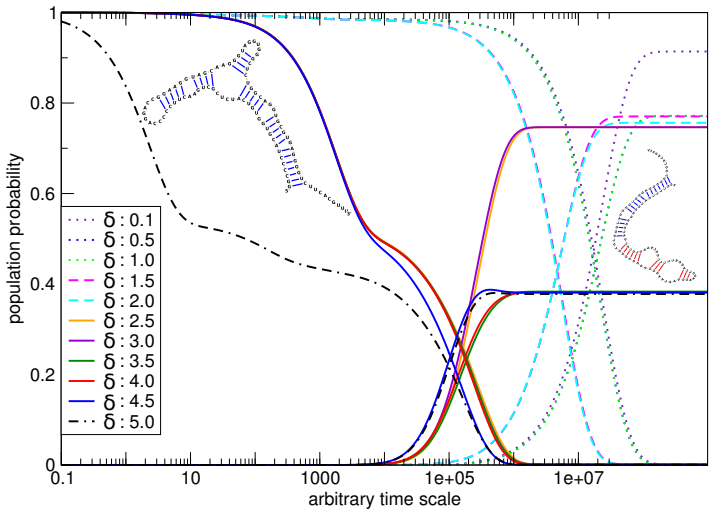

(a) `RNAscout.pl` – $\gamma = 0.4$

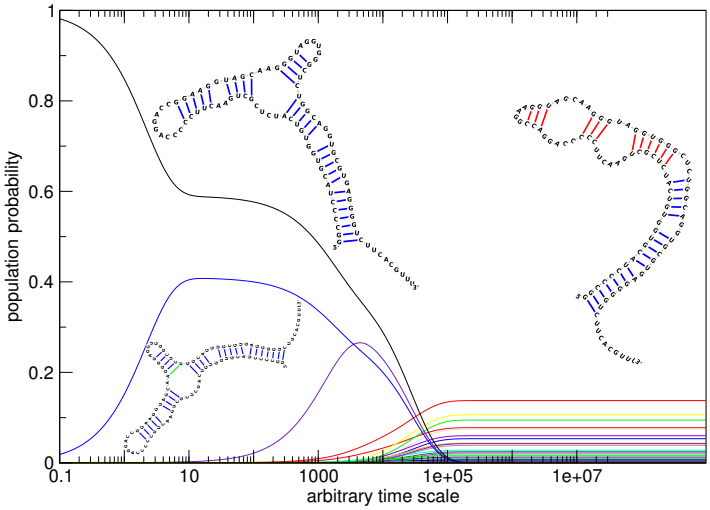

(b) `barriers`

Figure 4.6: Caption on page 87

Figure 4.6: `treekin` simulations of the SRP_00209 RNA. **(a)** Comparison of eleven simulations based on different `RNAscout.pl` networks. While the guiding potential is constant with $\gamma = 0.4$, the energy range δ varies from 0.1 kcal/mol up to 5.0 kcal/mol. For each simulation, the starting and MFE trajectories are shown (in the same color). The two structure comics are the starting and MFE structure, respectively. Blue base-pairs in the MFE structure remain constant during the simulation, red base-pairs are different from the starting conformation. **(b)** A `treekin` simulation based on a folding landscape that considers micro-rates (between single structures) instead of macro-rates (between gradient basins). Structures correspond to the closest trajectories. Blue base-pairs are those initially formed by the starting structure. The first upcoming sequence has *one* different base-pair (marked in green), new base-pairs formed by the MFE secondary structure are shown in red.

time. In case of guiding stringency $\gamma = 0.4$ we need an energy range δ of at least 2.5 kcal/mol.

Interestingly, this section showed that the coarse-graining level of `barriers`, even though it just merges gradient basins, has a high impact on subsequent simulations. In contrast, heuristic landscapes that consider solely the local minima obtained from barrier trees show a smaller impact on subsequent simulations.

4.4 Evaluation of a synthetic riboswitch

As discussed in section 1.4, the primary incitement to implement the `RNAscout.pl` algorithm was to provide a basis for the *in silico* evaluation of synthetic riboswitches.

The basic concept of the riboswitch published by Isaacs et al. [1] is to use two sequences that fold into certain stable structures as soon as they are transcribed. The cis-repressed

Trajectory distance								
δ \ γ	2.0	1.0	0.9	0.8	0.7	0.6	0.5	0.4
0.1 vs. 0.5	0.38	0.16	0.10	0.10	0.11	0.68	0.09	5.77
0.5 vs. 1.0	1.49	0.00	0.01	0.02	0.71	0.00	6.06	0.00
1.0 vs. 1.5	0.00	0.02	0.70	0.71	5.95	5.92	4.74	33.19
1.5 vs. 2.0	0.00	0.69	0.07	13.08	27.57	30.92	13.85	0.07
2.0 vs. 2.5	1.06	14.17	30.55	8.22	0.43	150.23	146.60	202.27
2.5 vs. 3.0	215.81	187.12	151.99	146.67	145.26	0.12	3.78	0.08
3.0 vs. 3.5	0.00	0.00	0.00	0.00	0.40	3.79	23.14	66.56
3.5 vs. 4.0	0.00	0.00	0.00	0.41	0.41	23.21	66.35	0.03
4.0 vs. 4.5	0.00	0.00	0.00	0.42	22.03	66.46	0.91	1.44
4.5 vs. 5.0	0.00	0.20	2.60	90.77	66.86	0.95	0.00	68.76

Table 4.5: Distances of trajectories in response to changes in the energy range δ. High values indicate a qualitative change in respect to the time scale and/or a quantitative change in relation to the population density. Background colors highlight the major trajectory-shifts. Dark gray: a quantitative and qualitative shift in response to the new barrier height obtained. Medium gray: Quantitative shift in equilibrium population density. Light gray: Quantitative shift of the starting trajectory.

RNA (crRNA) needs to have a conformation with a blocked ribosome binding site (RBS) and a loop interaction motive. The structure of the trans activation RNA (taRNA) must expose an interaction motive complementary to the crRNA (see figure 1.2). Both structures should be energetically stable if transcribed independently, but rearrange fast if they are transcribed together. Isaacs et al. have shown that their two synthetic RNA sequences are functional in Escherichia coli. Here we will kinetically evaluate the RNA molecules with `RNAscout.pl`.

For two reasons, the refolding time cannot be estimated by `barriers`. Firstly, the maximum of structures that barriers can handle is around 10^7. For our sequence this means that we are allowed to increase the energy range to about 12 kcal/mol. However, within this energy range there is no energetic barrier. Instead, the `findpath` heuristic estimates a barrier height of 17.10 kcal/mol. The second problem is shown in figure 3.5. As the best refolding path has a pseudoknotted intermediate, it is not predictable by conventional structure prediction. The `pk_findpath` barrier for our example is at 9.20 kcal/mol.

Table 4.6 shows the influence of γ and δ on the size of the generated network and the changes in the starting and MFE trajectories during different `treekin` simulations. Both RNA molecules together are 126 nucleotides long and they can fold into very distant conformations. The set of energetically good structures within Q_{pk} is therefore very high, such that a guiding stringency $\gamma = 1.8$ in combination with an energy range $\delta = 0.1$ kcal/mol already results in a heuristic $\tilde{Q}_{pk}$ network of 745 vertices. The minimum barrier height found is always 9.20 kcal/mol, which is exactly the barrier height predicted by `pk_findpath`. The trajectory distances are computed using equation 3.17. All starting and MFE trajectories are very similar, independently of the size of the generated network. Higher distances between trajectories (such as γ: 3.5 and δ: 2.5 vs. 3.0) are small qualitative changes concerning the population density (data not shown).

Network size					
δ \ γ	3.5	3.0	2.5	2.0	1.8
0.1	101	127	264	533	745
0.5	108	173	331	630	871
1.0	144	244	395	741	1022
1.5	151	267	458	836	
2.0	178	310	534	963	
2.5	194	385	600		
3.0	303	456	657		
3.5	327	496	706		
4.0	351	568	805		
4.5	411	629			
5.0	446	677			

Trajectory distance					
δ \ γ	3.5	3.0	2.5	2.0	1.8
0.1 vs. 0.5	0.00	0.03	0.02	3.34	0.95
0.5 vs. 1.0	0.00	26.72	0.21	1.49	0.50
1.0 vs. 1.5	0.04	0.00	0.00	0.04	
1.5 vs. 2.0	7.09	0.01	0.11	0.49	
2.0 vs. 2.5	0.00	1.95	0.00		
2.5 vs. 3.0	31.32	0.01	1.86		
3.0 vs. 3.5	0.00	0.00	0.02		
3.5 vs. 4.0	0.00	0.00	0.29		
4.0 vs. 4.5	0.02	0.12			
4.5 vs. 5.0	0.00	0.00			

Table 4.6: Network size: Amount of structures in the `RNAscout.pl` network for different values of δ and γ. Empty cells indicate that the parameters are too loose, such that the consumptions exceed available memory of 20 GB. All networks predicted a barrier height of 9.2 kcal/mol, which is exactly the barrier found by `pk_findpath`. Trajectory distance: As all networks contain the same minimum barrier structure, the starting and MFE trajectories are weakly influenced by network expansion. Bigger changes are exclusively quantitative.

Figure 4.7a shows a summary of trajectories computed from a network with $\gamma = 2.5$ and and δ ranging from 0.1 up to 4.0. As discussed above, there are no significant changes within the different simulations. We can therefore assume that the heuristic $\tilde{Q}_{pk}$ networks are a sufficient approximation of the full Q_{pk}. Figure 4.7b shows the full output for $\gamma = 2.5$ and $\delta = 4.0$. We find that the intermediate state predicted by `RNAscout.pl` is indeed similar to the transition state published by Isaacs et al.

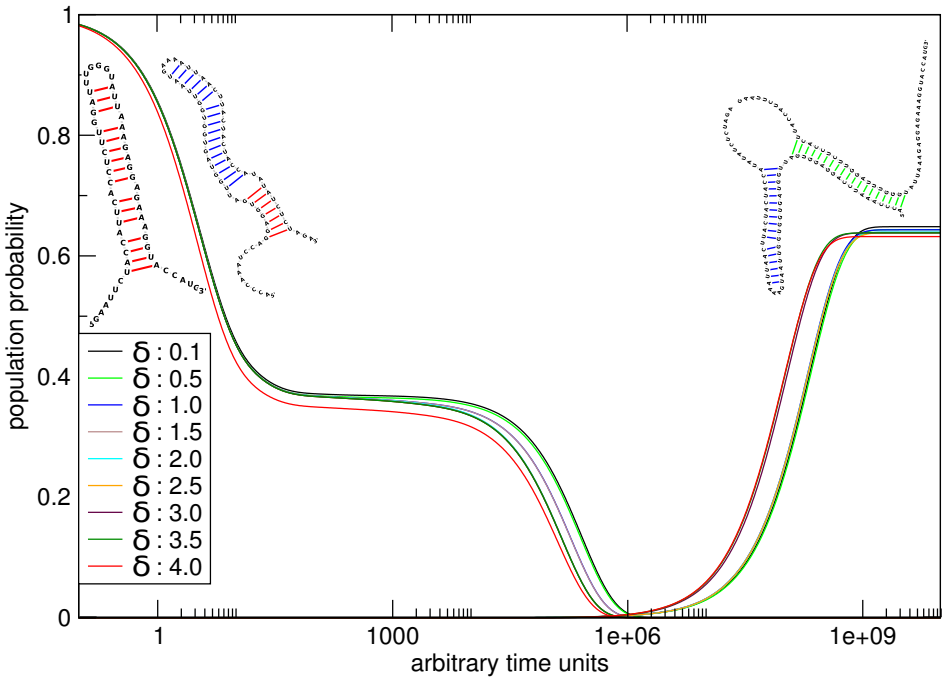

(a) `RNAscout.pl` – $\gamma = 2.5$

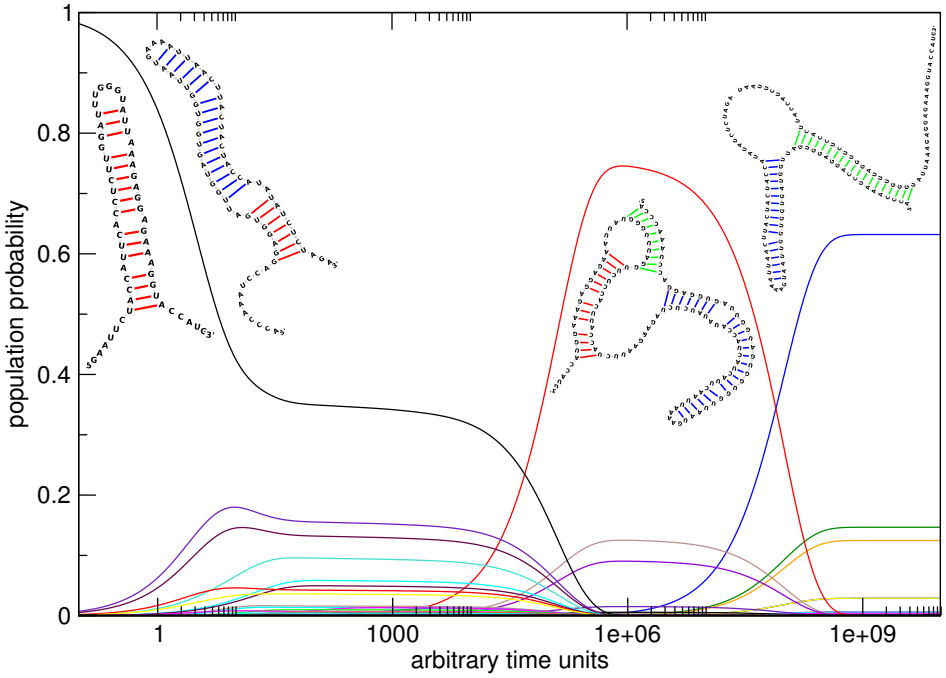

(b) `RNAscout.pl` – $\gamma = 2.5$, $\delta = 4.0$

Figure 4.7: Caption on page 93

Figure 4.7: `treekin` simulations of heuristically estimated riboswitch folding landscapes. **(a)**: Comparison of nine simulations from `RNAscout.pl` networks in respect to a change of the energy range δ. For each simulation, starting and MFE trajectories are shown (same color). The simulation starts with two independently folded RNA conformations (see squiggle plots). The MFE secondary structure is an RNA duplex. Blue base-pairs remain constant during the simulation, red base-pairs are opened an green base-pairs are closed. **(b)**: Full output of the `treekin` simulation with parameters $\gamma = 2.5$ and $\delta = 4.0$ kcal/mol. Additionally to starting and MFE structures, we see the squiggle plot of the most populated intermediate structure. The green base-pairs form a pseudoknot interaction with a hairpin loop. When refolding into the MFE secondary structure, red base-pairs open and green base-pairs close consecutively.

5 Conclusion & Perspective

We have discussed that the amount of suboptimal RNA secondary structures (i. e. the conformation space) for a given molecule increases exponentially with sequence length. The exhaustive computation of an RNA conformation space is therefore impossible for long RNA molecules. Current algorithms restrict the conformation space to a subset of computationally tractable, biologically reliable RNA secondary structures. These algorithms, however, neglect certain natural RNA secondary structure motives (e. g. pseudoknots), that have comparatively low impact on the MFE secondary structure prediction, but may have a significant impact on folding kinetics.

The `RNAscout.pl` heuristic has been implemented to compute folding kinetics between two RNA secondary structures including a wider set of RNA conformations, so called bisecondary structures. Our approach generates a heuristic image of the underlying conformation space, bounded by two parameters. The energy range defines the set of energetically relevant conformations, the guiding stringency excludes conformations that are structurally distant from the input structures. Based on this heuristic image, we can estimate refolding kinetics of both large RNA molecules and RNA molecules that are able to form pseudoknot conformations.

5.1 Discussion of Results

Inspection of a well established data set of RNA sequences (from the RNAstrand database) has shown that the majority of RNA molecules have lower barrier heights than shuffled sequences with the same dinucleotide content. This leads to the assumption that RNA molecules are optimized, such that they are able to fold into their MFE secondary structure quickly. However, we have also seen that it is not possible to compute the maximum barrier height of RNA folding landscapes from long RNA sequences exhaustively. Furthermore, estimation of barriers with direct path heuristics is only reliable for small structural arrangements up to a barrier height of 6.4 kcal/mol.

The predictions from `pk_findpath` are predominantly equal to those from `findpath`, suggesting that the inspected RNA molecules do not tend to form pseudoknotted intermediates on direct paths. However, lowering the pseudoknot penalty shows different results. A better energy model for pseudoknot interactions would therefore be highly appreciated.

The parameters of `RNAscout.pl` need to be adjusted carefully dependent on the type of refolding path. Stringent parameters might exclude important structures and therefore result in bad estimations of folding kinetics, loose parameters result in a computationally intractable set of RNA conformations. Recomputation of precomputed barrier heights has shown that automatic adjustment of the guiding stringency is often not sufficient, but `RNAscout.pl` performs better than direct path heuristics in general.

When inspecting single refolding pathways, the variation of both parameters usually allows to compute heuristic estimations of a conformation space that are sufficient to compute folding kinetics. We have seen this in the case of a manually selected sequence from the RNAstrand database. The quantitative description of population probabilities is not possible, as we cannot estimate basins of attraction based on single local minimum con-

formations. The qualitative description of the refolding time does also vary compared to full simulations, but allows to quantify the influence of certain intermediate states. The simulation of a synthetic riboswitch in response to its activating RNA molecule has underlined the importance of the assumed intermediate state. This supports the ability of `RNAscout.pl` to generate reliable heuristic images of the conformation space.

5.2 Perspective – Synthetic riboswitches

Due to the cellular function of RNA as a regulatory molecule, utilization of artificial RNA is of great importance in a (synthetic) cell. The small section of optimized RNA-triggered RNA switches allows a fast and versatile regulation of gene expression. In the simple case, given by Isaacs et al. [1], one taRNA refolds one crRNA. This model can easily be expanded such that various taRNAs are able to induce expression of different crRNAs.

Another interesting aspect concerning the utilization of RNA triggered switches is shown by Friedland et al. [101]. They presented a method to initiate translation of crRNA in response to different amounts of Arabinose pulses. Such models are very interesting in respect to time management within a synthetic cell.

Based on the ability of `RNAscout.pl` to quantify the refolding time of riboswitches, it should be possible to optimize refolding paths of certain RNA molecules by selective mutations. However, the first step towards new synthetic riboswitches is the *in silico* design. A potent approach to this has been shown by Flamm et al. in 2001 [189]. The algorithm of `switch.pl`[1] designs RNA sequences that are compatible with two different input structures. In a nutshell, an initially random RNA sequence is iteratively optimized to enhance the stability of *both* structures. In combination with `RNAscout.pl` one might establish a

[1] part of the `Vienna RNA package`

computational setup that suggests selected mutations, improving the refolding potential between the generated RNA secondary structures. The combination of `switch.pl` and `RNAscout.pl` could therefore lead to a efficient tool for both the design and evaluation of synthetic RNA molecules that may form complex networks in synthetic biology.

A Appendix

```
ACCCAAAUCCAGGAGGUGAUUGGUAGUGGUGGUUAAUGAAAAUUAACUUACUACUACCAUAUAUCUCUAGA&GAAUUCUACCAUUCACCUCUUGGAUUUGGGUAUUAAAGAGGAGAAAGGUACCAUG
...........(((((((..(((((((((((((((((((....))))))).)))))))))))..)))))))...&......((((.(((.((((((.(((......))).))))))..)))..))))..... -42.40
...........(((((((..(((((((((((((((((((....))))))).)))))))))))..)))))))...&.......(((.(((.((((((.(((......))).))))))..)))..)))..... -41.10
...........(((((((..(((((((((((((((((((....))))))).)))))))))))..)))))))...&........((.(((.((((((.(((......))).))))))..)))..))..... -40.30
...........(((((((..(((((((((((((((((((....))))))).)))))))))))..)))))))...&.........(.(((.((((((.(((......))).))))))..)))..).... -36.50
...........(((((((..(((((((((((((((((((....))))))).)))))))))))..)))))))...&...........(((.((((((.(((......))).))))))..)))..... -37.20
............((((((..(((((((((((((((((((....))))))).)))))))))))..))))))....&...........(((.((((((.(((......))).))))))..)))..... -36.80
............((((((..(((((((((((((((((((....))))))).)))))))))))..))))))....&............((.((((((.(((......))).))))))..))..... -35.60
............((((((..(((((((((((((((((((....))))))).)))))))))))..))))))....&.............(.((((((.(((......))).))))))..)..... -34.00
............((((((..(((((((((((((((((((....))))))).)))))))))))..))))))....&..............((((((.(((......))).))))))..... -35.40
............(((((...(((((((((((((((((((....))))))).)))))))))))...)))))....&..............((((((.(((......))).))))))..... -34.50
............((((....(((((((((((((((((((....))))))).)))))))))))....))))....&..............((((((.(((......))).))))))..... -32.80
............(((.....(((((((((((((((((((....))))))).)))))))))))).....)))....&..............((((((.(((......))).))))))..... -31.80
............((.....(((((((((((((((((((....))))))).)))))))))))).....))).....&..............((((((.(((......))).))))))..... -28.40
............(.....(((((((((((((((((((....))))))).)))))))))))).....).......&..............((((((.(((......))).))))))..... -27.30
.....................(((((((((((((((((((....))))))).)))))))))))...........&..............((((((.(((......))).))))))..... -28.40
.................(..(((((((((((((((((((....))))))).)))))))))))...........&.............).((((((.(((......))).))))))..... -26.40
.................((.(((((((((((((((((((....))))))).)))))))))))...........&............)).((((((.(((......))).))))))..... -27.80
................(((.(((((((((((((((((((....))))))).)))))))))))...........&...........)))((((((.(((......))).))))))..... -29.10
................(((.(((((((((((((((((((....))))))).)))))))))))...........&...........))).(((((.(((......))).)))))..... -25.30
...............((((.(((((((((((((((((((....))))))).)))))))))))...........&...........))))(((((.(((......))).)))))..... -28.70
...............((((.(((((((((((((((((((....))))))).)))))))))))...........&...........)))).((((.(((......))).))))..... -25.80
..............(((((.(((((((((((((((((((....))))))).)))))))))))...........&...........)))))((((.(((......))).))))..... -29.10
..............(((((.(((((((((((((((((((....))))))).)))))))))))...........&...........)))))..(((.(((......))).)))..... -27.50
.............((((((.(((((((((((((((((((....))))))).)))))))))))...........&...........))))))((.(((......))).)).....  -28.60
.............((((((.(((((((((((((((((((....))))))).)))))))))))...........&...........))))))..(((......))).))..... -25.70
............(((((((.(((((((((((((((((((....))))))).)))))))))))...........&...........)))))))((.(((......))).))..... -29.10
............(((((((.(((((((((((((((((((....))))))).)))))))))))...........&...........)))))))..(.(((......))).)..... -28.20
............(((((((.(((((((((((((((((((....))))))).)))))))))))...........&...........)))))))...(((......)))..... -30.00
............(((((((.(((((((((((((((((((....))))))).)))))))))))...........&...........)))))))....((......))..... -29.10
............(((((((.(((((((((((((((((((....))))))).)))))))))))...........&...........)))))))..... (......)..... -27.80
............(((((((.(((((((((((((((((((....))))))).)))))))))))...........&...........)))))))..... -32.00
.............(((((((.(((((((((((((((((((....))))))).)))))))))))...........&...........)))))))..... -33.10
..............(((((((.(((((((((((((((((((....))))))).)))))))))))...........&...........)))))))..... -33.30
................(((((((((.(((((((((((((((((((....))))))).)))))))))))...........&...........)))))))..... -36.30
..................(((((((((.(((((((((((((((((((....))))))).)))))))))))...........&...........)))))))..... -39.60
.(.....(((((((((((.(((((((((((((((((((....))))))).)))))))))))...........&...........)))))))))).....)..... -37.40
.((.....(((((((((((.(((((((((((((((((((....))))))).)))))))))))...........&...........)))))))))).....)).... -40.90
.(((....(((((((((((.(((((((((((((((((((....))))))).)))))))))))...........&...........)))))))))).....))).... -44.40
.(((...(((((((((((((.(((((((((((((((((((....))))))).)))))))))))...........&...........)))))))))))...))).... -46.40
.((((..(((((((((((((.(((((((((((((((((((....))))))).)))))))))))...........&...........)))))))))))..)))).... -48.80
.((((..(((((((((((((..(((((((((((((((((....))))))).)))))))))))...........&...........)))))))))))..)))).... -47.80
.((((..(((((((((((((...(((((((((((((((....))))))).)))))))))))...........&...........)))))))))))..)))).... -44.90
.((((..(((((((((((((..(((((((((((((((....))))))).)))))))))))...........&.........)..)))))))))))..)))).... -44.60
.((((..(((((((((((((..(.(((((((((((((....))))))).)))))))))))...........&.........)..)))))))))))..)))).... -41.20
.((((..(((((((((((((..(((((((((((((((....))))))).)))))))))))...........&........))..)))))))))))..)))).... -45.00
.((((.(((((((((((((..(((((((((((((((....))))))).)))))))))))...........&........))..)))))))))))).)))).... -46.60
.((((((((((((((((((..(((((((((((((((....))))))).)))))))))))...........&........))..)))))))))))))))).... -50.30
.((((((((((((((((((..((.(((((((((((....))))))).)))))))))))...........&........))..)))))))))))))))).... -48.80
.((((((((((((((((((..(((((((((((((((....))))))).)))))))))))...........&.......)))..)))))))))))))))).... -49.60
.((((((((((((((((((..(((.(((((((((((....))))))).)))))))))))...........&.......)))..)))))))))))))))).... -48.90
.((((((((((((((((((..(((((((((((((((....))))))).)))))))))))...........&......))))..)))))))))))))))).... -50.30
.((((((((((((((((((..((((.(((((((((((....))))))).)))))))))))...........&......))))..)))))))))))))))).... -46.90
.((((((((((((((((((..(((((((((((((((....))))))).)))))))))))...........&.....))))))..)))))))))))))))).... -50.00
.((((((((((((((((((.(((((((((((((((....))))))).)))))))))))...........&.....))))))).)))))))))))))))).... -52.20
((((((((((((((((((.(((((((((((((((....))))))).)))))))))))...........&.....))))))).))))))))))))))))).... -53.20
```

Table A.1: `findpath` output for the taRNA-crRNA pair of Isaacs et al. '&' separates the two structures.

ACCCAAAUCCAGGAGGUGAUUGGUAGUGGUGGUUAAUGAAAAUUAACUUACUACUACCAUAUAUCUCUAGA&GAAUUCUACCAUUCACCUCUUGGAUUUGGGUAUUAAAGAGGAGAAAGGUACCAUG	
...........(((((((..(((((((((((((((((....))))))).)))))))))))..)))))))...&.....((((.(((.((((((.(((......))).))))))).))).)))).....	-42.40
.[.........(((((((..(((((((((((((((((....))))))).)))))))))))..)))))))...&.....((((.(((.((((((.(((....].))).))))))).))).)))).....	-33.20
.[[........(((((((..(((((((((((((((((....))))))).)))))))))))..)))))))...&.....((((.(((.((((((.(((...]].))).))))))).))).)))).....	-36.50
.[[[.......(((((((..(((((((((((((((((....))))))).)))))))))))..)))))))...&.....((((.(((.((((((.(((..]]].))).))))))).))).)))).....	-39.40
.[[[[......(((((((..(((((((((((((((((....))))))).)))))))))))..)))))))...&.....((((.(((.((((((.(((.]]]].))).))))))).))).)))).....	-40.60
[[[[[......(((((((..(((((((((((((((((....))))))).)))))))))))..)))))))...&.....((((.(((.((((((.(((.]]]]].))).))))))).))).)))).....	-41.60
[[[[[[.....(((((((..(((((((((((((((((....))))))).)))))))))))..)))))))...&.....((((.(((.((((((.(((]]]]]]))).))))))).))).)))).....	-42.50
[[[[[[.....(((((((..(((((((((((((((((....))))))).)))))))))))..)))))))....&.....((((.(((.((((((.(((]]]]]]))).))))))).))).)))).....	-42.10
[[[[[[.....((((((..(((((((((((((((((....))))))).)))))))))))..))))))....&.....((((.(((.((((((..(]]]]]]))..))))))).))).)))).....	-41.40
[[[[[[.....((((((..(((((((((((((((((....))))))).)))))))))))..))))))....&.....((((.(((.((((((..(.]]]]].)..))))))).))).)))).....	-39.40
[[[[[[.....((((((..(((((((((((((((((....))))))).)))))))))))..))))))....&.....((((.(((.((((((....]]]]].....))))))).))).)))).....	-40.70
[[[[[[[.....((((((..(((((((((((((((((....))))))).)))))))))))..))))))....&.....((((.(((.((((((...]]]]]].....))))))).))).)))).....	-41.70
[[[[[[[[....((((((..(((((((((((((((((....))))))).)))))))))))..))))))....&.....((((.(((.((((((..]]]]]]].....))))))).))).)))).....	-43.00
(((((((((...((((((..(((((((((((((((((....))))))).)))))))))))..))))))....&.....[[[[.[[[.[[[[[[.))))))))))....]]]]].]]].]]]].....	-46.40
(((((((((..((((((..(((((((((((((((((....))))))).)))))))))))..))))))....&.....[[[[.[[[.[[[[[[)))))))))))....]]]]].]]].]]]].....	-49.30
(((((((((..((((((..(((((((((((((((((....))))))).)))))))))))..))))))....&.....[[[[.[[[.[[[[[.))))))))))).....]]]]].]]].]]]].....	-47.00
((((((((((.((((((..(((((((((((((((((....))))))).)))))))))))..))))))....&.....[[[[.[[[.[[[[[)))))))))))).....]]]]].]]].]]]].....	-48.20
((((((((((.((((((..(((((((((((((((((....))))))).)))))))))))..))))))....&.....[[[[.[[[.[[[[.))))))))))).....]]]].]]].]]]].....	-46.80
((((((((((((((((..(((((((((((((((((....))))))).)))))))))))..))))))....&.....[[[[.[[[.[[[[)))))))))))).....]]]].]]].]]]].....	-47.40
((((((((((((((((..(((((((((((((((((....))))))).)))))))))))..))))))....&.....[[[[.[[[.[[[.))))))))))).....].]]].]]].]]]].....	-44.10
((((((((((((((((..(((((((((((((((((....))))))).)))))))))))..))))))....&.....[[[[.[[[.[[..))))))))))).....].].]]].]]].]]]].....	-42.70
((((((((((.(((((..(((((((((((((((((....))))))).)))))))))))..))))))....&.....[[[[.[[[.[[..))))))))))).....].].]]].]]].]]]].....	-39.30
((((((((((((((((..(((((((((((((((((....))))))).)))))))))))..))))))....&.....[[[[.[[[.[[.))))))))))).....].].]]].]]].]]]].....	-42.20
((((((((((.(((((..(((((((((((((((((....))))))).)))))))))))..))))))....&.....[[[[.[[[.[[.))))))))))).....].].]]].]]].]]]].....	-41.10
((((((((((((((((..(((((((((((((((((....))))))).)))))))))))..))))))....&.....[[[[.[[[.[[)))))))))))).....].].]]].]]].]]]].....	-42.70
((((((((((((((((..(((((((((((((((((....))))))).)))))))))))..))))))....&.....[[[[.[[[.[..))))))))))).....]..]]].]]].]]]].....	-39.30
((((((((((((((((..(((((((((((((((((....))))))).)))))))))))..))))))....&.....[[[[.[[[...))))))))))).....]]].]]].]]]].....	-40.50
((((((((((((((.(((..(((((((((((((((((....))))))).)))))))))))..)))))))....&.....[[[[.[[[...))))))))))).....]]].]]].]]]].....	-38.00
((((((((((((((((..(((((((((((((((((....))))))).)))))))))))..)))))))....&.....[[[[.[[[..))))))))))).....]]].]]].]]]].....	-40.90
((((((((((((((.((..(((((((((((((((((....))))))).)))))))))))..))))))))....&.....[[[[.[[[..))))))))))).....]]].]]].]]]].....	-39.30
((((((((((((((((..(((((((((((((((((....))))))).)))))))))))..))))))))....&.....[[[[.[[[.))))))))))).....]]].]]].]]]].....	-43.10
((((((((((((((((...(((((((((((((((((....))))))).)))))))))))...))))))))....&.....[[[[.[[[.))))))))))).....]]].]]].]]]].....	-42.20
((((((((((((((((....(((((((((((((((((....))))))).)))))))))))............&.....[[[[.[[[.))))))))))).....]]].]]].]]]].....	-44.70
((((((((((((((((...(((((((((((((((((....))))))).)))))))))))............&.....[[[[.[[[))))))))))).....]]].]]].]]]].....	-45.50
((((((((((((((((...(((((((((((((((((....))))))).)))))))))))............&.....[[[[.[[.))))))))))).....]]].]]].]]]].....	-41.70
((((((((((((((((..(((((((((((((((((....))))))).)))))))))))............&.....[[[[.[[))))))))))).....]]].]]].]]]].....	-44.70
((((((((((((((((..(((((((((((((((((....))))))).)))))))))))............&.....[[[[.[.))))))))))).....].]]].]]].]]]].....	-43.74
((((((((((((((((..(((((((((((((((((....))))))).)))))))))))............&.....[[[[..))))))))))).....]]]].]]].]]]].....	-46.11
((((((((((((((((.(((((((((((((((((....))))))).)))))))))))............&.....[[[[..))))))))))).....]]]].]]].]]]].....	-47.51
((((((((((((((((.(((((((((((((((((....))))))).)))))))))))............&.....[[[..))))))))))).....]]].]]].]]]].....	-46.21
((((((((((((((((.(((((((((((((((((....))))))).)))))))))))............&.....[[..))))))))))).....]].]]].]]]].....	-45.41
((((((((((((((((.(((((((((((((((((....))))))).)))))))))))............&.....[..))))))))))).....].]]].]]]].....	-41.61
((((((((((((((((.(((((((((((((((((....))))))).)))))))))))............&.....))))))))))).....]]].]]].]]]].....	-55.10
((((((((((((((((..(((((((((((((((....))))))).)))))))))).............&.....))))))))))).....]]].]]].]]]].....	-54.10
((((((((((((((((.(((((((((((((((....))))))).)))))))))).............&.....).))))))))))).....]]].]]].]]]].....	-53.00
((((((((((((((((.(.(((((((((((((....))))))).)))))))))).............&.....).))))))))))).....]]].]]].]]]].....	-50.10
((((((((((((((((.(((((((((((((....))))))).)))))))))).............&.....)).))))))))))).....]]].]]].]]]].....	-53.10
((((((((((((((((.((.(((((((((((....))))))).)))))))))).............&.....)).))))))))))).....]]].]]].]]]].....	-49.70
((((((((((((((((.(((((((((((((....))))))).)))))))))).............&.....))).))))))))))).....]]].]]].]]]].....	-53.50
((((((((((((((((.(((.(((((((((....))))))).)))))))))).............&.....))).))))))))))).....]]].]]].]]]].....	-52.00
((((((((((((((((.(((((((((((((....))))))).)))))))))).............&.....))))).))))))))))).....]]].]]].]]]].....	-52.80
((((((((((((((((.((((.(((((((....))))))).))))))))).............&.....))))).))))))))))).....]]].]]].]]]].....	-52.10
((((((((((((((((.(((((((((((((....))))))).))))))))).............&......)))))).))))))))))).....]]].]]].]]]].....	-53.50
((((((((((((((((.(((((.(((((((....))))))).))))))))).............&......)))))).))))))))))).....]]].]]].]]]].....	-50.10
((((((((((((((((.(((((((((((((....))))))).))))))))).............&.....)))))).))))))))))).....]]].]]].]]]].....	-53.20

Table A.2: `pk_findpath` output for the taRNA-crRNA pair of Isaacs et al. '&' separates the two structures.

Bibliography

[1] F. Isaacs, D. Dwyer, C. Ding, D. Pervouchine, C. Cantor, and J. Collins, "Engineered riboregulators enable post-transcriptional control of gene expression," *Nature biotechnology*, vol. 22, no. 7, pp. 841–847, 2004.

[2] I. Hofacker, W. Fontana, P. Stadler, L. Bonhoeffer, M. Tacker, and P. Schuster, "Fast folding and comparison of RNA secondary structures," *Monatshefte f "ur Chemie/Chemical Monthly*, vol. 125, no. 2, pp. 167–188, 1994.

[3] K. Kruger, P. Grabowski, A. Zaug, J. Sands, D. Gottschling, and T. Cech, "Self-splicing RNA: autoexcision and autocyclization of the ribosomal RNA intervening sequence of Tetrahymena," *Cell*, vol. 31, no. 1, pp. 147–157, 1982.

[4] C. Guerrier-Takada, K. Gardiner, T. Marsh, N. Pace, and S. Altman, "The RNA moiety of ribonuclease P is the catalytic subunit of the enzyme," *Cell*, vol. 35, no. 3, pp. 849–857, 1983.

[5] N. Kresge, R. Simoni, and R. Hill, "Ribonuclease P and the Discovery of Catalytic RNA: the Work of Sidney Altman," *Journal of Biological Chemistry*, vol. 282, no. 7, p. e5, 2007.

[6] H. Amrein and R. Axel, "Genes expressed in neurons of adult male Drosophila," *Cell*, vol. 88, no. 4, pp. 459–469, 1997.

[7] J. Lee and R. Jaenisch, "Long-range cis effects of ectopic X-inactivation centres on a mouse autosome," 1997.

[8] L. Herzing, J. Romer, J. Horn, and A. Ashworth, "Xist has properties of the X-chromosome inactivation centre," 1997.

[9] H. Willard and H. Salz, "Remodelling chromatin with RNA," *Nature a-z index*, vol. 386, no. 6622, pp. 228–229, 1997.

[10] S. Eddy, "Noncoding RNA genes," *Current Opinion in Genetics & Development*, vol. 9, no. 6, pp. 695–699, 1999.

[11] W. Winkler, A. Nahvi, and R. Breaker, "Thiamine derivatives bind messenger RNAs directly to regulate bacterial gene expression," *Nature*, vol. 419, no. 6910, pp. 952–956, 2002.

[12] J. Mattick, "RNA regulation: a new genetics?," *Nature Reviews Genetics*, vol. 5, no. 4, pp. 316–323, 2004.

[13] E. Lander, L. Linton, B. Birren, C. Nusbaum, M. Zody, J. Baldwin, K. Devon, K. Dewar, M. Doyle, W. FitzHugh, *et al.*, "Initial sequencing and analysis of the human genome," *Nature*, vol. 409, no. 6822, pp. 860–921, 2001.

[14] M. HATTORI, "Finishing the euchromatic sequence of the human genome," *Protein, Nucleic Acid and Enzyme*, vol. 50, no. 2, pp. 162–168, 2005.

[15] C. Thomas Jr, "The genetic organization of chromosomes.," *Annual Review of Genetics*, vol. 5, p. 237, 1971.

[16] T. Gregory, "Coincidence, coevolution, or causation? DNA content, cell size, and the C-value enigma," *Biological Reviews*, vol. 76, no. 01, pp. 65–101, 2001.

[17] R. Taft, M. Pheasant, and J. Mattick, "The relationship between non-protein-coding DNA and eukaryotic complexity," *Bioessays*, vol. 29, no. 3, pp. 288–299, 2007.

[18] L. Goodstadt and C. Ponting, "Phylogenetic reconstruction of orthology, paralogy, and conserved synteny for dog and human," *PLoS Comput Biol*, vol. 2, no. 9, p. e133, 2006.

[19] R. Waterston, K. Lindblad-Toh, E. Birney, J. Rogers, J. Abril, P. Agarwal, R. Agarwala, R. Ainscough, M. Alexandersson, P. An, *et al.*, "Initial sequencing and comparative analysis of the mouse genome," *Nature*, vol. 420, pp. 520–562, 2002.

[20] L. Hillier, W. Miller, E. Birney, W. Warren, R. Hardison, C. Ponting, P. Bork, D. Burt, M. Groenen, M. Delany, *et al.*, "Sequence and comparative analysis of the chicken genome provide unique perspectives on vertebrate evolution," *Nature*, vol. 432, no. 7018, pp. 695–716, 2004.

[21] S. Aparicio, J. Chapman, E. Stupka, N. Putnam, J. Chia, P. Dehal, A. Christoffels, S. Rash, S. Hoon, A. Smit, *et al.*, "Whole-genome shotgun assembly and analysis of the genome of Fugu rubripes," *Science*, vol. 297, no. 5585, p. 1301, 2002.

[22] L. Stein, Z. Bao, D. Blasiar, T. Blumenthal, M. Brent, N. Chen, A. Chinwalla, L. Clarke, C. Clee, A. Coghlan, *et al.*, "The genome sequence of Caenorhabditis briggsae: a platform for comparative genomics," *PLoS Biol*, vol. 1, no. 2, p. E45, 2003.

[23] S. Misra, M. Crosby, C. Mungall, B. Matthews, K. Campbell, P. Hradecky, Y. Huang, J. Kaminker, G. Millburn, S. Prochnik, *et al.*, "Annotation of the Drosophila melanogaster euchromatic genome: a systematic review," *Genome biology*, vol. 3, no. 12, 2002.

[24] J. Mattick, "The hidden genetic program of complex organisms.," *Scientific American*, vol. 291, no. 4, p. 60, 2004.

[25] A. Eyre-Walker, "Evidence of selection on silent site base composition in mam-

mals: potential implications for the evolution of isochores and junk DNA," *Genetics*, vol. 152, no. 2, p. 675, 1999.

[26] F. Costa, "Non-coding RNAs, epigenetics and complexity," *Gene*, vol. 410, no. 1, pp. 9–17, 2008.

[27] R. Taft and J. Mattick, "Increasing biological complexity is positively correlated with the relative genome-wide expansion of non-protein-coding DNA sequences," *Genome Biology*, vol. 5, no. 1, pp. 1–1, 2004.

[28] M. Gagen and J. Mattick, "Failed" nonaccelerating" models of prokaryote gene regulatory networks," *Arxiv preprint q-bio/0312022*, 2003.

[29] L. Croft, M. Lercher, M. Gagen, and J. Mattick, "Is prokaryotic complexity limited by accelerated growth in regulatory overhead?," *Genome Biology*, vol. 5, no. 1, pp. 2–2, 2004.

[30] T. Gregory, "Synergy between sequence and size in large-scale genomics," *Nature Reviews Genetics*, vol. 6, no. 9, pp. 699–708, 2005.

[31] J. Ewan Birney, R. Anindya Dutta, R. Thomas, H. Elliott, M. Zhiping Weng, T. Emmanouil, A. John, E. Robert, S. Michael, M. Christopher, *et al.*, "Identification and analysis of functional elements in 1% of the human genome by the ENCODE pilot project," *Nature*, vol. 447, no. 7146, pp. 799–816, 2007.

[32] A. Bompf
"unewerer, C. Flamm, C. Fried, G. Fritzsch, I. Hofacker, J. Lehmann, K. Missal, A. Mosig, B. M
"uller, S. Prohaska, *et al.*, "Evolutionary patterns of non-coding RNAs," *Theory in Biosciences*, vol. 123, no. 4, pp. 301–369, 2005.

[33] J. Mattick, "The genetic signatures of noncoding RNAs," *PLoS genetics*, vol. 5, no. 4, 2009.

[34] J. Mattick and I. Makunin, "Non-coding RNA," *Human molecular genetics*, vol. 15, no. Review Issue 1, p. R17, 2006.

[35] T. Nilsen, "The spliceosome: the most complex macromolecular machine in the cell?," *Bioessays*, vol. 25, no. 12, pp. 1147–1149, 2003.

[36] K. Kwek, S. Murphy, A. Furger, B. Thomas, W. O'Gorman, H. Kimura, N. Proudfoot, and A. Akoulitchev, "U1 snRNA associates with TFIIH and regulates transcriptional initiation," *Nature Structural & Molecular Biology*, vol. 9, no. 11, pp. 800–805, 2002.

[37] W. O'Gorman, B. Thomas, K. Kwek, A. Furger, and A. Akoulitchev, "Analysis of U1 small nuclear RNA interaction with cyclin H," *Journal of Biological Chemistry*, vol. 280, no. 44, p. 36920, 2005.

[38] U. Meier, "The many facets of H/ACA ribonucleoproteins," *Chromosoma*, vol. 114, no. 1, pp. 1–14, 2005.

[39] J. Cavaillé, K. Buiting, M. Kiefmann, M. Lalande, C. Brannan, B. Horsthemke, J. Bachellerie, J. Brosius, and A. Hüttenhofer, "Identification of brain-specific and imprinted small nucleolar RNA genes exhibiting an unusual genomic organization," *Proceedings of the National Academy of Sciences of the United States of America*, vol. 97, no. 26, p. 14311, 2000.

[40] J. Cavaillé, P. Vitali, E. Basyuk, A. Hüttenhofer, and J. Bachellerie, "A novel brain-specific box C/D small nucleolar RNA processed from tandemly repeated introns of a noncoding RNA gene in rats," *Journal of Biological Chemistry*, vol. 276, no. 28, p. 26374, 2001.

[41] Y. Zeng, R. Yi, and B. Cullen, "MicroRNAs and small interfering RNAs can inhibit mRNA expression by similar mechanisms," *Proceedings of the National Academy of Sciences of the United States of America*, vol. 100, no. 17, p. 9779, 2003.

[42] B. Cullen, "Derivation and function of small interfering RNAs and microRNAs," *Virus research*, vol. 102, no. 1, pp. 3–9, 2004.

[43] A. Fire, "RNA-triggered gene silencing," *Trends in Genetics*, vol. 15, no. 9, pp. 358–363, 1999.

[44] D. Bartel, "MicroRNAs:: Genomics, Biogenesis, Mechanism, and Function," *Cell*, vol. 116, no. 2, pp. 281–297, 2004.

[45] L. He and G. Hannon, "MicroRNAs: small RNAs with a big role in gene regulation," *Nature Reviews Genetics*, vol. 5, no. 7, pp. 522–531, 2004.

[46] V. Ambros, "The functions of animal microRNAs," *Nature*, vol. 431, no. 7006, pp. 350–355, 2004.

[47] Z. HE and E. SONTHEIMER, "siRNAs and miRNAs: A meeting report on RNA silencing," *RNA*, vol. 10, no. 8, p. 1165, 2004.

[48] V. Ambros, "MicroRNA Pathways in Flies and Worms:: Growth, Death, Fat, Stress, and Timing," *Cell*, vol. 113, no. 6, pp. 673–676, 2003.

[49] M. Klein, S. Impey, and R. Goodman, "Role reversal: the regulation of neuronal gene expression by microRNAs," *Current opinion in neurobiology*, vol. 15, no. 5, pp. 507–513, 2005.

[50] A. Giraldez, R. Cinalli, M. Glasner, A. Enright, J. Thomson, S. Baskerville, S. Hammond, D. Bartel, and A. Schier, "MicroRNAs regulate brain morphogenesis in zebrafish," *Science*, vol. 308, no. 5723, p. 833, 2005.

[51] I. Naguibneva, M. Ameyar-Zazoua, A. Polesskaya, S. Ait-Si-Ali, R. Groisman, M. Souidi, S. Cuvellier, and A. Harel-Bellan, "The microRNA miR-181 targets the homeobox protein Hox-A11 during mammalian myoblast differentiation," *Nature cell biology*, vol. 8, no. 3, pp. 278–284, 2006.

[52] S. Hatfield, H. Shcherbata, K. Fischer, K. Nakahara, R. Carthew, and H. Ruohola-Baker, "Stem cell division is regulated by the microRNA pathway," *Nature*, vol. 435, no. 7044, pp. 974–978, 2005.

[53] E. Bernstein and C. Allis, "RNA meets chromatin," *Genes & development*, vol. 19, no. 14, p. 1635, 2005.

[54] T. Mercer, M. Dinger, and J. Mattick, "Long non-coding RNAs: insights into functions," *Nature Reviews Genetics*, vol. 10, no. 3, pp. 155–159, 2009.

[55] J. Rinn, M. Kertesz, J. Wang, S. Squazzo, X. Xu, S. Brugmann, L. Goodnough, J. Helms, P. Farnham, E. Segal, *et al.*, "Functional demarcation of active and silent chromatin domains in human HOX loci by noncoding RNAs," *Cell*, vol. 129, no. 7, pp. 1311–1323, 2007.

[56] Y. Ogawa, B. Sun, and J. Lee, "Intersection of the RNA interference and X-inactivation pathways," *Science*, vol. 320, no. 5881, p. 1336, 2008.

[57] X. Wang, S. Arai, X. Song, D. Reichart, K. Du, G. Pascual, P. Tempst, M. Rosenfeld, C. Glass, and R. Kurokawa, "Induced ncRNAs allosterically modify RNA-binding proteins in cis to inhibit transcription," *Nature*, vol. 454, no. 7200, pp. 126–130, 2008.

[58] J. Feng, C. Bi, B. Clark, R. Mady, P. Shah, and J. Kohtz, "The Evf-2 noncoding RNA is transcribed from the Dlx-5/6 ultraconserved region and functions as a Dlx-2 transcriptional coactivator," *Science's STKE*, vol. 20, no. 11, p. 1470, 2006.

[59] I. Martianov, A. Ramadass, A. Barros, N. Chow, and A. Akoulitchev, "Repression of the human dihydrofolate reductase gene by a non-coding interfering transcript," *Nature*, vol. 445, no. 7128, pp. 666–670, 2007.

[60] M. Beltran, I. Puig, C. Peña, J. García, A. Álvarez, R. Peña, F. Bonilla, and A. De Herreros, "A natural antisense transcript regulates Zeb2/Sip1 gene expres-

sion during Snail1-induced epithelial–mesenchymal transition," *Genes & development*, vol. 22, no. 6, p. 756, 2008.

[61] V. Vagin, A. Sigova, C. Li, H. Seitz, V. Gvozdev, and P. Zamore, "A distinct small RNA pathway silences selfish genetic elements in the germline," *Science*, vol. 313, no. 5785, p. 320, 2006.

[62] H. Lee, S. Chang, S. Choudhary, A. Aalto, M. Maiti, D. Bamford, and Y. Liu, "qiRNA is a new type of small interfering RNA induced by DNA damage," *Nature*, vol. 459, no. 7244, pp. 274–277, 2009.

[63] S. Choudhuri, "Lesser known relatives of miRNA," *Biochemical and biophysical research communications*, vol. 388, no. 2, pp. 177–180, 2009.

[64] G. Calin, C. Liu, M. Ferracin, T. Hyslop, R. Spizzo, C. Sevignani, M. Fabbri, A. Cimmino, E. Lee, S. Wojcik, *et al.*, "Ultraconserved regions encoding ncRNAs are altered in human leukemias and carcinomas," *Cancer Cell*, vol. 12, no. 3, pp. 215–229, 2007.

[65] J. Finnerty, W. Wang, S. Hébert, B. Wilfred, G. Mao, and P. Nelson, "The miR-15/107 group of microRNA genes: evolutionary biology, cellular functions, and roles in human diseases," *Journal of molecular biology*, 2010.

[66] C. Christov, E. Trivier, and T. Krude, "Noncoding human Y RNAs are overexpressed in tumours and required for cell proliferation," *British journal of cancer*, vol. 98, no. 5, pp. 981–988, 2008.

[67] A. Esquela-Kerscher and F. Slack, "OncomirsmicroRNAs with a role in cancer," *Nature Reviews Cancer*, vol. 6, no. 4, pp. 259–269, 2006.

[68] D. Perez, T. Hoage, J. Pritchett, A. Ducharme-Smith, M. Halling, S. Ganapathiraju, P. Streng, and D. Smith, "Long, abundantly expressed non-coding transcripts are altered in cancer," *Human molecular genetics*, vol. 17, no. 5, p. 642, 2008.

[69] E. Reis, H. Nakaya, R. Louro, F. Canavez, Á. Flatschart, G. Almeida, C. Egidio,

A. Paquola, A. Machado, F. Festa, *et al.*, "Antisense intronic non-coding RNA levels correlate to the degree of tumor differentiation in prostate cancer," *Oncogene*, vol. 23, no. 39, pp. 6684–6692, 2004.

[70] M. Szymanski, M. Barciszewska, V. Erdmann, and J. Barciszewski, "A new frontier for molecular medicine: noncoding RNAs," *Biochimica et Biophysica Acta (BBA)-Reviews on Cancer*, vol. 1756, no. 1, pp. 65–75, 2005.

[71] W. Gilbert, "Origin of life: The RNA world," *Nature*, vol. 319, no. 6055, 1986.

[72] M. Powner, B. Gerland, and J. Sutherland, "Synthesis of activated pyrimidine ribonucleotides in prebiotically plausible conditions," *Nature*, vol. 459, no. 7244, pp. 239–242, 2009.

[73] P. Purnick and R. Weiss, "The second wave of synthetic biology: from modules to systems," *Nature Reviews Molecular Cell Biology*, vol. 10, no. 6, pp. 410–422, 2009.

[74] T. Gardner, C. Cantor, and J. Collins, "Construction of a genetic toggle switch in Escherichia coli," *Nature*, vol. 403, no. 6767, pp. 339–342, 2000.

[75] B. Kramer, A. Viretta, M. Daoud-El Baba, D. Aubel, W. Weber, and M. Fussenegger, "An engineered epigenetic transgene switch in mammalian cells," *Nature biotechnology*, vol. 22, no. 7, pp. 867–870, 2004.

[76] B. Kramer and M. Fussenegger, "Hysteresis in a synthetic mammalian gene network," *Proceedings of the National Academy of Sciences of the United States of America*, vol. 102, no. 27, p. 9517, 2005.

[77] T. Deans, C. Cantor, and J. Collins, "A tunable genetic switch based on RNAi and repressor proteins for regulating gene expression in mammalian cells," *Cell*, vol. 130, no. 2, pp. 363–372, 2007.

[78] J. Dueber, B. Yeh, K. Chak, and W. Lim, "Reprogramming control of an allosteric sig-

naling switch through modular recombination," *Science*, vol. 301, no. 5641, p. 1904, 2003.

[79] J. Anderson, C. Voigt, and A. Arkin, "Environmental signal integration by a modular AND gate," *Molecular systems biology*, vol. 3, no. 1, 2007.

[80] C. Guet *et al.*, "Combinatorial synthesis of genetic networks," *Science*, vol. 296, no. 5572, p. 1466, 2002.

[81] O. Rackham and J. Chin, "Cellular logic with orthogonal ribosomes," *J. Am. Chem. Soc*, vol. 127, no. 50, pp. 17584–17585, 2005.

[82] K. Rinaudo, L. Bleris, R. Maddamsetti, S. Subramanian, R. Weiss, and Y. Benenson, "A universal RNAi-based logic evaluator that operates in mammalian cells," *Nature biotechnology*, vol. 25, no. 7, pp. 795–801, 2007.

[83] M. Stojanovic and D. Stefanovic, "A deoxyribozyme-based molecular automaton," *Nature Biotechnology*, vol. 21, no. 9, pp. 1069–1074, 2003.

[84] M. Win and C. Smolke, "A modular and extensible RNA-based gene-regulatory platform for engineering cellular function," *Proceedings of the National Academy of Sciences*, vol. 104, no. 36, p. 14283, 2007.

[85] M. Win and C. Smolke, "Higher-order cellular information processing with synthetic RNA devices," *Science*, vol. 322, no. 5900, p. 456, 2008.

[86] T. Bayer and C. Smolke, "Programmable ligand-controlled riboregulators of eukaryotic gene expression," *Nature Biotechnology*, vol. 23, no. 3, pp. 337–343, 2005.

[87] H. Kobayashi, M. Kærn, M. Araki, K. Chung, T. Gardner, C. Cantor, and J. Collins, "Programmable cells: interfacing natural and engineered gene networks," *Proceedings of the National Academy of Sciences of the United States of America*, vol. 101, no. 22, p. 8414, 2004.

[88] S. Basu, Y. Gerchman, C. Collins, F. Arnold, and R. Weiss, "A synthetic multicellular system for programmed pattern formation," *Nature*, vol. 434, no. 7037, pp. 1130–1134, 2005.

[89] S. Basu, R. Mehreja, S. Thiberge, M. Chen, and R. Weiss, "Spatiotemporal control of gene expression with pulse-generating networks," *Proceedings of the National Academy of Sciences of the United States of America*, vol. 101, no. 17, p. 6355, 2004.

[90] M. Elowitz and S. Leibler, "A synthetic oscillatory network of transcriptional regulators," *Nature*, vol. 403, no. 6767, pp. 335–338, 2000.

[91] M. Atkinson, M. Savageau, J. Myers, and A. Ninfa, "Development of genetic circuitry exhibiting toggle switch or oscillatory behavior in Escherichia coli," *Cell*, vol. 113, no. 5, pp. 597–607, 2003.

[92] E. Fung, W. Wong, J. Suen, T. Bulter, S. Lee, and J. Liao, "A synthetic gene–metabolic oscillator," *Nature*, vol. 435, no. 7038, pp. 118–122, 2005.

[93] J. Stricker, S. Cookson, M. Bennett, W. Mather, L. Tsimring, and J. Hasty, "A fast, robust and tunable synthetic gene oscillator," *Nature*, vol. 456, no. 7221, pp. 516–519, 2008.

[94] M. Tigges, T. Marquez-Lago, J. Stelling, and M. Fussenegger, "A tunable synthetic mammalian oscillator," *Nature*, vol. 457, no. 7227, pp. 309–312, 2009.

[95] T. Danino, O. Mondragón-Palomino, L. Tsimring, and J. Hasty, "A synchronized quorum of genetic clocks," *Nature*, vol. 463, no. 7279, pp. 326–330, 2010.

[96] T. Ham, S. Lee, J. Keasling, and A. Arkin, "Design and construction of a double inversion recombination switch for heritable sequential genetic memory," *PloS one*, vol. 3, no. 7, p. 2815, 2008.

[97] C. Ajo-Franklin, D. Drubin, J. Eskin, E. Gee, D. Landgraf, I. Phillips, and P. Silver,

"Rational design of memory in eukaryotic cells," *Genes & development*, vol. 21, no. 18, p. 2271, 2007.

[98] S. Hooshangi, S. Thiberge, and R. Weiss, "Ultrasensitivity and noise propagation in a synthetic transcriptional cascade," *Proceedings of the National Academy of Sciences of the United States of America*, vol. 102, no. 10, p. 3581, 2005.

[99] T. Sohka, R. Heins, R. Phelan, J. Greisler, C. Townsend, and M. Ostermeier, "An externally tunable bacterial band-pass filter," *Proceedings of the National Academy of Sciences*, vol. 106, no. 25, p. 10135, 2009.

[100] T. Ellis, X. Wang, and J. Collins, "Diversity-based, model-guided construction of synthetic gene networks with predicted functions," *Nature biotechnology*, vol. 27, no. 5, pp. 465–471, 2009.

[101] A. Friedland, T. Lu, X. Wang, D. Shi, G. Church, and J. Collins, "Synthetic gene networks that count," *Science*, vol. 324, no. 5931, p. 1199, 2009.

[102] J. Tabor, H. Salis, Z. Simpson, A. Chevalier, A. Levskaya, E. Marcotte, C. Voigt, and A. Ellington, "A synthetic genetic edge detection program," *Cell*, vol. 137, no. 7, pp. 1272–1281, 2009.

[103] A. Levskaya, A. Chevalier, J. Tabor, Z. Simpson, L. Lavery, M. Levy, E. Davidson, A. Scouras, A. Ellington, E. Marcotte, *et al.*, "Synthetic biology: engineering Escherichia coli to see light," *Nature*, vol. 438, no. 7067, pp. 441–442, 2005.

[104] A. Levskaya, O. Weiner, W. Lim, and C. Voigt, "Spatiotemporal control of cell signalling using a light-switchable protein interaction," *Nature*, vol. 461, no. 7266, pp. 997–1001, 2009.

[105] T. Lu and J. Collins, "Dispersing biofilms with engineered enzymatic bacteriophage," *Proceedings of the National Academy of Sciences*, vol. 104, no. 27, p. 11197, 2007.

[106] J. Anderson, E. Clarke, A. Arkin, and C. Voigt, "Environmentally controlled invasion

of cancer cells by engineered bacteria," *Journal of molecular biology*, vol. 355, no. 4, pp. 619–627, 2006.

[107] T. Lu and J. Collins, "Engineered bacteriophage targeting gene networks as adjuvants for antibiotic therapy," *Proceedings of the National Academy of Sciences*, vol. 106, no. 12, p. 4629, 2009.

[108] D. Ro, E. Paradise, M. Ouellet, K. Fisher, K. Newman, J. Ndungu, K. Ho, R. Eachus, T. Ham, J. Kirby, *et al.*, "Production of the antimalarial drug precursor artemisinic acid in engineered yeast," *Nature*, vol. 440, no. 7086, pp. 940–943, 2006.

[109] J. Bath, S. Green, and A. Turberfield, "A Free-Running DNA Motor Powered by a Nicking Enzyme," *Angewandte Chemie*, vol. 117, no. 28, pp. 4432–4435, 2005.

[110] P. Yin, H. Yan, X. Daniell, A. Turberfield, and J. Reif, "A unidirectional DNA walker that moves autonomously along a track," *Angewandte Chemie International Edition*, vol. 43, no. 37, pp. 4906–4911, 2004.

[111] J. Shin and N. Pierce, "A synthetic DNA walker for molecular transport," *J. Am. Chem. Soc*, vol. 126, no. 35, pp. 10834–10835, 2004.

[112] B. Yurke, "Using DNA to power the nanoworld," *Controlled Nanoscale Motion*, pp. 331–347, 2007.

[113] V. Balzani, A. Credi, F. Raymo, and J. Stoddart, "Artificial molecular machines," *Angewandte Chemie International Edition*, vol. 39, no. 19, pp. 3348–3391, 2000.

[114] G. Kottas, L. Clarke, D. Horinek, and J. Michl, "Artificial molecular rotors," *Chem. Rev*, vol. 105, no. 4, pp. 1281–1376, 2005.

[115] J. Bath and A. Turberfield, "DNA nanomachines," *Nature nanotechnology*, vol. 2, no. 5, pp. 275–284, 2007.

[116] E. Bromley, N. Kuwada, M. Zuckermann, R. Donadini, L. Samii, G. Blab, G. Gem-

men, B. Lopez, P. Curmi, N. Forde, *et al.*, "The Tumbleweed: towards a synthetic protein motor," 2009.

[117] B. Canton, A. Labno, and D. Endy, "Refinement and standardization of synthetic biological parts and devices," *Nature biotechnology*, vol. 26, no. 7, pp. 787–793, 2008.

[118] I. Cases and V. Lorenzo, "Genetically modified organisms for the environment: stories of success and failure and what we have learned from them," *International microbiology*, vol. 8, pp. 213–222, 2005.

[119] D. Savage, J. Way, and P. Silver, "Defossiling fuel: How synthetic biology can transform biofuel production," *ACS Chemical Biology*, vol. 3, no. 1, pp. 13–16, 2008.

[120] D. Ro, E. Paradise, M. Ouellet, K. Fisher, K. Newman, J. Ndungu, K. Ho, R. Eachus, T. Ham, J. Kirby, *et al.*, "Production of the antimalarial drug precursor artemisinic acid in engineered yeast," *Nature*, vol. 440, no. 7086, pp. 940–943, 2006.

[121] R. Gil, F. Silva, J. Peretó, and A. Moya, "Determination of the core of a minimal bacterial gene set," *Microbiology and Molecular Biology Reviews*, vol. 68, no. 3, p. 518, 2004.

[122] G. Murtas, "Question 7: construction of a semi-synthetic minimal cell: a model for early living cells," *Origins of Life and Evolution of Biospheres*, vol. 37, no. 4, pp. 419–422, 2007.

[123] E. Bromley, K. Channon, E. Moutevelis, and D. Woolfson, "Peptide and protein building blocks for synthetic biology: from programming biomolecules to self-organized biomolecular systems," *ACS Chemical Biology*, vol. 3, no. 1, pp. 38–50, 2008.

[124] P. Schwille and S. Diez, "Synthetic biology of minimal systems," 2009.

[125] A. Forster and G. Church, "Towards synthesis of a minimal cell," *Molecular Systems Biology*, vol. 2, no. 1, 2006.

[126] J. Szostak, D. Bartel, and P. Luisi, "Synthesizing life," *Nature*, vol. 409, no. 6818, pp. 387–390, 2001.

[127] I. Chen and J. Szostak, "Membrane growth can generate a transmembrane pH gradient in fatty acid vesicles," *Proceedings of the National Academy of Sciences of the United States of America*, vol. 101, no. 21, p. 7965, 2004.

[128] K. Wilson and P. von Hippel, "Transcription termination at intrinsic terminators: the role of the RNA hairpin," *Proceedings of the National Academy of Sciences*, vol. 92, no. 19, p. 8793, 1995.

[129] A. Garst and R. Batey, "A switch in time: Detailing the life of a riboswitch," *Biochimica et Biophysica Acta (BBA)-Gene Regulatory Mechanisms*, vol. 1789, no. 9-10, pp. 584–591, 2009.

[130] R. Montange and R. Batey, "Riboswitches: emerging themes in RNA structure and function," *Annu. Rev. Biophys.*, vol. 37, pp. 117–133, 2008.

[131] J. D. Watson and F. H. Crick, "Molecular structure of nucleic acids; a structure for deoxyribose nucleic acid.," *Nature*, vol. 171, pp. 737–738, April 1953.

[132] G. Varani and W. H. McClain, "The G x U wobble base pair. a fundamental building block of rna structure crucial to rna function in diverse biological systems.," *EMBO Rep*, vol. 1, pp. 18–23, July 2000.

[133] N. Leontis, J. Stombaugh, and E. Westhof, "The non-Watson–Crick base pairs and their associated isostericity matrices," *Nucleic acids research*, vol. 30, no. 16, p. 3497, 2002.

[134] J. Šponer, P. Kulhánek, J. Leszczynski, and J. Šponer, "Non-Watson- Crick Base

Pairing in RNA. Quantum Chemical Analysis of the cis Watson- Crick/Sugar Edge Base Pair Family," *J. Phys. Chem. A*, vol. 109, no. 10, pp. 2292–2301, 2005.

[135] P. Brion and E. Westhof, "Hierarchy and dynamics of RNA folding," *Annual review of biophysics and biomolecular structure*, vol. 26, no. 1, pp. 113–137, 1997.

[136] R. Das, J. Karanicolas, and D. Baker, "Atomic accuracy in predicting and designing non-canonical RNA structure," *Nature methods*, vol. 7, no. 4, p. 291, 2010.

[137] S. Sharma, F. Ding, and N. Dokholyan, "ifoldrna: three-dimensional RNA structure prediction and folding," *Bioinformatics*, vol. 24, no. 17, p. 1951, 2008.

[138] M. Rother, K. Rother, T. Puton, and J. Bujnicki, "ModeRNA: a tool for comparative modeling of RNA 3D structure," *Nucleic acids research*, vol. 39, no. 10, p. 4007, 2011.

[139] Y. Itoh, S. Chiba, S. Sekine, and S. Yokoyama, "Crystal structure of human selenocysteine tRNA," *Nucleic Acids Research*, vol. 37, no. 18, p. 6259, 2009.

[140] P. Stadler and C. Haslinger, "RNA structures wth pseudo-knots," *Working Papers*, 1997.

[141] K. Wiese, E. Glen, and A. Vasudevan, "jviz. rna-a java tool for RNA secondary structure visualization," *NanoBioscience, IEEE Transactions on*, vol. 4, no. 3, pp. 212–218, 2005.

[142] R. Nussinov and A. Jacobson, "Fast algorithm for predicting the secondary structure of single-stranded RNA," *Proceedings of the National Academy of Sciences of the United States of America*, vol. 77, no. 11, p. 6309, 1980.

[143] C. Do, D. Woods, and S. Batzoglou, "Contrafold: RNA secondary structure prediction without physics-based models," *Bioinformatics*, vol. 22, no. 14, p. e90, 2006.

[144] J. SantaLucia, "A unified view of polymer, dumbbell, and oligonucleotide DNA

nearest-neighbor thermodynamics," *Proceedings of the National Academy of Sciences of the United States of America*, vol. 95, no. 4, p. 1460, 1998.

[145] A. Walter, D. Turner, J. Kim, M. Lyttle, P. M
"uller, D. Mathews, and M. Zuker, "Coaxial stacking of helixes enhances binding of oligoribonucleotides and improves predictions of RNA folding," *Proceedings of the National Academy of Sciences*, vol. 91, no. 20, p. 9218, 1994.

[146] D. Mathews, J. Sabina, M. Zuker, and D. Turner, "Expanded sequence dependence of thermodynamic parameters improves prediction of RNA secondary structure1," *Journal of molecular biology*, vol. 288, no. 5, pp. 911–940, 1999.

[147] C. Flamm, I. Hofacker, and P. Stadler, "Computational chemistry with rna secondary structures," *Kemija u industriji*, vol. 53, pp. 315–322, 2004.

[148] J. Jaeger, D. Turner, and M. Zuker, "Improved predictions of secondary structures for RNA," *Proceedings of the National Academy of Sciences of the United States of America*, vol. 86, no. 20, p. 7706, 1989.

[149] M. Zuker and P. Stiegler, "Optimal computer folding of large RNA sequences using thermodynamics and auxiliary information," *Nucleic acids research*, vol. 9, no. 1, p. 133, 1981.

[150] I. L. Hofacker and P. F. Stadler, *RNA Secondary Structures*, pp. 439–489. Wiley-VCH Verlag GmbH, 2008.

[151] M. Zuker, "On finding all suboptimal foldings of an RNA molecule," *Science*, vol. 244, no. 4900, p. 48, 1989.

[152] S. Wuchty, W. Fontana, I. Hofacker, P. Schuster, *et al.*, "Complete suboptimal folding of RNA and the stability of secondary structures," *Biopolymers*, vol. 49, no. 2, pp. 145–165, 1999.

[153] M. S. Waterman, "Secondary structure of single - stranded nucleic acids," *Studies*

on foundations and combinatorics, Advances in mathematics supplementary studies, Academic Press N.Y., vol. 1, pp. 167–212, 1978.

[154] J. McCaskill, "The equilibrium partition function and base pair binding probabilities for RNA secondary structure," *Biopolymers*, vol. 29, no. 6-7, pp. 1105–1119, 1990.

[155] D. Konings and R. Gutell, "A comparison of thermodynamic foldings with comparatively derived structures of 16s and 16s-like rRNAs.," *Rna*, vol. 1, no. 6, p. 559, 1995.

[156] A. Loria and T. Pan, "Domain structure of the ribozyme from eubacterial ribonuclease p.," *Rna*, vol. 2, no. 6, p. 551, 1996.

[157] H. Mann, Y. Ben-Asouli, A. Schein, S. Moussa, and N. Jarrous, "Eukaryotic RNase p:: Role of RNA and protein subunits of a primordial catalytic ribonucleoprotein in RNA-based catalysis," *Molecular cell*, vol. 12, no. 4, pp. 925–935, 2003.

[158] D. Staple and S. Butcher, "Pseudoknots: RNA structures with diverse functions," *PLoS biology*, vol. 3, no. 6, p. e213, 2005.

[159] T. Cech, "Conserved sequences and structures of group i introns: building an active site for RNA catalysis–a review," *Gene*, vol. 73, no. 2, pp. 259–271, 1988.

[160] C. Theimer, C. Blois, and J. Feigon, "Structure of the human telomerase RNA pseudoknot reveals conserved tertiary interactions essential for function," *Molecular cell*, vol. 17, no. 5, pp. 671–682, 2005.

[161] J. Paillart, E. Skripkin, B. Ehresmann, C. Ehresmann, and R. Marquet, "A loop-loop" kissing" complex is the essential part of the dimer linkage of genomic hiv-1 RNA," *Proceedings of the National Academy of Sciences of the United States of America*, vol. 93, no. 11, p. 5572, 1996.

[162] J. Reeder and R. Giegerich, "Design, implementation and evaluation of a practi-

cal pseudoknot folding algorithm based on thermodynamics," *BMC bioinformatics*, vol. 5, no. 1, p. 104, 2004.

[163] A. Condon, B. Davy, B. Rastegari, S. Zhao, and F. Tarrant, "Classifying RNA pseudoknotted structures," *Theoretical Computer Science*, vol. 320, no. 1, pp. 35–50, 2004.

[164] C. Reidys, F. Huang, J. Andersen, R. Penner, P. Stadler, and M. Nebel, "Topology and prediction of RNA pseudoknots," *Bioinformatics*, vol. 27, no. 8, p. 1076, 2011.

[165] T. Akutsu, "Dynamic programming algorithms for RNA secondary structure prediction with pseudoknots," *Discrete Applied Mathematics*, vol. 104, no. 1-3, pp. 45–62, 2000.

[166] A. Gultyaev, F. Van Batenburg, and C. Pleij, "An approximation of loop free energy values of RNA h-pseudoknots.," *RNA*, vol. 5, no. 5, p. 609, 1999.

[167] M. Andronescu, C. Pop, and A. Condon, "Improved free energy parameters for RNA pseudoknotted secondary structure prediction," *RNA*, vol. 16, no. 1, p. 26, 2010.

[168] J. Bois, S. Venkataraman, H. Choi, A. Spakowitz, Z. Wang, and N. Pierce, "Topological constraints in nucleic acid hybridization kinetics," *Nucleic acids research*, vol. 33, no. 13, p. 4090, 2005.

[169] H. Isambert, "The jerky and knotty dynamics of RNA," *Methods*, vol. 49, no. 2, pp. 189–196, 2009.

[170] A. Xayaphoummine, T. Bucher, and H. Isambert, "Kinefold web server for RNA/DNA folding path and structure prediction including pseudoknots and knots," *Nucleic acids research*, vol. 33, no. suppl 2, p. W605, 2005.

[171] J. Ren, B. Rastegari, A. Condon, and H. Hoos, "HotKnots: heuristic prediction of RNA secondary structures including pseudoknots," *Rna*, vol. 11, no. 10, p. 1494, 2005.

[172] J. Sperschneider and A. Datta, "Dotknot: pseudoknot prediction using the probability dot plot under a refined energy model," *Nucleic Acids Research*, vol. 38, no. 7, p. e103, 2010.

[173] A. Gultyaev, F. Van Batenburg, and C. Pleij, "The computer simulation of RNA folding pathways using a genetic algorithm," *Journal of Molecular Biology*, vol. 250, no. 1, pp. 37–51, 1995.

[174] L. Cai, R. Malmberg, and Y. Wu, "Stochastic modeling of RNA pseudoknotted structures: a grammatical approach," *Bioinformatics*, vol. 19, no. suppl 1, p. i66, 2003.

[175] S. Cao and S. Chen, "Predicting RNA pseudoknot folding thermodynamics," *Nucleic acids research*, vol. 34, no. 9, p. 2634, 2006.

[176] S. Cao and S. Chen, "Predicting structures and stabilities for H-type pseudoknots with interhelix loops," *RNA*, vol. 15, no. 4, p. 696, 2009.

[177] E. Rivas and S. Eddy, "A dynamic programming algorithm for RNA structure prediction including pseudoknots," *Journal of molecular biology*, vol. 285, no. 5, pp. 2053–2068, 1999.

[178] R. Dirks and N. Pierce, "A partition function algorithm for nucleic acid secondary structure including pseudoknots," *Journal of Computational Chemistry*, vol. 24, no. 13, pp. 1664–1677, 2003.

[179] W. Beyer, "RNA secondary structure prediction including pseudoknots," *Master Thesis*, 2004.

[180] C. Reidys and P. Stadler, "Combinatorial landscapes," *SIAM review*, pp. 3–54, 2002.

[181] B. Hajek, "Cooling schedules for optimal annealing," *Mathematics of operations research*, pp. 311–329, 1988.

[182] M. Wolfinger, W. Svrcek-Seiler, C. Flamm, I. Hofacker, and P. Stadler, "Efficient computation of RNA folding dynamics," *Journal of Physics A: Mathematical and General*, vol. 37, p. 4731, 2004.

[183] C. Flamm, W. Fontana, I. Hofacker, and P. Schuster, "RNA folding at elementary step resolution.," *Rna*, vol. 6, no. 3, p. 325, 2000.

[184] M. Wolfinger, "Landscapes of biopolymers," *PHD Thesis*, 2004.

[185] M. Tacker, W. Fontana, P. Stadler, and P. Schuster, "Statistics of RNA melting kinetics," *European biophysics journal*, vol. 23, no. 1, pp. 29–38, 1994.

[186] M. Wolfinger, "The energy landscape of RNA folding," *Diplomarbeit*, 2001.

[187] J. Maňuch, C. Thachuk, L. Stacho, and A. Condon, "NP-completeness of the energy barrier problem without pseudoknots and temporary arcs," *Natural Computing*, pp. 1–15, 2011.

[188] S. Morgan and P. Higgs, "Barrier heights between ground states in a model of RNA secondary structure," *Journal of Physics A: Mathematical and General*, vol. 31, p. 3153, 1998.

[189] C. Flamm, I. Hofacker, S. Maurer-Stroh, P. Stadler, and M. Zehl, "Design of multi-stable RNA molecules.," *Rna*, vol. 7, no. 2, p. 254, 2001.

[190] I. Dotu, W. Lorenz, P. Van Hentenryck, and P. Clote, "Computing folding pathways between RNA secondary structures," *Nucleic acids research*, vol. 38, no. 5, p. 1711, 2010.

[191] M. Andronescu, V. Bereg, H. Hoos, and A. Condon, "RNA STRAND: the RNA secondary structure and statistical analysis database," *BMC bioinformatics*, vol. 9, no. 1, p. 340, 2008.

[192] M. Rosenblad, J. Gorodkin, B. Knudsen, C. Zwieb, and T. Samuelsson, "SRPDB:

Signal recognition particle database," *Nucleic acids research*, vol. 31, no. 1, p. 363, 2003.

Curriculum Vitae

Stefan Badelt

March 2, 1985, Vienna, Austria

http://www.tbi.univie.ac.at/~stef

stef@tbi.univie.ac.at

Educational Background

2004 –	Studies in Molecular Biology, University of Vienna
2003 – 2004	Diploma Thesis with Prof. Ivo Hofacker: *Design of artificial RNA* Military Service
1995 – 2003	Secondary School (Albertus Magnus School, Vienna)

Professional Experience

2009/05 –	**Diploma Thesis** – Bioinformatics Design of artificial RNA *Institute for Theoretical Chemistry, Vienna, Austria* (Theoretical Biochemistry Group)
2008/07 – 2008/09	**Rotation** – Molecular Medicine Chromosome degradation in apoptotic cells *Max Planck Institute for Molecular Genetics, Berlin, Germany* (Group Ullmann – Molecular Cytogenetics)

2008/03 – 2008/04 **Rotation** – Immunology

Interaction of Stat1-GRDBD-Stat1 and GRE

Max F. Perutz Laboratories, Vienna, Austria

(Group Kovarik – Infection Biology)

2006/07 – 2009/03 **Technician** – plasmid library administration, genotyping

Max F. Perutz Laboratories, Vienna, Austria

(Group Kovarik – Infection Biology)

Skills

- Languages: German (native), English, Perl, C, Bash, Latex, R, HTML
- Lab-Techniques: PCR, Real Time PCR, Tissue Culture work (including Nucleofection), Immunfluorescence, Immunoprecipitation, Nuclear Extract, Western Blot Analysis, Electrophoretic Mobility Shift Assay, DNA/RNA Extraction, DNA/RNA Gel Electrophoresis, Reverse Transcription, Array CGH, Oligoarray, BAC Array, ChIP on Chip.

Conferences, Talks

- *TBI Winterseminar* in Bled, Slovenia, Feb 13 - 20, 2011
  Title: Energy barriers in pseudoknot conformation space
- *Herbstseminar Bioinformatik* in Vysoká Lípa, Czech Republic, Oct 5 - 10, 2010
  Title: Design & future aspects of artificial RNA-switches in synthetic biology
- *TBI Winterseminar* in Bled, Slovenia, Feb 14 - 21, 2010
  Title: Design of artificial RNA-switches